JUAN ESTEBAN SUAREZ PATIÑO

INCREASING DISTRIBUTED ENERGY RESOURCES HOSTING CAPACITY IN DISTRIBUTION SYSTEMS USING D-STATCOM DEVICES AND RECONFIGURATION

LONDRINA
2025

JUAN ESTEBAN SUAREZ PATIÑO

INCREASING DISTRIBUTED ENERGY RESOURCES HOSTING CAPACITY IN DISTRIBUTION SYSTEMS USING D-STATCOM DEVICES AND RECONFIGURATION

A dissertation submitted to the Electrical Engineering Graduate Program at the State University of Londrina in fulfillment of the requirements for the degree of Master of Science in Electrical Engineering.

Supervisor:
Prof. Dr. Luis Alfonso Gallego Pareja

LONDRINA
2025

Ficha de identificação da obra elaborada pelo autor, através do Programa de Geração Automática do Sistema de Bibliotecas da UEL

P298i Patiño, Juan Esteban Suarez.
Increasing distributed energy resources hosting capacity in distribution systems using d-statcom devices and reconfiguration / Juan Esteban Suarez Patiño. - Londrina, 2025.
122 f. : il.

Orientador: Luis Alfonso Gallego Pareja.
Dissertação (Mestrado em Engenharia Elétrica) - Universidade Estadual de Londrina, Centro de Tecnologia e Urbanismo, Programa de Pós-Graduação em Engenharia Elétrica, 2025.
Inclui bibliografia.

1. Generação Distribuída - Tese. 2. Transição Energética - Tese. 3. FACTS - Tese. 4. Programação Linear Inteira Mista - Tese. I. Pareja, Luis Alfonso Gallego . II. Universidade Estadual de Londrina. Centro de Tecnologia e Urbanismo. Programa de Pós-Graduação em Engenharia Elétrica. III. Título.

CDU 62

JUAN ESTEBAN SUAREZ PATIÑO

INCREASING DISTRIBUTED ENERGY RESOURCES HOSTING CAPACITY IN DISTRIBUTION SYSTEMS USING D-STATCOM DEVICES AND RECONFIGURATION

A dissertation submitted to the Electrical Engineering Graduate Program at the State University of Londrina in fulfillment of the requirements for the degree of Master of Science in Electrical Engineering.

EXAMINATION BOARD

Prof. Dr. Luis Alfonso Gallego Pareja
Universidade Estadual de Londrina – UEL
Supervisor

Prof(a). Dr(a). Juliani Chico Piai Paiva
Universidade Estadual de Londrina – UEL

Prof. Dr. Edgar Manuel Carreño Franco
Universidade Estadual do Oeste do Paraná – UNIOESTE/CECE-Foz

Londrina, March 26, 2025

ACKNOWLEDGEMENTS

I would like to express my deepest gratitude to my advisor, Luis Alfonso Gallego Pareja, for their support and feedback throughout the development of this thesis. I also extend my sincere appreciation to the members of the examination board, Juliani Chico Piai Paiva and Edgar Manuel Carreño Franco, for their constructive suggestions and critical evaluations, which have significantly enriched the quality of this work.

My heartfelt thanks go to my family and loved ones, whose unwavering support, encouragement, and understanding have been a constant source of motivation during this academic journey. I am equally grateful to my fellow master's colleagues for the stimulating discussions, collaboration, and companionship that have made this experience both enriching and memorable.

Finally, I acknowledge the financial support provided by the Araucária Foundation (Fundação Araucária de Apoio ao Desenvolvimento Científico e Tecnológico do Estado do Paraná), which was essential for the development of this work.

SUAREZ, J. E. **Aumento da Capacidade de Acomodação de Recursos Energéticos Distribuídos em Sistemas de Distribuição Usando Dispositivos D-STATCOM e Reconfiguração**. 121f. Dissertação (Mestrado em Engenharia Elétrica) – Universidade Estadual de Londrina, Londrina, 2025.

RESUMO

A crescente inserção de recursos energéticos distribuídos (RED), como a geração solar fotovoltaica (FV), em sistemas de distribuição de energia elétrica (SDEE) apresenta desafios operacionais significativos. A capacidade de acomodação (CA) é considerada um indicador do nível aceitável de inserção de RED em SDEE, razão pela qual são feitos esforços para aumentar seu valor. Este estudo propõe uma metodologia para aumentar a CA de RED em SDEE por meio da integração de dispositivos D-STATCOM e da reconfiguração de redes. Alinhada aos Objetivos de Desenvolvimento Sustentável (ODS) das Nações Unidas (NU), a abordagem proposta utiliza modelos matemáticos para determinar a localização ótima de dispositivos D-STATCOM e resolver o problema de reconfiguração de sistemas de distribuição (RSD), garantindo uma integração mais segura e eficiente dos RED. Todos os modelos são baseados em fluxo de potência para SDEE radiais e formulados como modelos de otimização de programação linear inteira mista (PLIM). Até o momento, tais modelos PLIM para dispositivos D-STATCOM e para RSD e D-STATCOMs simultaneamente não foram encontrados na literatura especializada. A reconfiguração mostra-se altamente versátil para melhorar as condições gerais do sistema, enquanto os dispositivos D-STATCOM, apesar de eficazes, apresentam limitações que indicam a necessidade de análises adicionais para explorar todo o seu potencial. A metodologia envolve um processo iterativo para calcular a CA, incorporando os modelos de D-STATCOM e DSR em cada iteração. A principal contribuição deste trabalho é a introdução de um modelo combinado que integra simultaneamente a reconfiguração e os dispositivos D-STATCOM, fornecendo uma solução robusta para enfrentar os desafios associados à crescente penetração de RED em SDEE. A metodologia proposta foi validada utilizando os sistemas de teste de 33, 69 e 136 barras, amplamente referenciados na literatura especializada. Os resultados demonstram que a combinação dessas duas abordagens aumenta significativamente a CA, alcançando melhorias de até 95% em casos com limitações iniciais críticas. Os resultados também demonstram a precisão do método iterativo para calcular a CA, bem como a eficácia e eficiência dos dispositivos D-STATCOM e da RSD no aumento da CA e na melhoria das condições operacionais dos SDEE.

Palavras-chave: Generação Distribuída. Transição Energética. FACTS. Programação Linear Inteira Mista. Otimização.

SUAREZ, J. E. **Increasing Distributed Energy Resources Hosting Capacity in Distribution Systems Using D-STATCOM Devices and Reconfiguration**. 121p. Master's Thesis (Master of Science in Electrical Engineering) – State University of Londrina, Londrina, 2025.

ABSTRACT

The increasing penetration of distributed energy resources (DER), such as solar photovoltaic (PV) generation, in power distribution systems (PDS) poses significant operational challenges. Hosting capacity (HC) is considered an indicator of the acceptable level of DER integration in a PDS, which is why efforts are made to increase its value. This study presents a methodology to enhance the HC of DER in PDS through the integration of distribution static compensator (D-STATCOM) devices and network reconfiguration. Aligned with the United Nations' (UN) Sustainable Development Goals (SDG), the proposed approach employs mathematical models to determine the optimal placement of D-STATCOMs and solve the distribution systems reconfiguration (DSR) problem, ensuring a safer and more efficient integration of DER. All models are based on a power flow for radial PDS and are formulated as mixed-integer linear programming (MILP) optimization models. To date, such MILP models for D-STATCOM devices and for DSR and D-STATCOMs simultaneously have not been found in the specialized literature. Reconfiguration proves to be highly versatile in improving the overall conditions of the system, while the D-STATCOM devices, despite its effectiveness, has limitations that suggest the need for further analysis to explore its full potential. The methodology involves an iterative process to calculate the HC, incorporating D-STATCOM and DSR models in each iteration. The main contribution of this work is the introduction of a combined model that simultaneously integrates reconfiguration and D-STATCOM devices, providing a robust solution to address the challenges associated with the growing penetration of DER in PDS. The proposed methodology was validated using the 33, 69, and 136-bus benchmark test systems, widely referenced in specialized literature. The results demonstrate that the combination of these two approaches significantly increases HC, achieving up to 95% improvement in cases with critical initial limitations. The results also demonstrate the accuracy of the iterative method for calculating HC, as well as the effectiveness and efficiency of D-STATCOM devices and DSR in increasing HC and improving the operational conditions of PDS.

Keywords: Distributed Generation. Energy Transition. FACTS. Mixed Integer Linear Programming. Optimization.

LIST OF FIGURES

LIST OF TABLES

LIST OF ABBREVIATIONS AND ACRONYMS

CIGRÉ	Conseil International des Grands Réseaux Électrique
DER	Distributed Energy Resources
DG	Distributed Generation
DSO	Distribution System Operator
DSR	Distribution Systems Reconfiguration
D-STATCOM	Distribution Static Synchronous Compensator
EPRI	Electric Power Research Institute
FACTS	Flexible AC Transmission Systems
HC	Hosting Capacity
MILP	Mixed-Integer Linear Programming
NCRES	Non-Conventional Renewable Energy Sources
PDS	Power Distribution Systems
PV	Photovoltaic
SDG	Sustainable Development Goals
UN	United Nations

LIST OF SYMBOLS

Sets

Ω_b	Set of buses
Ω_l	Set of branches
Ω_t	Set of periods

Parameters

$\overline{I_{ij}}$	Upper current limit for branch ij
K_V	Overvoltage penalty factor
$m^s_{ij,t,y}$	Slope of the y_{th} block of the load flow in the branch ij during period t
N	Number of buses
$N^{STATCOM}_{max}$	Maximum number of devices available for installation in the system
$P^d_{i,t}$	Active power demand at bus i during period t
$Q^d_{i,t}$	Reactive power demand at bus i during period t
$Q^{STATCOM}_{max}$	Maximum allowed capacity for each D-STATCOM
R_{ij}	Resistance of branch ij
S	Number of discretizations for the linearization of $V^{sqr}_{j,t} I^{sqr}_{ij,t}$
$\overline{V}$	Upper voltage limit
$\underline{V}$	Lower voltage limit
V_{nom}	Nominal voltage
X_{ij}	Reactance of branch ij
Y	Number of blocks in the segmented linearization of $P^2_{ij,t}$ and $Q^2_{ij,t}$
Z_{ij}	Impedance of branch ij
$\Delta^S_{ij,t}$	Limit of each block of the power flow in branch ij during period t
$\overline{\Delta}^V$	Discretization step for the linearization of $V^{sqr}_{j,t} I^{sqr}_{ij,t}$

Continuous variables

$b_{ij,t}$	Slack variable for the voltage drop constraint in reconfiguration
$I_{ij,t}$	Current in branch ij during period t
$I^{sqr}_{ij,t}$	Squared current in branch ij during period t
$P_{ij,t}$	Active power flow in branch ij during period t
$P_{ki,t}$	Active power flow in branch ki during period t
$P^{c}_{j,t,s}$	Power correction used in $V^{sqr}_{j,t} I^{sqr}_{ij,t}$
$P^{s}_{i,t}$	Active power supplied by the substation at bus i during period t
$P^{+}_{ij,t}$, $P^{-}_{ij,t}$	Auxiliary variables for the direction of $P_{ij,t}$
$Q_{ij,t}$	Reactive power flow in branch ij during period t
$Q_{ki,t}$	Reactive power flow in branch ki during period t
$Q^{s}_{i,t}$	Reactive power supplied by the substation at bus i during period t
$Q^{STATCOM}_{i,t}$	Reactive power delivered or absorbed by the D-STATCOM connected at bus i during period t
$Q^{+}_{ij,t}$, $Q^{-}_{ij,t}$	Auxiliary variables for the direction of $Q_{ij,t}$
$V_{i,t}$	Voltage at bus i during period t
$V_{j,t}$	Voltage at bus j during period t
$V^{sqr}_{i,t}$	Squared voltage at bus i during period t
$V^{sqr}_{j,t}$	Squared voltage at bus j during period t
$\Delta P_{ij,t,y}$	Value of the y_{th} block of $\lvert P_{ij,t} \rvert$
$\Delta Q_{ij,t,y}$	Value of the y_{th} block of $\lvert Q_{ij,t} \rvert$

Binary variables

w_i	Binary variable indicating where a D-STATCOM is located
$x^{V}_{i,t,s}$	Binary variable used in the discretization of $V^{sqr}_{i,t}$
$y^{+}_{ij,t}$, $y^{-}_{ij,t}$	Binary variables related to the direction of the power flow in branch ij

CONTENTS

1 INTRODUCTION

In recent decades, the growing concern over the effects of climate change and the need to reduce greenhouse gas emissions have driven an energy transition towards cleaner and renewable sources. The United Nations' (UN) Sustainable Development Goals (SDG) are a set of global objectives aimed at addressing various social, economic, and environmental challenges to achieve a more sustainable future by 2030 [1]. Among these objectives, renewable energy in the electric sector is given special recognition for its role in mitigating the effects of climate change, while also contributing to the decentralization, diversification, and democratization of the sector. In this context, distributed energy resources (DER), which include technologies such as solar photovoltaic (PV), wind, and other renewable sources, have gained prominence in power systems. Unlike centralized generation systems, where energy is produced in large power plants and transmitted to consumption centers through long transmission lines, DER allow for the production of electricity close to the point of consumption, thereby reducing transmission losses and enhancing system efficiency.

This decentralization of energy production has been promoted by energy policies and regulations aimed at encouraging consumer participation in energy generation, transforming them into "prosumers". In the case of Brazil, Figure 1 illustrates the installed solar generation capacity over the past few years, highlighting the exponential growth observed during this period. The micro and mini distributed generation (DG) of electric energy has experienced growth driven by regulatory actions, such as the establishment of the possibility of compensation for excess energy produced by smaller systems (Net Metering). In 2023, micro and mini DG reached 30,950 GWh with an installed capacity of 26,627 MW, notably in PV solar sources, which accounted for 29,813 GWh and 26,366 MW of generation and installed capacity, respectively [2].

However, the massive integration of these DER presents significant challenges in the operation and control of power distribution systems (PDS), which were not originally designed to accommodate large volumes of DER. One of the main issues is the inherent variability of renewable sources, such as solar and wind, which depend on weather conditions. This variability can cause fluctuations in voltage levels, affecting the quality of electricity supply and leading to stability issues in the grid. Moreover, PDS are primarily designed to operate with unidirectional power flows, from generation centers to end users. With the integration of DER, power flows can become bidirectional, complicating system operation. Distribution system operators (DSOs) must address issues such as overvoltages, power quality problems, overloading in lines and transformers, as well as the need for enhanced coordination in protection systems, which may not be equipped to handle

Figure 1 – Installed capacity in Brazil - Solar generation

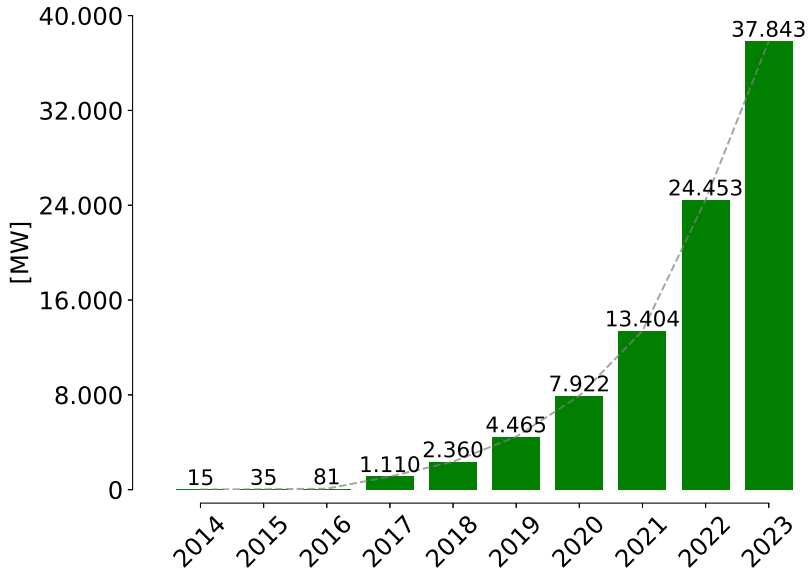

Source: Adapted from [3]

these new operational scenarios [4]. These factors, collectively, limit the ability of the PDS to accommodate high levels of DER without compromising supply reliability and safety.

The calculation of hosting capacity (HC) in PDS allows for identifying the maximum acceptable level of DER integration without compromising power quality or system reliability [5]. In this way, by having a technical and measurable criterion for decision-making regarding the integration of DER into the system, it is possible to find a balance that meets the goals of the energy transition while maintaining the operational limits of PDS. With a methodology for calculating HC, DSOs can determine the maximum level of DER that can be integrated without affecting system operation. Additionally, the results obtained can identify the factors that limit integration in their systems and provide relevant information for future investments.

To increase HC and maximize the safe integration of DER in PDS, various techniques have been proposed [6–9]. Among these, reactive power control has proven to be highly effective, including control through devices such as distribution static synchronous compensator (D-STATCOM) [4]. D-STATCOMs are devices based on power electronic converters that provide dynamic reactive power compensation, enabling more precise voltage regulation in PDS. Unlike traditional compensators, D-STATCOMs can quickly respond to changes in the network, adjusting their injection or absorption of reactive power in real-time [10]. This enhances system robustness and allows the grid to accommodate higher levels of DER without compromising supply quality.

On the other hand, distribution systems reconfiguration (DSR) is an effective technique for better managing loads and improving the system's operating conditions. The DSR problem involves modifying the network topology by opening and closing switches, allowing for the redistribution of currents among different branches of the system. This strategy optimizes the use of existing infrastructure, alleviates overloads, and reduces network losses. Therefore, due to its benefits, DSR has also been proposed as a method to increase HC in PDS [11].

Thus, the HC in PDS was evaluated in this work, defining a methodology and performance indices to determine the maximum allowable DER integration. Additionally, the impact of advanced reactive power control, such as D-STATCOM devices, on the HC of DER was examined. The effect of another well-known and widely used technique, DSR, was also assessed. Finally, the simultaneous use of both techniques was proposed, and their impact was evaluated in PDS with high DER penetration. All models presented are based on linear power flow, making them mixed-integer linear programming (MILP) models, which can be solved using commercial software such as IBM-CPLEX.

1.1 General Objective

Implement a methodology to calculate HC in PDS and evaluate solutions based on MILP models to increase it, considering a well-studied and widely applied technique such as DSR, as well as a modern approach that incorporates new technologies, such as FACTS devices, particularly D-STATCOM devices.

1.2 Specific Objectives

- Conduct a literature review on HC, its calculation methods, limitations, and approaches to enhance it in PDS. Additionally, review the location of D-STATCOM devices in PDS and the techniques to address the DSR problem.
- Calculate the HC of DER in PDS by selecting a calculation method for its evaluation.
- Evaluate the impact of integrating D-STATCOM devices in PDS with high DER penetration.
- Implement a solution for the DSR problem in PDS to improve overall system performance in the presence of DER.
- Propose a combined model for the optimal integration of D-STATCOMs and DSR, aimed at maximizing performance indices in the presence of high DER penetration.
- Validate the proposed models and techniques using benchmark systems available in the specialized literature.

1.3 Relevance and Contribution

This work presents a methodology for evaluating the HC of DER in PDS, including mathematical models to assess the impact of D-STATCOM devices and DSR in PDS with high DER integration. Among the models detailed in Chapter 4, the formulation for the placement of D-STATCOM devices in PDS is notable for its mixed-integer linear nature, a type of model not encountered in the specialized literature. Moreover, the objective function incorporates a factor aimed at mitigating one of the primary challenges of DER integration: overvoltages. The results contribute to efforts toward achieving the UN SDGs by ensuring the secure integration of DER into PDS. In addition, the analytical tools described in this work assist DSOs and planners in optimizing the incorporation of DER, particularly renewable sources, into existing PDS.

1.4 Document Structure

In this section, the organization of the document is described, outlining the chapters and their content as follows:

- **Chapter 2 - Hosting Capacity:** This chapter highlights the importance of HC, as well as the techniques used for its evaluation and enhancement.
- **Chapter 3 - Distribution Static Compensator Devices:** This chapter describes FACTS devices in general, providing a more detailed description of D-STATCOM devices. Additionally, a review of the planning of PDS considering D-STATCOM devices is conducted.
- **Chapter 4 - Distribution Systems Reconfiguration:** This chapter explains the DSR problem as well as the techniques used to address it.
- **Chapter 5 - Mathematical Models:** This chapter presents the mathematical models of power flow in a radial PDS, the optimal placement and sizing of D-STATCOM devices, and the DSR problem. All models are formulated as a MILP model.
- **Chapter 6 - Test and Results:** This chapter describes the proposed methodology and presents the results obtained, along with the discussions on its application using the models described in Chapter 4.
- **Chapter 7 - Conclusions:** This chapter contains the conclusions drawn from this work.

2 HOSTING CAPACITY

Hosting capacity is a concept that has existed since the initial implementation of DER in power systems. In 2004, as part of the EU-DEEP project (EUropean Distributed EnErgy Partnership), HC was defined as an indicator of the acceptable level of penetration of DER under given circumstances [12]. Likewise, EPRI (Electric Power Research Institute) defines HC as the amount of DER that can be accommodated without adversely impacting power quality or reliability under existing control configurations and without requiring infrastructure upgrades [5]. Although it is a topic of great importance, various terms have been used to refer to HC, and in fact, there is no standard for its definition, evaluation, or calculation.

Figure 2 shows a basic representation of the HC concept. Here, the x-axis represents the integration of DER, and the y-axis represents an index that measures system performance, such as the maximum voltage at one or more buses, the maximum current in one or more lines, or the power quality within the system. In this way, by defining a maximum limit (red dashed line), it is possible to calculate the index as a function of DER integration (blue line) to determine the HC (green dashed line) at the point where the index reaches its maximum allowable limit.

Figure 2 – Basic representation of HC

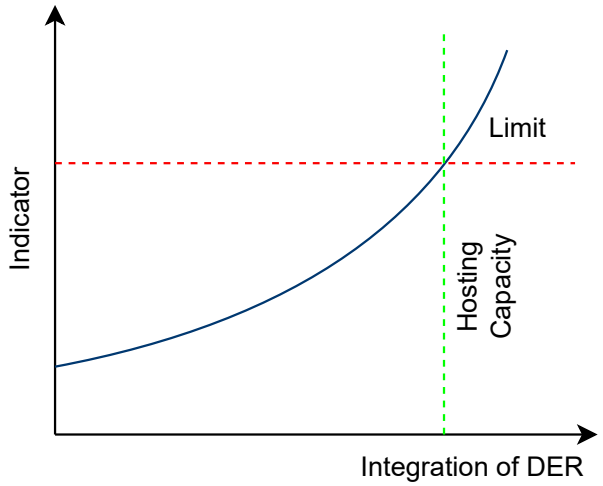

Source: Created by the author

As can also be observed in Figure 2, HC is highly dependent on the chosen indicator. In practice, more than one indicator can be selected, and the resulting HC would be the minimum value among all those found. However, considering a large number of

factors that impact HC can be challenging, if not impossible [13]. Table 1 presents some of the factors that most significantly affect the assessment of HC in a PDS.

Table 1 – Impact factors that most affect HC

Related to	**HC impact factor**
DER	Location
	Type or technology
	Smart inverter
	Communication and control
PDS	Voltage control scheme
	Configuration / Reconfiguration
	Load level
	Phasing information
	Protection system design

Source: Adapted from [13]

The assessment of HC is a complex process that combines input information, such as models and historical operation data, a methodology, impact factors, and a specific purpose. Therefore, HC is not a single value, and the result depends on the chosen conditions [14]. Thus, HC results are estimates and have limitations, making it necessary to consider the specific application to understand these limitations and ensure a satisfactory outcome. Additionally, HC is a value that can change over time, which makes it necessary to perform the calculation regularly using the same considerations in order to obtain the updated DER value that the system can support.

HC has many applications, including but not limited to those mentioned in [14]: interconnection, planning, and mapping. For interconnection, an engineer gains prior knowledge of how much DER integration a specific location can support, serving as an indicator without replacing detailed interconnection studies. Planning studies consider a planning horizon in which DER integration in PDS may need to be addressed. Therefore, a HC study that considers DER integration at multiple locations simultaneously can identify feeders that may benefit from new investments. Finally, mapping has become a solution to inform DER investors using HC results. Figure 3 shows an example of this type of application, where attractive system locations can be identified, and by selecting a specific location, its associated constraints can be observed.

2.1 Importance of HC

The UN SDG are a set of global objectives aimed at addressing various social, economic, and environmental challenges to achieve a more sustainable future by 2030 [1]. Among these objectives, renewable energy in the electric sector is given special recognition for its role in mitigating the effects of climate change, while also contributing to the decentralization, diversification, and democratization of the sector. In line with these objectives, governments have promoted the integration of non-conventional renewable en-

Figure 3 – Example of mapping using HC results

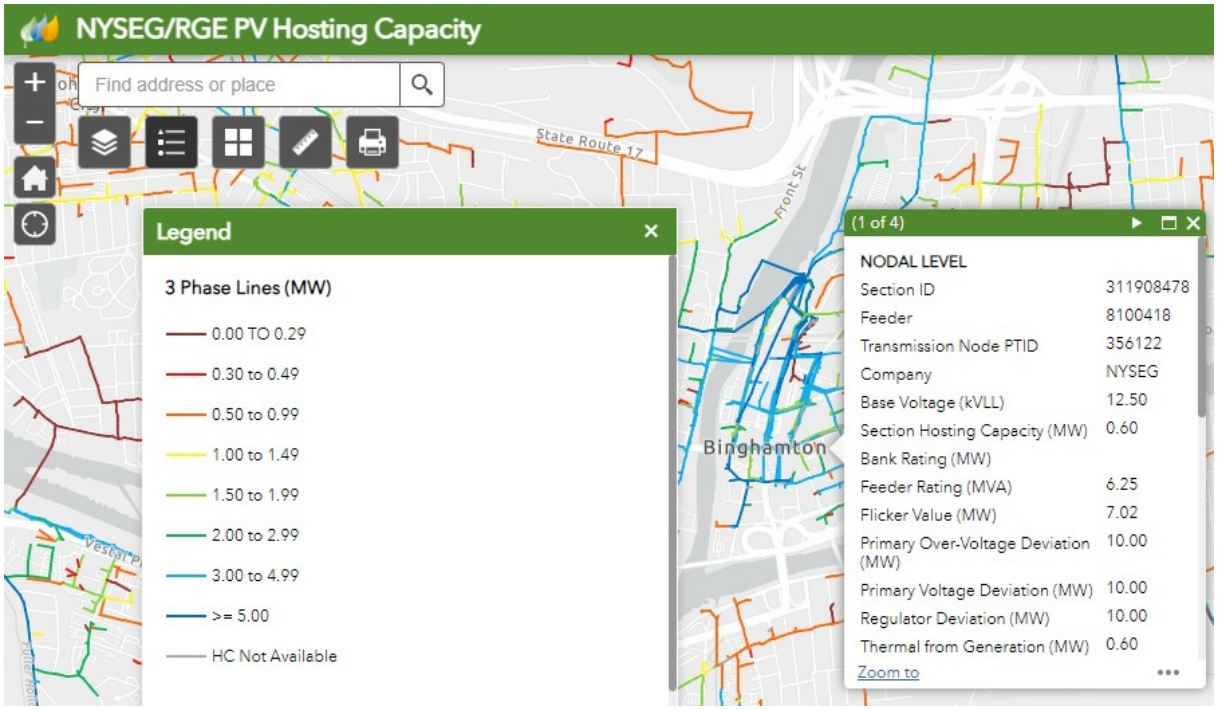

Source: [15]

ergy sources (NCRES). In Colombia, the Ministry of Mines and Energy (MME) issued Law 1715 of 2014 with the aim of regulating and promoting the integration of NCRES into the Colombian electrical system [16]. In Brazil, with legal frameworks such as Law 14300 of 2022 [17], the country has been actively investing in NCRES, including wind and PV solar generation, with PV solar power plants, rooftop solar installations, and community solar initiatives, aiming to diversify its energy matrix and reduce its dependence on fossil fuels. In 2023, PV solar generation plants increased their installed capacity by approximately 55% compared to 2022, reaching a total of 37,843 GW [3].

However, in the case of PDS, excessive integration of renewable DER can negatively impact system performance, causing issues such as voltage problems, harmonics, or protection malfunctions [18]. For this reason, it is necessary to assess the system's capacity to integrate new DER without exceeding operational limits. This situation has created a conflict between DER investors and DSOs, as investors seek to increase DER integration into the system, while DSOs aim to maintain system conditions within operational limits [4].

In this context, where the interests of achieving the UN SDG, investors' goals of increasing DER integration, and the objectives of DSOs to maintain PDS performance intersect, a clear and fair solution is needed to decide when to accept or reject the connection of new DER. HC offers a solution by providing clear performance indices as evaluation criteria for DER integration. Thus, under given conditions, it is possible to establish a technical and measurable criterion for decision-making.

2.2 Assessment of HC

The CIGRÉ (Conseil International des Grands Réseaux Électriques) Working Group C6.24 studied the HC limits of PDS, as well as methods to increase it. To achieve this, the group evaluated practices adopted by DSOs in various countries across Africa, Asia, Europe, and North America, which developed methodologies and rules of thumb to assess HC quickly and reliably without the need for detailed studies [19]. These methodologies have been employed, primarily, due to the pressure on DSOs to meet the demand for grid access while simultaneously ensuring that the connection of new DER does not violate the system's operational limits. As a result of the study, it was found that all DSOs assess whether a new DER connection causes a violation of the capacity limits in network elements. In some cases, HC is expressed as a percentage of the capacity of the transformer, feeder, or circuit breaker. This limit is sometimes further constrained by considering the system's N-1 contingency condition. Additionally, another common requirement is that the short-circuit capacity remains below the design threshold, limiting the DER contribution to fault currents. Other practices identified include limiting voltage rise and the increase in losses due to DER connection.

On the other hand, in [13] EPRI presented four methods for evaluating HC, as well as common misconceptions, their advantages, disadvantages, and recommendations. The methods presented are known in the industry as: Stochastic, Streamlined, Iterative, and Hybrid (DRIVE). The following describes each of these methods.

2.2.1 Stochastic

This approach begins with a base case of the system, followed by the generation of a representative set of cases by adding DER of varying sizes at different locations. The objective is to identify the range of impacts that DER integration may have on the system. However, the stochastic method does not allow for the identification of impacts at a specific location of interest, as DER are placed in multiple locations simultaneously. Figure 4 shows an example of the results obtained using this approach. Here, three regions are observed: one where all cases are acceptable regardless of the location, another where acceptability depends on the location, and a third where all cases are unacceptable regardless of the location.

2.2.2 Streamlined

This method was developed with the recognition that modeling all DER integration scenarios requires significant resources and simulation time. It applies a set of equations and algorithms to evaluate the impact of DER at each system node. Since it neither models nor simulates directly, this method reduces the time needed to assess a large number of scenarios. In this case, only one location is considered at a time, making it

Figure 4 – Example of the results from applying the stochastic method

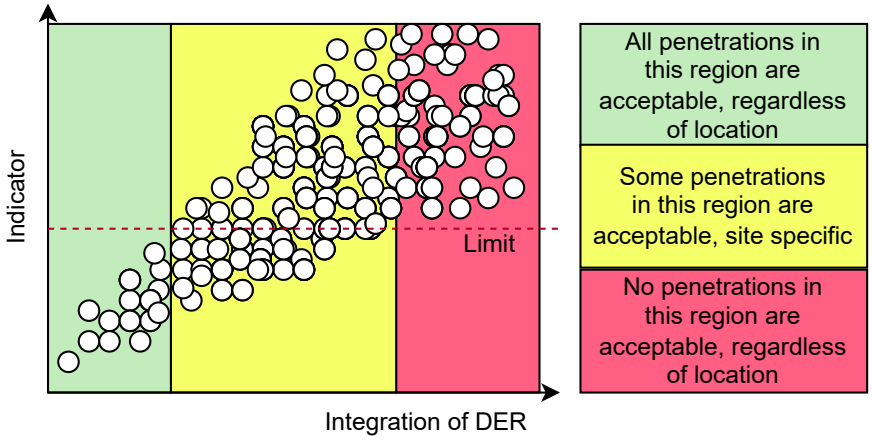

Source: Adapted from [13]

impossible to identify the impact of aggregated DER. The detailed description of this method can be found in PG&E's (Pacific Gas and Electric Company) Demonstration Projects A and B Final Reports, December 27, 2016 [13].

2.2.3 Iterative

The iterative method consists of gradually increasing DER integration, typically considering a single location, until an operational limit is breached. Figure 5 illustrates the basic process of this approach.

Since the iterative process is applied to each of the considered locations, the processing time can be lengthy. However, modifications can be made to the PDS simulation methods, as well as to the DER integration search algorithm, to improve computational efficiency.

2.2.4 Hybrid (DRIVE)

The Distribution Resource Integration and Value Estimation (DRIVE) HC method is the successor to the stochastic and detailed methods previously developed by EPRI. The DRIVE method involves selecting a number of cases to characterize the system and performing calculations to determine the impact of DER. However, the method has also evolved towards more detailed studies and continues to do so. In practice, this method has proven to be a streamlined approach while achieving results comparable to a detailed analysis [13]. For more information on this EPRI method, see [20].

Figure 5 – Basic diagram of the iterative method

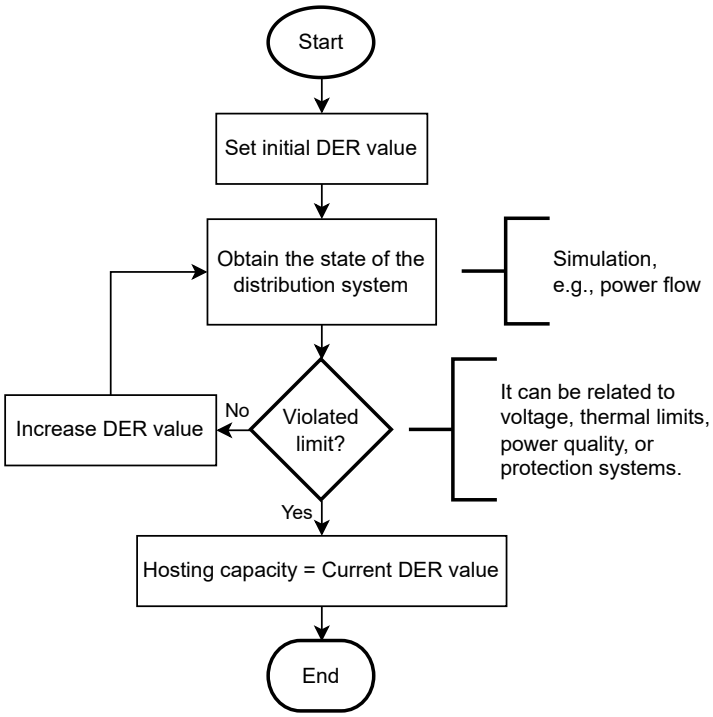

Source: Created by the author

2.3 Techniques to Increase HC

The main issues that limit HC in PDS are overvoltages, system overloads and power losses, power quality problems, and electrical protections [4]. Various techniques have been presented in the literature to address these issues and increase HC [6–9].

Overvoltages are one of the most common problem and most studied when evaluating HC. Reactive power control is an effective option for addressing this limitation in PDS, including techniques such as static var compensator (SVC) or D-STATCOM devices, as well as control through smart inverters in DER [4]. Additionally, other techniques such as on-load tap changers (OLTC) have also been used. In [6], the authors evaluated various voltage control techniques to increase HC in PDS. The techniques used were OLTC, inverter reactive power control, network reinforcement, and hybrid approaches.

Other limitations of HC include equipment capacities and system losses, which means that high DER integration can create issues with these operational limits. The authors in [7] evaluated the optimal conductor selection technique to increase HC, considering thermal limits and voltage limits as performance indices. Additionally, in the proposed optimization model, the objective function aimed to minimize the cost of losses and the investment cost.

The growing presence of non-linear loads in PDS, combined with the integration of DER through power electronics-based devices, can create power quality issues that limit HC. To address such problems, [8] presented the design of a passive filter aimed at increasing the harmonic-constrained HC in a test system.

Although less studied in the specialized literature, but no less important, the high integration of DER in PDS also has adverse effects on protection systems. In particular, changes in the magnitude and direction of short-circuit currents can cause protection systems to fail. To avoid the costly and complex task of modifying a system's protection scheme, [9] presented a method for the optimal placement of DER aimed at maximizing the system's HC without altering the original protection scheme.

In addition to the techniques mentioned earlier, there are other methods to increase HC by considering multiple performance indices. For example, DSR can be used to address network imbalances, voltage issues, and overloads. Another example is D-STATCOM devices, which can correct power quality issues, reduce losses, and regulate voltage when equipped with the appropriate control system.

3 TECHNIQUES APPLIED IN THIS WORK

This chapter describes the techniques applied in this study to increase HC and improve the operational conditions of PDS: D-STATCOMs and reconfiguration. Additionally, a review of the solution methods employed in the specialized literature for their implementation is presented.

3.1 Distribution Static Compensator Devices

In this section, FACTS devices are described in general, including their historical development and classification, with a more detailed explanation of D-STATCOM devices. Additionally, a review of the application of D-STATCOM devices in PDS planning is presented.

3.1.1 FACTS Devices

Flexible AC Transmission Systems (FACTS) devices are a category of equipment used in electrical power transmission to enhance the capacity and flexibility of power grids [21]. The concept of "Custom Power" or "distribution FACTS" (D-FACTS) refers to FACTS devices installed in PDS. Despite sharing the same base technology, they serve different purposes and have distinct economic justifications [22].

FACTS are electronic devices that enable fast and dynamic control of various parameters in the electric power transmission system, such as power flow, voltage, and system stability. These devices utilize power electronics components such as thyristors, high-power transistors, and static converters. The main benefits of FACTS are [23]:

- **Increased Transmission Capacity:** FACTS can increase the transmission capacity of an existing line without the need to build new infrastructure, which is a significant advantage in terms of cost and time.
- **Improvement of System Stability:** FACTS help improve power system stability, both transient and steady-state stability, by providing a rapid response to disturbances.
- **Control of Power Flow:** FACTS enable precise control of power flow in transmission lines, which helps optimize network utilization and prevent overloads in certain lines.
- **Voltage Regulation:** FACTS can maintain voltage levels within desired limits, improving power quality and reducing losses.

- **Integration of Renewable Energies:** FACTS facilitate the integration of renewable energy sources into the electrical grid, which can be intermittent and variable.

All these benefits optimize the grid by enhancing the utilization of existing infrastructure, thereby delaying or eliminating the need to construct new transmission lines. They also help manage congestion in the network, facilitating more efficient and reliable operations. Additionally, they reduce voltage fluctuations and improve the quality of the electrical supply.

On the other hand, FACTS devices present some challenges, such as their initial costs and technical complexity. The implementation of FACTS devices can be expensive, although it is offset by long-term benefits. Moreover, their implementation and maintenance require an advanced understanding of power electronics and electrical system dynamics [24].

3.1.1.1 History of FACTS Devices

Its origin can be traced back to the exponential increase in electricity demand following World War II, driven by industrial growth and increased electrification [25]. Electrical networks had to be expanded and upgraded to handle greater loads and transmit electricity over long distances. However, with the growing need to expand the networks, significant challenges arose, including limitations in transmission capacity and stability issues [26].

During the 1970s, the first reactive power control devices were developed, such as thyristor-switched capacitors (TSCs) and thyristor-switched reactors (TSRs) [27]. These devices allowed for basic control over voltage and reactive power flow, although their capacity was limited, they laid the groundwork for future developments. By the end of this decade, engineers began to explore the idea of using power electronics devices for more precise and dynamic control of electrical system parameters.

In the 1980s, power semiconductor technology advanced rapidly, enabling the development of more efficient and robust devices. The SVC was the first device developed and commercially implemented for applications in transmission systems [28]. Utilizing thyristor-controlled reactors and capacitors (TCRs and TCCs), SVCs provided rapid voltage regulation and improved grid stability, especially under fluctuating load conditions.

The increasing complexity of electrical networks and the need for greater flexibility led to the development of the first concepts of FACTS. In 1988, engineer Narain Hingorani of EPRI coined the term “FACTS” and outlined his vision for more flexible transmission systems using emerging power electronics technology [29]. Similarly, in 1995, he introduced the concept of “Custom Power” referring to power electronics devices applied to PDS, focused on reliability and power quality [22]. His idea was to enable dynamic,

real-time control of power flow, something that previous technologies could not achieve efficiently.

The development of the static synchronous compensator (STATCOM) marked a significant advancement in the field of reactive power compensation. Utilizing voltage source converters (VSC) based on high-power transistors, STATCOMs provided an even faster response and more precise control of reactive power compared to SVCs. This was a historic milestone in the FACTS initiative promoted by EPRI, further enhancing the stability and capacity of the grid [30]. The first commercial installation of a STATCOM took place in 1996 at the Sullivan substation in Tennessee, USA.

The unified power flow controller (UPFC) was developed as a combination of a STATCOM and a series static synchronous compensator (SSSC). This device could simultaneously control both active and reactive power flow in a transmission line, offering unprecedented flexibility. The first UPFC was installed in 1998 in Inez, Kentucky, providing comprehensive control capability over the power flow in the transmission line [31].

With globalization and the interconnection of electrical networks, the implementation of FACTS devices expanded worldwide. Thyristor-controlled series capacitors (TCSCs) [32,33] and thyristor-controlled phase shifters (TCPSs) [34] were widely implemented to enhance the stability and transmission capacity of electrical networks.

On the other hand, the increasing integration of NCRES, such as solar and wind, created new challenges for the stability and management of the electrical grid [35]. FACTS devices played a crucial role in adapting the networks to these intermittent sources, providing voltage regulation and dynamic stability support. Likewise, advances in semiconductor materials and digital control technologies continued to enhance the efficiency and capability of FACTS devices [36]. Furthermore, the growing concern for sustainability and the need to reduce carbon emissions further propelled the adoption of these technologies to optimize the use of existing infrastructure and facilitate the transition to a smarter and more resilient electrical grid.

The future of FACTS devices is closely tied to the evolution of the electrical grid towards smarter and more flexible systems. The integration of artificial intelligence and machine learning in the control of FACTS devices promises to further enhance the efficiency and responsiveness of electrical networks [37]. Additionally, the growing digitalization and the implementation of new technologies will enable more precise control and greater optimization of the grid [38].

3.1.1.2 Types of FACTS Devices

Figure 6 presents the classification of FACTS devices. As mentioned earlier, there are devices designed for transmission applications (FACTS) and for distribution applica-

tions (D-FACTS). Both are similar in terms of technology, with power electronics being the technical foundation in both cases. However, their performance objectives differ. FACTS are used to address issues in the transmission system, including increasing efficiency, providing flexible demand control, improving voltage stability, controlling power flow, and reducing energy losses [23]. D-FACTS are used to mitigate issues in the PDS, particularly to improve system reliability and resolve power quality problems, such as power factor, voltage profile, and voltage stability [22].

On the other hand, FACTS devices can be classified into two generations based on their technological characteristics [39]. The first generation uses thyristors, while the second generation employs VSC as controlled switches. The second generation offers better performance compared to the first, as VSC-based controllers do not encounter the resonance issues faced by thyristor-based controllers.

Similarly, FACTS or D-FACTS devices can be classified by their connection mode. The types of devices include series-connected, shunt-connected, combined series-series, and combined shunt-series configurations [40].

Figure 6 – Classification of FACTS devices

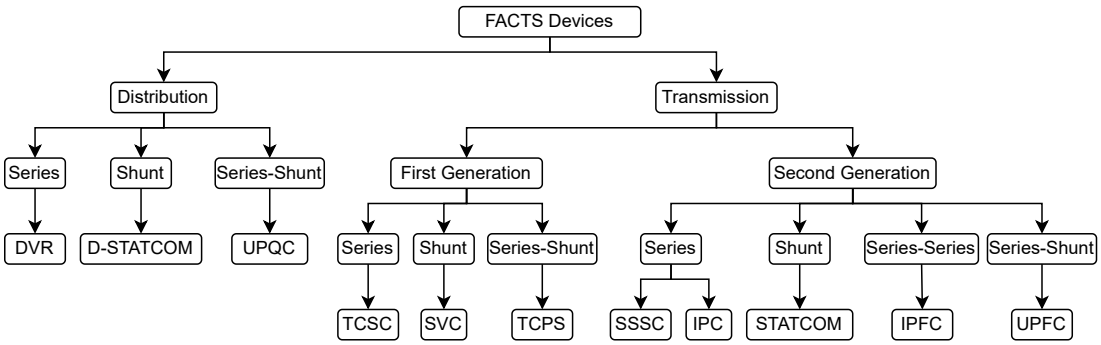

Source: Created by the author

3.1.1.3 D-STATCOM

The static synchronous compensator is a shunt-connected compensation device capable of generating and/or absorbing reactive power, with its output adjustable to maintain control of specific parameters in the power system to which it is connected [10]. This device typically consists of VSC and a set of converter controls that adjust the output voltage of the STATCOM, as shown in Figure 7.

The term “static” is used to indicate that it is based on solid-state power electronic devices without any moving or rotating components. The terms “synchronous” and “compensator” indicate that it is analogous to an ideal synchronous machine that generates a balanced set of three-phase sinusoidal voltages at a fundamental frequency

Figure 7 – D-STATCOM schematic

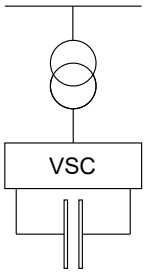

Source: Created by the author

A D-STATCOM is structurally identical to a STATCOM, with differences in its objectives and control techniques. The initial application of a D-STATCOM was for voltage control at the fundamental frequency, providing a rapid response even under reduced voltage conditions.

The advantages of using a D-STATCOM include limiting overvoltages caused by capacitor switching, reducing voltage drops due to common feeder faults, and controlling voltage fluctuations caused by load variations [41]. As a result, the need for switching operations in other mechanical devices is reduced, aiding in maintenance. Additionally, it increases the system's maximum loadability, for example, by enhancing the maximum amount of induction motor load that can remain stable during a disturbance.

3.1.2 D-STATCOM in PDS Planning

The planning of PDS has experienced significant transformations in recent years. While the traditional objectives of improving voltage profile, reducing power losses, avoiding line overloads, and increasing reliability and power quality remain, new conditions have emerged that influence the planning process [42]. The use of multiple DER in PDS adds uncertainty to operations due to the variability of primary energy sources. Furthermore, PDS, which have historically operated in a radial manner with unidirectional power flow, now face the possibility of bidirectional power flows, creating new operational challenges. Additionally, the construction of new lines has become increasingly constrained due to the high associated costs and environmental and space restrictions in large consumption centers. Consequently, the planning of PDS must focus on optimizing the use of existing assets.

To address the variability problem in DER and optimize the use of existing assets in PDS, FACTS devices emerge as an attractive solution. Given the high complexity of the technology used in these devices, various studies are necessary to determine whether a FACTS device can resolve an identified issue in the network [43]. Typically, the follow-

ing studies are considered: steady-state power flow, transient stability, electromagnetic transients, harmonic studies, and short-circuit fault current calculations.

One of the most efficient devices to tackle these challenges in PDS is the D-STATCOM. The D-STATCOM is a shunt compensation device capable of generating or absorbing reactive power as needed by the network [44]. The advantages of using a D-STATCOM include limiting overvoltages caused by capacitor switching, reducing voltage drops due to common faults in feeders, and controlling voltage fluctuations resulting from load variations [41]. Due to the cost and impact that D-STATCOM devices can have on the network, their location and sizing must be carefully planned to ensure maximum benefit. Various techniques have been proposed in the specialized literature to address the problem of placement and sizing D-STATCOM devices in PDS. These techniques can be classified into: 1. Analytical techniques, 2. Metaheuristic techniques, 3. Hybrid techniques, and 4. Classical optimization techniques.

3.1.2.1 Analytical Techniques

Analytical techniques are straightforward and easy-to-implement methods that provide acceptable solutions [45]. Due to their general approach to the problem, they lack consideration for the nonlinearities and complexities that such problems may present. Typically, for D-STATCOM devices, they are used to determine the optimal location. In [46], the problem of locating a D-STATCOM device in PDS was addressed. The power stability index (PSI) and the power loss index (PLI) were used to select the best location. In this case, the D-STATCOM device was not sized. Tests were conducted on the IEEE 12-bus radial system.

In [47], several analytical approaches were proposed to determine the optimal location of D-STATCOM devices. Both normal load and load increase were taken into account, as well as different load profiles for seasons, such as summer and winter. To size the device, its capacity was varied from a minimum value up to the reactive power capacity of the feeder in constant steps to achieve the minimum system losses. The results obtained for each of the indices considered were compared using a 38-bus meshed distribution system.

A voltage stability indicator (VSI) was used to identify the weakest bus in [48]. A D-STATCOM device was located at the identified bus to maintain the voltage at 1 pu, thus having no limits on the device's capacity. The index used allows for the selection of the bus as the location for a D-STATCOM device to improve the system's voltage profile. The system used for testing was the IEEE 33-bus radial distribution system.

The same VSI used in [48] was employed to determine the location of a D-STATCOM device in [49]. The analysis was conducted on an unbalanced radial distribution system of 25 buses, considering low, medium, and high load scenarios. To size

the device, similar to [47], the device's capacity was varied from a minimum value up to the reactive load capacity of the feeder in constant increments to minimize the system losses. Additionally, the impact of the D-STATCOM device on the cost of energy losses was analyzed.

3.1.2.2 Metaheuristic Techniques

Metaheuristic techniques are methods, often inspired by nature, used to solve highly complex problems. Their main advantage is the high versatility they offer, being able to address problems with multiple objectives and nonlinearities, providing more than acceptable solutions when correctly implemented [40]. On the other hand, their disadvantage is that they do not guarantee a global optimal solution; that is, they may converge to a local optimum or even fail to converge to an acceptable solution. A gravitational search algorithm (GSA) for determining the optimal location and sizing of D-STATCOMs was proposed in [50]. The optimization objectives were to reduce voltage deviation, minimize energy losses, and maximize annual energy savings. Tests were conducted on the IEEE radial distribution systems of 33 and 69 buses. Additionally, the effectiveness of the proposed algorithm was compared with other existing algorithms in the literature and some analytical techniques.

Another type of algorithm used for the placement and sizing of D-STATCOM is genetic algorithms (GAs). In [51], a non-dominated sorting genetic algorithm-II (NSGA-II) was implemented for the location and sizing of D-STATCOMs. The NSGA-II creates a set of solutions known as the Pareto front, where the best solution is identified using a fuzzy decision making engine. Uncertainty in the loads was considered using Monte Carlo simulation technique. The proposed methodology was tested on the IEEE radial distribution system of 33 buses and a 94-bus distribution system.

The authors in [52] implemented a new metaheuristic tool called the lightning search algorithm (LSA) for the simultaneous location and sizing of DG and D-STATCOMs. The algorithm was tested on the IEEE radial distribution systems of 33 and 69 buses. The dimensions of the installed devices were identified for different load percentages in the system. Thus, a curve fitting was performed on the obtained results to formulate an equation that models the dimension as a function of changes in load percentage.

In [53], an improved particle swarm optimization algorithm based on success rate (IPSO-SR) was presented for the optimal location of DG or D-STATCOM. The optimization function considered a combination of technical, economic, and social objectives. Comparative studies were conducted with other evolutionary algorithms in the IEEE distribution systems of 33 and 69 buses to validate the effectiveness of the proposed algorithm. Additionally, a comparison was made between the optimal locations of DG as an active power source and D-STATCOM as a reactive power source.

In addition to those mentioned, several other well-established algorithms have been applied for the placement and sizing of D-STATCOMs, including the vortex search algorithm (VSA) [54], the generalized normal distribution optimizer (GNDO) [55], and the discrete version of the sine-cosine algorithm (SCA) [56].

3.1.2.3 Hybrid Techniques

Hybrid techniques are methods that combine the strengths of both analytical and metaheuristic approaches [57]. Some hybrid techniques utilize analytical methods to reduce the search space and decrease the computation time of a metaheuristic algorithm. Another approach involves a two-stage process. In the first stage, the location is determined using an analytical technique, while in the second stage, the sizing is performed using a metaheuristic technique. A hybrid approach was proposed in [58] to determine the location and size of DG and D-STATCOM. The loss sensitivity factor (LSF) was used for the location, identifying the optimal locations concerning active and reactive power. For sizing, the bacterial foraging optimization algorithm (BFOA) was proposed. The method was validated through tests on IEEE radial distribution systems of 33 and 119 buses, placing DG and D-STATCOM in various scenarios, both separately and simultaneously.

Another hybrid methodology involving the LSF for the location of D-STATCOMs was presented in [59] to identify the optimal locations. The sizing and selection of the number of devices to be installed were carried out using a particle swarm optimization (PSO) algorithm, aiming to minimize total energy losses, voltage deviations, and overloaded lines. The methodology was validated on the IEEE radial distribution system of 33 buses, considering different levels of DG penetration.

In [60], a hybrid analytical and metaheuristic method was proposed for the optimal location and sizing of both DG and D-STATCOM. The VSI was utilized to determine the best location, while the sizing was performed using a SCA. The optimization objective was to minimize active power losses in the system. The proposed method was applied to the IEEE distribution systems of 12 and 69 buses, comparing its effectiveness with other methods available in the literature.

Another hybrid analytical-metaheuristic method for identifying the optimal location and sizing of one or more D-STATCOM devices was presented in [61]. In this case, a metric called the voltage stability factor (VSF) was utilized to determine the optimal locations for one or more devices. For sizing, a metaheuristic algorithm inspired by the behavior of bats was implemented. The primary optimization objective was defined as minimizing the total active power losses in the system. The performance of the method was tested on the IEEE radial distribution system of 33 buses, under low, medium, and high load conditions. Additionally, the obtained results were compared with other existing analytical techniques and evolutionary algorithms.

3.1.2.4 Classical Optimization Techniques

Classical optimization techniques are methods that allow for finding the global optimum of the problem. Depending on the complexity of the model, different levels of computational effort may be required. Typically, this type of approach is employed with the aim of ensuring that the model representing the problem is linear in nature. The main disadvantage is that for very complex problems with numerous variables and constraints, the computational time can be very high. In the case of locating and sizing FACTS devices, such approaches have not been as extensively explored compared to others. Nevertheless, D-STATCOM devices have been the most commonly selected for this type of analysis.

Among the research articles found, a mixed-integer nonlinear programming model (MINLP) for the optimal location and sizing of D-STATCOM devices was presented in [62]. The exact nonlinear model was separated into two stages: one for location and the other for sizing. The first stage was conducted using a mixed-integer quadratic convex approximation (MIQC), while for sizing, the initial model was transformed into an equivalent second-order cone programming model. The resulting models were solved using the Gurobi solver on radial distribution systems of 33 and 69 buses, considering a daily active and reactive demand profile.

A similar approach for solving the location and sizing problem of D-STATCOM devices in PDS was proposed in [63]. As in [62], the location of the devices was performed using a MIQC approximation. For sizing, with the solution from the first stage, the original MINLP model results in a nonlinear programming (NLP) model. The model from the first stage was solved using CVX and the Gurobi solver, while the second stage was solved using GAMS and the BONMIN solver. The proposed methodology was applied to the 33-bus distribution system considering both radial and meshed operation, as well as daily load profiles for residential, industrial, and commercial sectors.

A mixed-integer second-order cone programming (MI-SOCP) model was proposed in [64] to address the location and sizing problem of D-STATCOM devices in PDS. The proposed model was applied to the 33-bus radial distribution system, considering active and reactive demand profiles for a day of operation. The optimization objective was to minimize the cost of energy losses and the investment cost in D-STATCOM devices. Several analyses were conducted, such as varying the maximum number of devices available for installation and considering different weights for the two components of the objective function.

The model proposed in [64] was extended to consider converter losses and the probability of different generation-demand scenarios in [65]. The proposed model was tested on the modified 33-bus, 69-bus, and 85-bus distribution systems to account for the

integration of distributed PV generation. Similar analyses to those studied in [64] were conducted.

3.2 Distribution Systems Reconfiguration

PDS have primarily been designed in a radial configuration to simplify their operation. In some cases, to enhance reliability in specific areas, they are designed with meshed structures that include normally open switches [66]. Distribution systems reconfiguration involves modifying the network topology through these switches to achieve certain operational or planning objectives. The primary goal of DSR is to reduce active power losses; however, other objectives, such as improving power quality and reliability, have recently been considered [67]. Additionally, DSR can also be used for service restoration, aiming to maximize the amount of restored load [68].

Figure 8 presents an example of DSR in the 14-bus test system. Initially, the configuration on the left shows branches 8-12, 3-9, and 5-14 as normally open, with losses of 511,43 kW and the respective voltage profile. On the other hand, by closing branches 8-12 and 3-9 and opening branches 6-8 and 7-9, the configuration on the right is obtained, with losses of 466,12 kW and a new voltage profile. It can be observed that simply by modifying the system's topology, it was possible to reduce active power losses and improve the voltage profile, particularly at buses 8 and 9, which were connected to another feeder.

Figure 8 – Example of DSR in a small system

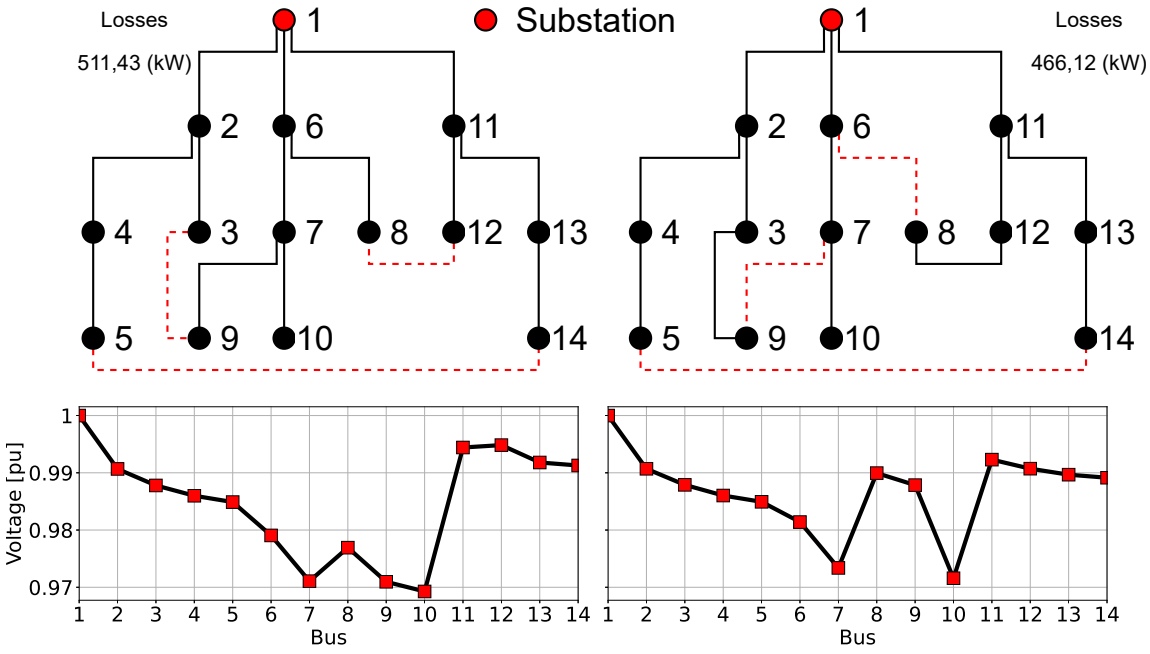

Source: Created by the author

Despite the simplicity of the DSR problem concept, its large search space makes finding a solution very challenging. Considering a system with n switches, the number

of possible configurations is 2^n. Therefore, DSR exhibits an exponential characteristic, and depending on the value of n, it becomes impossible to test all configurations to find the optimal solution [69]. For example, the system in Figure 8 has $2^{16} = 65.536$ possible configurations, assuming that all branches are equipped with switches, which is already a considerable number for a small-sized system.

On the other hand, in a traditional PDS, not all branches are equipped with controlled switches, and DSR is typically approached from a planning perspective. However, the implementation of smart grids and distribution system automation (DSA) allows for dynamic DSR through remotely controlled switches. DSA consists of network monitoring, decision-making algorithms, remotely controlled devices, and a robust communication infrastructure, all of which together enhance the real-time operation of the system [70].

3.2.1 Techniques for Solving the Reconfiguration Problem

DSR is a well-studied technique due to its ability to efficiently improve system conditions. It was initially proposed in [71], where a methodology based on DC power flow for a meshed system was presented, calculating the minimum-loss operating state. To achieve a radial configuration, branches with the lowest currents were opened in an iterative process, minimally perturbing the system's minimum-loss state. The results were demonstrated on several test systems, showcasing the proposal's effectiveness in reducing losses and delaying investments in the PDS.

In [72], an alternative methodology for DSR focusing on system losses was proposed. The methodology starts from a radial configuration and performs the switching of one closed branch and one open branch at a time, aiming to maintain the radial nature of the system. The variation in losses caused by transferring a load to a different feeder is estimated to select the best switch to open. This strategy enabled the execution of DSR without the need for numerous power flow analyses, thereby reducing computational demands.

Based on the work presented in [72], another approach to solve the DSR problem was proposed in [73]. Two new approximate methods for calculating power flow, and consequently the variation in losses due to changes in open and closed branches, were introduced. Reactive power was considered in the calculations, and the methodology was applied both for loss reduction and load balancing. Similarly, following the work presented in [71] but addressing its main drawbacks, a technique to solve the DSR problem was introduced in [74]. The main contributions included the use of a specialized AC power flow method for weakly meshed networks, the consideration of current limits in the branches and voltage limits at the buses, and the calculation of load currents at each iteration, since [71] assumed fixed current sources.

More recently, various metaheuristic techniques have been implemented to solve

the DSR problem. These methods are iterative processes, typically nature-inspired, that explore the search space intelligently. Furthermore, these techniques can be applied to solve any type of optimization problem with the appropriate implementation, making them the most widely used approaches for DSR in the literature. In [75], a GA was presented to solve the DSR problem for the first time, with the optimization objective of minimizing losses, subject to operational constraints such as voltage drop limits and current limits in lines and transformers. The PSO algorithm has also been used to solve the DSR problem. In [76] an improved PSO, which takes into account the history of local optima, was proposed. The objective was to minimize active power losses while maintaining system radiality and satisfying voltage and current constraints. In [77], an ant colony search (ACS) algorithm was presented to solve the DSR problem, another swarm intelligence-based algorithm. In this case, the presence of DER in the system was considered. The objective was to minimize active power losses and a load balancing index, while adhering to the system's operational constraints. Another type of metaheuristic algorithm used to solve the DSR problem is the simulated annealing (SA) algorithm. In [78], an efficient SA algorithm was proposed for the reconfiguration of PDS. The objective was to minimize active power losses while maintaining the system's operational constraints, using the power flow equations presented in [73] to compute the power flow.

Classical optimization techniques have also been used to solve the DSR problem, which offer the primary advantage of guaranteeing the optimal solution, as long as the computational effort remains acceptable. In [79], a convex mixed-integer conic programming (MICP) model and a MILP model were proposed to solve the DSR problem. Both models were validated on various test systems with the objective of minimizing active power losses. Another MILP model was proposed in [80] to address the DSR problem. In this case, the starting point was a MINLP model and two linearization techniques were applied resulting in the proposed model. Additionally, some constraints were introduced to improve the model's performance in terms of computational effort. The resulting model was tested on various systems available in the specialized literature. In [81], a MILP model was presented to solve, in this case, the dynamic DSR problem. The model also considered load demand and DER output variation in an unbalanced three-phase distribution system. The proposed model was validated on a modified version of the 34-bus test system. Furthermore, the DSR can be addressed simultaneously with the placement and sizing of different equipment in the PDS. A MILP model was proposed in [82] to simultaneously solve the reconfiguration and placement of capacitor banks in PDS. The presented model was tested on seven different benchmark systems available in the literature, demonstrating its effectiveness across various types of systems. Likewise, reconfiguration has been applied to increase the HC of PDS. The authors in [11] presented a MINLP model to assess the effectiveness of DSR in enhancing the HC of an active distribution system. Due to the complexity of the problem when considering multiple periods, a methodology

was proposed to reduce the problem size.

In recent years, with the increasing application of machine learning in electrical systems, methods based on reinforcement learning and artificial neural networks have been developed to address the DSR problem. Although they require substantial time and effort for training, once trained, they enable rapid solutions to the DSR problem [70].

4 MATHEMATICAL MODELS

This chapter presents the proposed mathematical models for the development of this dissertation. In the first section, the mathematical model of power flow in radial PDS is introduced, along with the linearizations employed to obtain a MILP model. Next, the necessary modifications to the linear power flow model for the optimal placement of D-STATCOM devices are presented. Following this, the modifications required to account for DSR are described. Finally, a model is proposed to simultaneously solve the problem of DSR and the placement of D-STATCOM devices in radial PDS.

4.1 Power Flow for Radial PDS

Power flow analysis is an essential tool for determining the operating state of power systems, which involves calculating bus voltages and branch currents under a given scenario [83]. Consequently, power flow analysis enables the evaluation of losses and the loadability of system components, such as generators, transformers, and lines. In general, power flow analysis consists of a set of nonlinear equations whose solution requires specialized algorithms, such as the iterative Newton-Raphson method [83] and the sweep method for PDS [84]. In the case of PDS, although meshed structures may exist, their operation is typically radial. This specific characteristic of PDS presents an advantage, as it reduces the complexity of the power flow problem.

4.1.1 Nonlinear Power Flow

The authors in [82] presented a nonlinear power flow model for radial PDS. The presented model includes the following considerations:

- The system is represented by a single-phase equivalent.
- Loads are represented as constant power.
- Only one electrical source (substation) is considered.
- Losses are concentrated at the sending bus.
- The capacitive reactance of the lines is not considered.

Equation (4.1) represents the objective function, which aims to minimize active power losses. Here, R_{ij} is the resistance of branch ij; $I_{ij,t}$ is the current in branch ij during period t; Ω_l is the set of branches; and Ω_t is the set of periods.

Figure 9 – Simplified representation of a distribution system

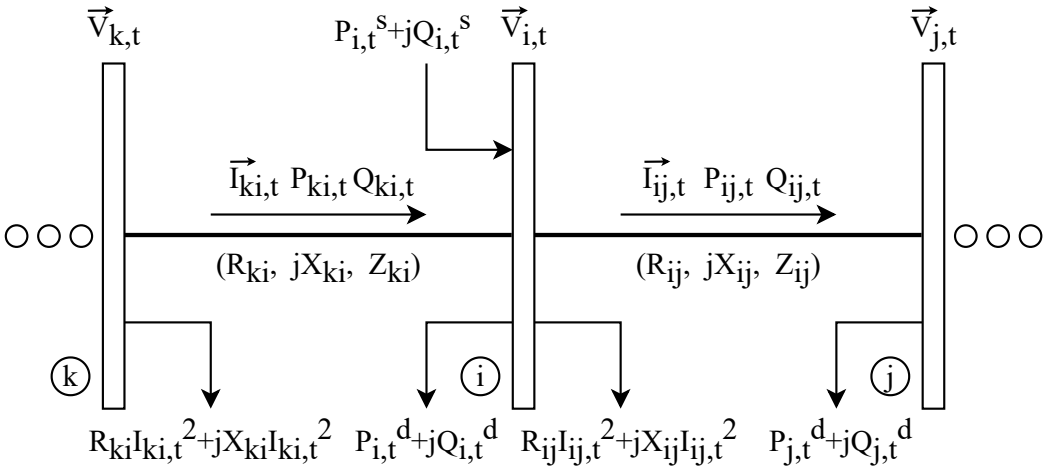

Source: Created by the author

$$Minimize\ f = \sum_{\forall ij \in \Omega_l} \sum_{\forall t \in \Omega_t} R_{ij} I_{ij,t}^2 \tag{4.1}$$

From Figure 9, the active and reactive power balance for each bus in the system is described by Equations (4.2) and (4.3), respectively. $P_{ki,t}$ and $P_{ij,t}$ represent the active power flow in the branches ki and ij during period t, while $Q_{ki,t}$ and $Q_{ij,t}$ represent the reactive power flow in the branches ki and ij during period t, respectively. $P_{i,t}^{s}$ and $Q_{i,t}^{s}$ denote the active and reactive power supplied by the substation at bus i during period t. $P_{i,t}^{d}$ and $Q_{i,t}^{d}$ are the active and reactive power demands at bus i during period t. X_{ij} is the reactance of branch ij. Finally, Ω_b is the set of buses.

$$\sum_{\forall ki \in \Omega_l} P_{ki,t} - \sum_{\forall ij \in \Omega_l} \left(P_{ij,t} + R_{ij} I_{ij,t}^2 \right) + P_{i,t}^{s} = P_{i,t}^{d}; \quad \forall\ i \in \Omega_b,\ \forall\ t \in \Omega_t \tag{4.2}$$

$$\sum_{\forall ki \in \Omega_l} Q_{ki,t} - \sum_{\forall ij \in \Omega_l} \left(Q_{ij,t} + X_{ij} I_{ij,t}^2 \right) + Q_{i,t}^{s} = Q_{i,t}^{d}; \quad \forall\ i \in \Omega_b,\ \forall\ t \in \Omega_t \tag{4.3}$$

Equation (4.4) relates the square of current times the square of voltage and the active and reactive power flows in each branch ij at period t. Here, $V_{j,t}$ represents the voltage at bus j during period t.

$$I_{ij,t}^2 V_{j,t}^2 = P_{ij,t}^2 + Q_{ij,t}^2; \quad \forall\ ij \in \Omega_l,\ \forall\ t \in \Omega_t \tag{4.4}$$

Equations (4.5) and (4.6) represent the limits in period t for the current through branch ij and the voltage at bus i, respectively. $V_{i,t}$ represents the voltage at bus i during period t, $\overline{V}$ and $\underline{V}$ represent the upper and lower voltage limits, while $\overline{I_{ij}}$ is the upper current limit for branch ij.

$$0 \leq I_{ij,t} \leq \overline{I_{ij}}; \quad \forall\ ij \in \Omega_l,\ \forall\ t \in \Omega_t \tag{4.5}$$

$$\underline{V} \leq V_{i,t} \leq \overline{V}; \quad \forall\ i \in \Omega_b,\ \forall\ t \in \Omega_t \tag{4.6}$$

Equation (4.7) models the voltage drop across each branch ij, where Z_{ij} represents the impedance of branch ij and $\overrightarrow{(*)}$ represents a phasor.

$$\overrightarrow{V_{i,t}} - \overrightarrow{V_{j,t}} = \overrightarrow{Z_{ij}}\overrightarrow{I_{ij,t}} = (R_{ij} + jX_{ij})\,\overrightarrow{I_{ij,t}} \tag{4.7}$$

Considering the complex power in branch ij during period t ($\overrightarrow{S_{ij,t}}$), where $()^*$ represents the conjugate:

$$\overrightarrow{S_{ij,t}} = \overrightarrow{V_{j,t}}\overrightarrow{I^*_{ij,t}} \longrightarrow \overrightarrow{I_{ij,t}} = \left(\frac{\overrightarrow{S_{ij,t}}}{\overrightarrow{V_{j,t}}}\right)^* = \left(\frac{P_{ij,t} - jQ_{ij,t}}{\overrightarrow{V^*_{j,t}}}\right) \tag{4.8}$$

Then substituting Equation (4.8) into Equation (4.7) and performing the operations, where θ_{ij} represents the angular difference between the voltage phasors at buses i and j:

$$\begin{aligned}
\overrightarrow{V_{i,t}} - \overrightarrow{V_{j,t}} &= (R_{ij} + jX_{ij})\left(\frac{P_{ij,t} - jQ_{ij,t}}{\overrightarrow{V^*_{j,t}}}\right) \\
\left(\overrightarrow{V_{i,t}} - \overrightarrow{V_{j,t}}\right)\overrightarrow{V^*_{j,t}} &= (R_{ij} + jX_{ij})\,(P_{ij,t} - jQ_{ij,t}) \\
V_{i,t}V_{j,t}\,(\cos\theta_{ij} + j\sin\theta_{ij}) - V^2_{j,t} &= (R_{ij} + jX_{ij})\,(P_{ij,t} - jQ_{ij,t})
\end{aligned} \tag{4.9}$$

Separating the real and imaginary parts:

$$V_{i,t}V_{j,t}\cos\theta_{ij} = V^2_{j,t} + (R_{ij}P_{ij,t} + X_{ij}Q_{ij,t}) \tag{4.10}$$

$$V_{i,t}V_{j,t}\sin\theta_{ij} = (X_{ij}P_{ij,t} - R_{ij}Q_{ij,t}) \tag{4.11}$$

Squaring and summing Equations (4.10) and (4.11):

$$V^2_{i,t}V^2_{j,t} = V^4_{j,t} + 2V^2_{j,t}\,(R_{ij}P_{ij,t} + X_{ij}Q_{ij,t}) + \left(R^2_{ij} + X^2_{ij}\right)\left(P^2_{ij,t} + Q^2_{ij,t}\right) \tag{4.12}$$

Dividing Equation (4.12) by $V_{j,t}^2$:

$$V_{i,t}^2 = V_{j,t}^2 + 2\left(R_{ij}P_{ij,t} + X_{ij}Q_{ij,t}\right) + \frac{\left(R_{ij}^2 + X_{ij}^2\right)\left(P_{ij,t}^2 + Q_{ij,t}^2\right)}{V_{j,t}^2} \tag{4.13}$$

Recalling that:

$$I_{ij,t}^2 = \frac{P_{ij,t}^2 + Q_{ij,t}^2}{V_{j,t}^2}; \qquad Z_{ij}^2 = R_{ij}^2 + X_{ij}^2 \tag{4.14}$$

Substituting (4.14) into (4.13) and rearranging yields Equation (4.15). The constraint given by Equation (4.15), similar to Equation (4.7), models the voltage drop across each branch ij. In this case, the phasors are removed from the optimization model, which in turn eliminates the angles as variables. Consequently, the magnitudes of the voltages are calculated based on the power flow in the branches and their electrical parameters.

$$V_{i,t}^2 - 2\left(R_{ij}P_{ij,t} + X_{ij}Q_{ij,t}\right) - Z_{ij}^2 I_{ij,t}^2 - V_{j,t}^2 = 0; \quad \forall\ ij \in \Omega_l,\ \forall\ t \in \Omega_t \tag{4.15}$$

For completeness, the entire nonlinear power flow model is presented in (4.16).

$$\begin{gathered}
Minimize\ f = \sum_{\forall ij \in \Omega_l} \sum_{\forall t \in \Omega_t} R_{ij} I_{ij,t}^2 \\
\sum_{\forall ki \in \Omega_l} P_{ki,t} - \sum_{\forall ij \in \Omega_l} \left(P_{ij,t} + R_{ij} I_{ij,t}^2\right) + P_{i,t}^s = P_{i,t}^d; \quad \forall\ i \in \Omega_b,\ \forall\ t \in \Omega_t \\
\sum_{\forall ki \in \Omega_l} Q_{ki,t} - \sum_{\forall ij \in \Omega_l} \left(Q_{ij,t} + X_{ij} I_{ij,t}^2\right) + Q_{i,t}^s = Q_{i,t}^d; \quad \forall\ i \in \Omega_b,\ \forall\ t \in \Omega_t \\
V_{i,t}^2 - 2\left(R_{ij}P_{ij,t} + X_{ij}Q_{ij,t}\right) - Z_{ij}^2 I_{ij,t}^2 - V_{j,t}^2 = 0; \quad \forall\ ij \in \Omega_l,\ \forall\ t \in \Omega_t \\
I_{ij,t}^2 V_{j,t}^2 = P_{ij,t}^2 + Q_{ij,t}^2; \quad \forall\ ij \in \Omega_l,\ \forall\ t \in \Omega_t \\
0 \leq I_{ij,t} \leq \overline{I_{ij}}; \quad \forall\ ij \in \Omega_l,\ \forall\ t \in \Omega_t \\
\underline{V} \leq V_{i,t} \leq \overline{V}; \quad \forall\ i \in \Omega_b,\ \forall\ t \in \Omega_t
\end{gathered} \tag{4.16}$$

4.1.2 Linear Power Flow

After presenting the nonlinear power flow, the authors in [82] applied and validated the linearization techniques presented below to obtain a MILP model of power flow in radial PDS.

By examining the model given by (4.16), it is evident that the variables $V_{i,t}$, $V_{j,t}$, and $I_{ij,t}$ only appear squared. Therefore, it is possible to perform the variable substitutions $V_{i,t}^2 = V_{i,t}^{sqr}$, $V_{j,t}^2 = V_{j,t}^{sqr}$, and $I_{ij,t}^2 = I_{ij,t}^{sqr}$, resulting in the model given by (4.17).

$$
\begin{aligned}
&Minimize\ f = \sum_{\forall ij \in \Omega_l} \sum_{\forall t \in \Omega_t} R_{ij} I^{sqr}_{ij,t} \\
&\sum_{\forall ki \in \Omega_l} P_{ki,t} - \sum_{\forall ij \in \Omega_l} \left(P_{ij,t} + R_{ij} I^{sqr}_{ij,t} \right) + P^s_{i,t} = P^d_{i,t}; \quad \forall\ i \in \Omega_b,\ \forall\ t \in \Omega_t \\
&\sum_{\forall ki \in \Omega_l} Q_{ki,t} - \sum_{\forall ij \in \Omega_l} \left(Q_{ij,t} + X_{ij} I^{sqr}_{ij,t} \right) + Q^s_{i,t} = Q^d_{i,t}; \quad \forall\ i \in \Omega_b,\ \forall\ t \in \Omega_t \\
&V^{sqr}_{i,t} - 2\left(R_{ij} P_{ij,t} + X_{ij} Q_{ij,t}\right) - Z^2_{ij} I^{sqr}_{ij,t} - V^{sqr}_{j,t} = 0; \quad \forall\ ij \in \Omega_l,\ \forall\ t \in \Omega_t \\
&I^{sqr}_{ij,t} V^{sqr}_{j,t} = P^2_{ij,t} + Q^2_{ij,t}; \quad \forall\ ij \in \Omega_l,\ \forall\ t \in \Omega_t \\
&0 \leq I^{sqr}_{ij,t} \leq \overline{I_{ij}}^2; \quad \forall\ ij \in \Omega_l,\ \forall\ t \in \Omega_t \\
&\underline{V}^2 \leq V^{sqr}_{i,t} \leq \overline{V}^2; \quad \forall\ i \in \Omega_b,\ \forall\ t \in \Omega_t
\end{aligned}
\tag{4.17}
$$

From Model (4.17), it can be observed that the only source of nonlinearity is equation $I^{sqr}_{ij,t} V^{sqr}_{j,t} = P^2_{ij,t} + Q^2_{ij,t}$, where the left-hand side involves the multiplication of continuous variables, while the right-hand side contains the sum of two continuous variables squared. The left-hand side of this equation can be linearized according to Equations (4.18) through (4.24). Equation (4.18) represents the linearization of the product of variables $V^{sqr}_{j,t}$ and $I^{sqr}_{ij,t}$, where $\overline{\Delta}^V$ is the discretization step, S is the number of discretizations and $P^c_{j,t,s}$ is the power correction used in $V^{sqr}_{j,t} I^{sqr}_{ij,t}$.

$$
I^{sqr}_{ij,t} V^{sqr}_{j,t} = \left(\underline{V}^2 + \frac{1}{2} \overline{\Delta}^V \right) I^{sqr}_{ij,t} + \sum_{s=1}^{S} P^c_{j,t,s} \tag{4.18}
$$

Equation (4.19) specifies the range of possible values for the voltage ($V^{sqr}_{i,t}$) in the proposed linearization. Here, $x^V_{i,t,s}$ is a binary variable used in the discretization of $V^{sqr}_{i,t}$.

$$
\underline{V}^2 + \overline{\Delta}^V \sum_{s=1}^{S} x^V_{i,t,s} \leq V^{sqr}_{i,t} \leq \underline{V}^2 + \overline{\Delta}^V + \overline{\Delta}^V \sum_{s=1}^{S} x^V_{i,t,s}; \quad \forall\ i \in \Omega_b,\ \forall\ t \in \Omega_t \tag{4.19}
$$

Equations (4.20) and (4.21) represent the limit of the power discretization steps and the limits of $P^c_{j,t,s}$, respectively.

$$
0 \leq \overline{\Delta}^V I^{sqr}_{ij,t} - P^c_{j,t,s} \leq \overline{\Delta}^V \overline{I_{ij}}^2 \left(1 - x^V_{j,t,s}\right); \quad \forall\ ij \in \Omega_l,\ \forall\ t \in \Omega_t,\ \forall\ s \in 1...S \tag{4.20}
$$

$$
0 \leq P^c_{j,t,s} \leq \overline{\Delta}^V \overline{I_{ij}}^2 x^V_{j,t,s}; \quad \forall\ ij \in \Omega_l,\ \forall\ t \in \Omega_t,\ \forall\ s \in 1...S \tag{4.21}
$$

Equation (4.22) states that the binary variable $x^V_{i,t,s-1}$ must be greater than the variable $x^V_{i,t,s}$. Equation (4.23) indicates the nature of the variable implemented in the linearization scheme (binary variable). Equation (4.24) is used to calculate $\overline{\Delta}^V$.

$$x^V_{i,t,s} \leq x^V_{i,t,s-1}; \quad \forall\ i \in \Omega_b,\ \forall\ t \in \Omega_t,\ \forall\ s \in 2...S \tag{4.22}$$

$$x^V_{i,t,s} \in \{0,1\}; \quad \forall\ i \in \Omega_b,\ \forall\ t \in \Omega_t,\ \forall\ s \in 1...S \tag{4.23}$$

$$\overline{\Delta}^V = \frac{\overline{V}^2 - \underline{V}^2}{S+1} \tag{4.24}$$

The right-hand side of the nonlinear equation can be linearized using Equations (4.25) through (4.34). Equation (4.25) represents the sum of the linearizations of the squared variables $P_{ij,t}$ and $Q_{ij,t}$. In this case, Y represents the number of blocks in the segmented linearization, $\Delta P_{ij,t,y}$ and $\Delta Q_{ij,t,y}$ represent the values of the y_{th} block of $|P_{ij,t}|$ and $|Q_{ij,t}|$, respectively, and $m^s_{ij,t,y}$ denotes the slope of the y_{th} block of the load flow in the branch ij.

$$P^2_{ij,t} + Q^2_{ij,t} = \sum_{y=1}^{Y} m^s_{ij,t,y} \Delta P_{ij,t,y} + \sum_{y=1}^{Y} m^s_{ij,t,y} \Delta Q_{ij,t,y} \tag{4.25}$$

Equations (4.26) and (4.27) represent the possible values of variables $P_{ij,t}$ and $Q_{ij,t}$ as a function of the auxiliary variables $P^+_{ij,t}$, $P^-_{ij,t}$, $Q^+_{ij,t}$, and $Q^-_{ij,t}$.

$$P^+_{ij,t} - P^-_{ij,t} = P_{ij,t}; \quad \forall\ ij \in \Omega_l,\ \forall\ t \in \Omega_t \tag{4.26}$$

$$Q^+_{ij,t} - Q^-_{ij,t} = Q_{ij,t}; \quad \forall\ ij \in \Omega_l,\ \forall\ t \in \Omega_t \tag{4.27}$$

Equations (4.28) and (4.29) indicate that $|P_{ij,t}|$ and $|Q_{ij,t}|$ are the sum of the values in each discretization block.

$$P^+_{ij,t} + P^-_{ij,t} = \sum_{y=1}^{Y} \Delta P_{ij,t,y}; \quad \forall\ ij \in \Omega_l,\ \forall\ t \in \Omega_t \tag{4.28}$$

$$Q^+_{ij,t} + Q^-_{ij,t} = \sum_{y=1}^{Y} \Delta Q_{ij,t,y}; \quad \forall\ ij \in \Omega_l,\ \forall\ t \in \Omega_t \tag{4.29}$$

Equations (4.30) and (4.31) define the upper and lower bounds of each block's contribution to $|P_{ij,t}|$ and $|Q_{ij,t}|$, respectively. Here, $\Delta^S_{ij,t}$ represents the maximum limit of each block of the power flow in branch ij.

$$0 \leq \Delta P_{ij,t,y} \leq \Delta^S_{ij,t}; \quad \forall\ ij \in \Omega_l,\ \forall\ t \in \Omega_t,\ \forall\ y \in 1...Y \tag{4.30}$$

$$0 \leq \Delta Q_{ij,t,y} \leq \Delta^{S}_{ij,t}; \quad \forall\ ij \in \Omega_l,\ \forall\ t \in \Omega_t,\ \forall\ y \in 1...Y \tag{4.31}$$

Equation (4.32) represents the non-negativity of the auxiliary variables $P^{+}_{ij,t}$, $P^{-}_{ij,t}$, $Q^{+}_{ij,t}$, and $Q^{-}_{ij,t}$. Equations (4.33) and (4.34) are used to calculate the values of $\Delta^{S}_{ij,t}$ and $m^{s}_{ij,t,y}$.

$$P^{+}_{ij,t};\ P^{-}_{ij,t};\ Q^{+}_{ij,t};\ Q^{-}_{ij,t} \geq 0; \quad \forall\ ij \in \Omega_l,\ \forall\ t \in \Omega_t \tag{4.32}$$

$$\Delta^{S}_{ij,t} = \frac{\overline{V}\ \overline{I_{ij}}}{Y}; \quad \forall\ ij \in \Omega_l,\ \forall\ t \in \Omega_t \tag{4.33}$$

$$m^{s}_{ij,t,y} = (2y-1)\,\Delta^{S}_{ij,t}; \quad \forall\ ij \in \Omega_l,\ \forall\ t \in \Omega_t,\ \forall\ y \in 1...Y \tag{4.34}$$

By adding Equations (4.19) through (4.24) and (4.26) through (4.34), and substituting Equations (4.18) and (4.25) into model (4.17), the MILP model for power flow in radial PDS, given by (4.35), is obtained.

$$\begin{gathered}
Minimize\ f = \sum_{\forall ij \in \Omega_l} \sum_{\forall t \in \Omega_t} R_{ij} I^{sqr}_{ij,t} \\
\sum_{\forall ki \in \Omega_l} P_{ki,t} - \sum_{\forall ij \in \Omega_l} \left(P_{ij,t} + R_{ij} I^{sqr}_{ij,t}\right) + P^{s}_{i,t} = P^{d}_{i,t}; \quad \forall\ i \in \Omega_b,\ \forall\ t \in \Omega_t \\
\sum_{\forall ki \in \Omega_l} Q_{ki,t} - \sum_{\forall ij \in \Omega_l} \left(Q_{ij,t} + X_{ij} I^{sqr}_{ij,t}\right) + Q^{s}_{i,t} = Q^{d}_{i,t}; \quad \forall\ i \in \Omega_b,\ \forall\ t \in \Omega_t \\
V^{sqr}_{i,t} - 2\left(R_{ij} P_{ij,t} + X_{ij} Q_{ij,t}\right) - Z^{2}_{ij} I^{sqr}_{ij,t} - V^{sqr}_{j,t} = 0; \quad \forall\ ij \in \Omega_l,\ \forall\ t \in \Omega_t \\
\left(\underline{V}^{2} + \frac{1}{2}\overline{\Delta}^{V}\right) I^{sqr}_{ij,t} + \sum_{s=1}^{S} P^{c}_{j,t,s} = \sum_{y=1}^{Y} m^{s}_{ij,t,y} \Delta P_{ij,t,y} + \sum_{y=1}^{Y} m^{s}_{ij,t,y} \Delta Q_{ij,t,y}; \quad \forall\ ij \in \Omega_l,\ \forall\ t \in \Omega_t \\
0 \leq I^{sqr}_{ij,t} \leq \overline{I_{ij}}^{2}; \quad \forall\ ij \in \Omega_l,\ \forall\ t \in \Omega_t \\
\underline{V}^{2} \leq V^{sqr}_{i,t} \leq \overline{V}^{2}; \quad \forall\ i \in \Omega_b,\ \forall\ t \in \Omega_t \\
\underline{V}^{2} + \overline{\Delta}^{V} \sum_{s=1}^{S} x^{V}_{i,t,s} \leq V^{sqr}_{i,t} \leq \underline{V}^{2} + \overline{\Delta}^{V} + \overline{\Delta}^{V} \sum_{s=1}^{S} x^{V}_{i,t,s}; \quad \forall\ i \in \Omega_b,\ \forall\ t \in \Omega_t \\
0 \leq \overline{\Delta}^{V} I^{sqr}_{ij,t} - P^{c}_{j,t,s} \leq \overline{\Delta}^{V} \overline{I_{ij}}^{2} \left(1 - x^{V}_{j,t,s}\right); \quad \forall\ ij \in \Omega_l,\ \forall\ t \in \Omega_t,\ \forall\ s \in 1...S \\
0 \leq P^{c}_{j,t,s} \leq \overline{\Delta}^{V} \overline{I_{ij}}^{2} x^{V}_{j,t,s}; \quad \forall\ ij \in \Omega_l,\ \forall\ t \in \Omega_t,\ \forall\ s \in 1...S \\
x^{V}_{i,t,s} \leq x^{V}_{i,t,s-1}; \quad \forall\ i \in \Omega_b,\ \forall\ t \in \Omega_t,\ \forall\ s \in 2...S \\
x^{V}_{i,t,s} \in \{0,1\}; \quad \forall\ i \in \Omega_b,\ \forall\ t \in \Omega_t,\ \forall\ s \in 1...S \\
\overline{\Delta}^{V} = \frac{\overline{V}^{2} - \underline{V}^{2}}{S+1}
\end{gathered} \tag{4.35}$$

$$P^{+}_{ij,t} - P^{-}_{ij,t} = P_{ij,t}; \quad \forall\ ij \in \Omega_l,\ \forall\ t \in \Omega_t$$

$$Q^{+}_{ij,t} - Q^{-}_{ij,t} = Q_{ij,t}; \quad \forall\ ij \in \Omega_l,\ \forall\ t \in \Omega_t$$

$$P^{+}_{ij,t} + P^{-}_{ij,t} = \sum_{y=1}^{Y} \Delta P_{ij,t,y}; \quad \forall\ ij \in \Omega_l,\ \forall\ t \in \Omega_t$$

$$Q^{+}_{ij,t} + Q^{-}_{ij,t} = \sum_{y=1}^{Y} \Delta Q_{ij,t,y}; \quad \forall\ ij \in \Omega_l,\ \forall\ t \in \Omega_t$$

$$0 \leq \Delta P_{ij,t,y} \leq \Delta^{S}_{ij,t}; \quad \forall\ ij \in \Omega_l,\ \forall\ t \in \Omega_t,\ \forall\ y \in 1...Y$$

$$0 \leq \Delta Q_{ij,t,y} \leq \Delta^{S}_{ij,t}; \quad \forall\ ij \in \Omega_l,\ \forall\ t \in \Omega_t,\ \forall\ y \in 1...Y$$

$$P^{+}_{ij,t};\ P^{-}_{ij,t};\ Q^{+}_{ij,t};\ Q^{-}_{ij,t} \geq 0; \quad \forall\ ij \in \Omega_l,\ \forall\ t \in \Omega_t$$

$$\Delta^{S}_{ij,t} = \frac{\overline{V}\ \overline{I_{ij}}}{Y}; \quad \forall\ ij \in \Omega_l,\ \forall\ t \in \Omega_t$$

$$m^{s}_{ij,t,y} = (2y-1)\,\Delta^{S}_{ij,t}; \quad \forall\ ij \in \Omega_l,\ \forall\ t \in \Omega_t,\ \forall\ y \in 1...Y$$

4.2 Placement of D-STATCOM Devices in PDS

D-STATCOM devices allow for the injection or absorption of reactive power as needed [10]. For this reason, D-STATCOM devices are considered in the following model as reactive power that varies according to the system's requirements. Although D-STATCOMs have a wide range of applications with appropriate control techniques, such as limiting overvoltages caused by capacitor switching, reducing voltage drops due to common feeder faults, and controlling voltage fluctuations caused by load variations [41], in this model, only their capability for voltage control at the fundamental frequency is considered. The modifications to the linear power flow model to account for the placement of D-STATCOM devices are detailed below.

The objective function in (4.35) is modified as shown in Equation (4.36). In this case, f_1 represents the system's active power losses and f_2 represents the voltage deviation. In f_2, voltages above the nominal voltage (V_{nom}) are penalized with a factor K_V, aiming to alleviate overvoltages caused by DER.

Normally, increasing voltages in PDS reduces losses. That is, the two components of the objective function are in conflict since decreasing one increases the other. The factor K_V allows controlling the priority level that the model assigns to reducing overvoltages in the mathematical formulation.

$$Minimize\ f = f_1 + f_2 \tag{4.36}$$

$$f_1 = \sum_{\forall ij \in \Omega_l} \sum_{\forall t \in \Omega_t} R_{ij} I^{sqr}_{ij,t}$$

$$f_2 = \begin{cases} K_V \cdot \sum\limits_{\forall i \in \Omega_b} \sum\limits_{\forall t \in \Omega_t} \left(V_{i,t}^{sqr} - V_{nom}^2 \right) & V_{i,t}^{sqr} \geq V_{nom}^2 \\ 0 & V_{i,t}^{sqr} < V_{nom}^2 \end{cases}$$

The reactive power balance equation is modified to account for the reactive power injection from D-STATCOM devices, resulting in Equation (4.37), where $Q_{i,t}^{STATCOM}$ is the reactive power delivered or absorbed by the D-STATCOM connected at bus i during period t.

$$\sum_{\forall ki \in \Omega_l} Q_{ki,t} - \sum_{\forall ij \in \Omega_l} \left(Q_{ij,t} + X_{ij} I_{ij,t}^{sqr} \right) + Q_{i,t}^{s} + Q_{i,t}^{STATCOM} = Q_{i,t}^{d}; \quad \forall\, i \in \Omega_b,\ \forall\, t \in \Omega_t \quad (4.37)$$

The equations for the optimal placement of D-STATCOMs are given by Equations (4.38) and (4.39). Equation (4.38) determines the power delivered/absorbed by the devices for period t and whether it is placed at bus i. $Q_{max}^{STATCOM}$ is the maximum allowed capacity for each D-STATCOM and w_i is a binary variable that equals 1 when a device is installed at bus i, and 0 otherwise.

$$-w_i \cdot Q_{max}^{STATCOM} \leq Q_{i,t}^{STATCOM} \leq w_i \cdot Q_{max}^{STATCOM}; \quad \forall\, i \in \Omega_b,\ \forall\, t \in \Omega_t \quad (4.38)$$

Finally, Equation (4.39) restricts the maximum number of D-STATCOM devices available for installation, where $N_{max}^{STATCOM}$ is the maximum number of devices available for installation in the system.

$$\sum_{\forall i \in \Omega_i} w_i \leq N_{max}^{STATCOM} \quad (4.39)$$

With the addition of (4.38) and (4.39), and the modifications of (4.36) and (4.37), the complete MILP model for the optimal placement of D-STATCOM devices is shown in (4.40).

$$Minimize\ f = f_1 + f_2$$

$$f_1 = \sum_{\forall ij \in \Omega_l} \sum_{\forall t \in \Omega_t} R_{ij} I_{ij,t}^{sqr}$$

$$f_2 = \begin{cases} K_V \cdot \sum\limits_{\forall i \in \Omega_b} \sum\limits_{\forall t \in \Omega_t} \left(V_{i,t}^{sqr} - V_{nom}^2 \right) & V_{i,t}^{sqr} \geq V_{nom}^2 \\ 0 & V_{i,t}^{sqr} < V_{nom}^2 \end{cases}$$

$$\sum_{\forall ki \in \Omega_l} P_{ki,t} - \sum_{\forall ij \in \Omega_l} \left(P_{ij,t} + R_{ij} I_{ij,t}^{sqr} \right) + P_{i,t}^{s} = P_{i,t}^{d}; \quad \forall\, i \in \Omega_b,\ \forall\, t \in \Omega_t$$

$$\sum_{\forall ki \in \Omega_l} Q_{ki,t} - \sum_{\forall ij \in \Omega_l} \left(Q_{ij,t} + X_{ij} I^{sqr}_{ij,t} \right) + Q^{s}_{i,t} + Q^{STATCOM}_{i,t} = Q^{d}_{i,t}; \quad \forall\, i \in \Omega_b,\ \forall\, t \in \Omega_t$$

$$V^{sqr}_{i,t} - 2\left(R_{ij} P_{ij,t} + X_{ij} Q_{ij,t}\right) - Z^2_{ij} I^{sqr}_{ij,t} - V^{sqr}_{j,t} = 0; \quad \forall\, ij \in \Omega_l,\ \forall\, t \in \Omega_t$$

$$\left(\underline{V}^2 + \frac{1}{2}\overline{\Delta}^V \right) I^{sqr}_{ij,t} + \sum_{s=1}^{S} P^{c}_{j,t,s} = \sum_{y=1}^{Y} m^{s}_{ij,t,y} \Delta P_{ij,t,y} + \sum_{y=1}^{Y} m^{s}_{ij,t,y} \Delta Q_{ij,t,y}; \quad \forall\, ij \in \Omega_l,\ \forall\, t \in \Omega_t$$

$$0 \le I^{sqr}_{ij,t} \le \overline{I_{ij}}^2; \quad \forall\, ij \in \Omega_l,\ \forall\, t \in \Omega_t$$

$$\underline{V}^2 \le V^{sqr}_{i,t} \le \overline{V}^2; \quad \forall\, i \in \Omega_b,\ \forall\, t \in \Omega_t$$

$$\underline{V}^2 + \overline{\Delta}^V \sum_{s=1}^{S} x^{V}_{i,t,s} \le V^{sqr}_{i,t} \le \underline{V}^2 + \overline{\Delta}^V + \overline{\Delta}^V \sum_{s=1}^{S} x^{V}_{i,t,s}; \quad \forall\, i \in \Omega_b,\ \forall\, t \in \Omega_t$$

$$0 \le \overline{\Delta}^V I^{sqr}_{ij,t} - P^{c}_{j,t,s} \le \overline{\Delta}^V \overline{I_{ij}}^2 \left(1 - x^{V}_{j,t,s}\right); \quad \forall\, ij \in \Omega_l,\ \forall\, t \in \Omega_t,\ \forall\, s \in 1...S$$

$$0 \le P^{c}_{j,t,s} \le \overline{\Delta}^V \overline{I_{ij}}^2 x^{V}_{j,t,s}; \quad \forall\, ij \in \Omega_l,\ \forall\, t \in \Omega_t,\ \forall\, s \in 1...S$$

$$x^{V}_{i,t,s} \le x^{V}_{i,t,s-1}; \quad \forall\, i \in \Omega_b,\ \forall\, t \in \Omega_t,\ \forall\, s \in 2...S \tag{4.40}$$

$$x^{V}_{i,t,s} \in \{0,1\}; \quad \forall\, i \in \Omega_b,\ \forall\, t \in \Omega_t,\ \forall\, s \in 1...S$$

$$\overline{\Delta}^V = \frac{\overline{V}^2 - \underline{V}^2}{S+1}$$

$$P^{+}_{ij,t} - P^{-}_{ij,t} = P_{ij,t}; \quad \forall\, ij \in \Omega_l,\ \forall\, t \in \Omega_t$$

$$Q^{+}_{ij,t} - Q^{-}_{ij,t} = Q_{ij,t}; \quad \forall\, ij \in \Omega_l,\ \forall\, t \in \Omega_t$$

$$P^{+}_{ij,t} + P^{-}_{ij,t} = \sum_{y=1}^{Y} \Delta P_{ij,t,y}; \quad \forall\, ij \in \Omega_l,\ \forall\, t \in \Omega_t$$

$$Q^{+}_{ij,t} + Q^{-}_{ij,t} = \sum_{y=1}^{Y} \Delta Q_{ij,t,y}; \quad \forall\, ij \in \Omega_l,\ \forall\, t \in \Omega_t$$

$$0 \le \Delta P_{ij,t,y} \le \Delta^{S}_{ij,t}; \quad \forall\, ij \in \Omega_l,\ \forall\, t \in \Omega_t,\ \forall\, y \in 1...Y$$

$$0 \le \Delta Q_{ij,t,y} \le \Delta^{S}_{ij,t}; \quad \forall\, ij \in \Omega_l,\ \forall\, t \in \Omega_t,\ \forall\, y \in 1...Y$$

$$P^{+}_{ij,t};\ P^{-}_{ij,t};\ Q^{+}_{ij,t};\ Q^{-}_{ij,t} \ge 0; \quad \forall\, ij \in \Omega_l,\ \forall\, t \in \Omega_t$$

$$\Delta^{S}_{ij,t} = \frac{\overline{V}\ \overline{I_{ij}}}{Y}; \quad \forall\, ij \in \Omega_l,\ \forall\, t \in \Omega_t$$

$$m^{s}_{ij,t,y} = (2y-1)\,\Delta^{S}_{ij,t}; \quad \forall\, ij \in \Omega_l,\ \forall\, t \in \Omega_t,\ \forall\, y \in 1...Y$$

$$-w_i \cdot Q^{STATCOM}_{max} \le Q^{STATCOM}_{i,t} \le w_i \cdot Q^{STATCOM}_{max}; \quad \forall\, i \in \Omega_b,\ \forall\, t \in \Omega_t$$

$$\sum_{\forall i \in \Omega_i} w_i \le N^{STATCOM}_{max}$$

4.3 Reconfiguration in PDS

To implement DSR in PDS, depending on the requirements, the objective function can be either the one presented in Model (4.35) or the equation given in (4.36). In this case, to control overvoltages caused by DER, the objective function is modified using Equation (4.36).

In addition to the objective function, other modifications must be made to the linear power flow model to account for reconfiguration [82]. The voltage drop equation in the branches of Model (4.35) must be modified, taking the form of Equation (4.41), where $b_{ij,t}$ is an auxiliary variable that depends on the state of the interconnection switches.

$$V_{i,t}^{sqr} - 2\left(R_{ij}P_{ij,t} + X_{ij}Q_{ij,t}\right) - Z_{ij}^{2}I_{ij,t}^{sqr} - V_{j,t}^{sqr} - b_{ij,t} = 0; \quad \forall\ ij \in \Omega_l,\ \forall\ t \in \Omega_t \tag{4.41}$$

The new current limit is represented by Equation (4.42), which is a function of the variables $y_{ij,t}^{+}$ and $y_{ij,t}^{-}$. The new limits for the variables $P_{ij,t}^{+}$ and $P_{ij,t}^{-}$ are represented by Equations (4.43) and (4.44). The new limit on the reactive power flow in branch ij during period t is represented by Equation (4.45). Equation (4.46) represents the limits on $b_{ij,t}$. This auxiliary variable is zero if the branch ij is closed according to (4.46); otherwise, is free within the limits defined by (4.46) in order to maintain and satisfy (4.41). Here, $y_{ij,t}^{+}$ and $y_{ij,t}^{-}$ represent binary variables related to the direction of the power flow in branch ij. If either of these variables equals one, the breaker in this branch is closed; if both variables are zero, the branch is open.

$$0 \leq I_{ij,t}^{sqr} \leq \overline{I_{ij}}^{2}\left(y_{ij,t}^{+} + y_{ij,t}^{-}\right); \quad \forall\ ij \in \Omega_l,\ \forall\ t \in \Omega_t \tag{4.42}$$

$$0 \leq P_{ij,t}^{+} \leq \overline{V}\ \overline{I}_{ij} y_{ij,t}^{+}; \quad \forall\ ij \in \Omega_l,\ \forall\ t \in \Omega_t \tag{4.43}$$

$$0 \leq P_{ij,t}^{-} \leq \overline{V}\ \overline{I}_{ij} y_{ij,t}^{-}; \quad \forall\ ij \in \Omega_l,\ \forall\ t \in \Omega_t \tag{4.44}$$

$$|Q_{ij,t}| \leq \overline{V}\ \overline{I}_{ij}\left(y_{ij,t}^{+} + y_{ij,t}^{-}\right); \quad \forall\ ij \in \Omega_l,\ \forall\ t \in \Omega_t \tag{4.45}$$

$$|b_{ij,t}| \leq \left(\overline{V}^{2} - \underline{V}^{2}\right)\left(1 - \left(y_{ij,t}^{+} + y_{ij,t}^{-}\right)\right); \quad \forall\ ij \in \Omega_l,\ \forall\ t \in \Omega_t \tag{4.46}$$

Since the system topology will be modified by reconfiguration, it is necessary to ensure that the new configuration remains radial [66]. This condition is given by Equations (4.47) through (4.49) [79,80], where N is the number of buses. Equation (4.50)

ensures that only one direction is selected, and the variables $y^{+}_{ij,t}$ and $y^{-}_{ij,t}$ are binary according to Equation (4.51).

$$\sum_{\forall ij \in \Omega_l} \left(y^{+}_{ij,t} + y^{-}_{ij,t} \right) = N - 1; \quad \forall\, t \in \Omega_t \tag{4.47}$$

$$\sum_{\forall ij \in \Omega_l} \left(y^{+}_{ij,t} \right) + \sum_{\forall ki \in \Omega_l} \left(y^{-}_{ki,t} \right) \geq 1; \quad \forall\, i = Substation \in \Omega_b,\ \forall\, t \in \Omega_t \tag{4.48}$$

$$\sum_{\forall ij \in \Omega_l} \left(y^{-}_{ij,t} \right) + \sum_{\forall ki \in \Omega_l} \left(y^{+}_{ki,t} \right) = 1; \quad \forall\, i \neq Substation \in \Omega_b,\ \forall\, t \in \Omega_t \tag{4.49}$$

$$\left(y^{+}_{ij,t} + y^{-}_{ij,t} \right) \leq 1; \quad \forall\, ij \in \Omega_l,\ \forall\, t \in \Omega_t \tag{4.50}$$

$$y^{+}_{ij,t},\ y^{-}_{ij,t}\ \ binary; \quad \forall\, ij \in \Omega_l,\ \forall\, t \in \Omega_t \tag{4.51}$$

Finally, the complete model for DSR in radial PDS is given in (4.52).

$$Minimize\ f = f_1 + f_2$$

$$f_1 = \sum_{\forall ij \in \Omega_l} \sum_{\forall t \in \Omega_t} R_{ij} I^{sqr}_{ij,t}$$

$$f_2 = \begin{cases} K_V \cdot \sum_{\forall i \in \Omega_b} \sum_{\forall t \in \Omega_t} \left(V^{sqr}_{i,t} - V^{2}_{nom} \right) & V^{sqr}_{i,t} \geq V^{2}_{nom} \\ 0 & V^{sqr}_{i,t} < V^{2}_{nom} \end{cases}$$

$$\sum_{\forall ki \in \Omega_l} P_{ki,t} - \sum_{\forall ij \in \Omega_l} \left(P_{ij,t} + R_{ij} I^{sqr}_{ij,t} \right) + P^{s}_{i,t} = P^{d}_{i,t}; \quad \forall\, i \in \Omega_b,\ \forall\, t \in \Omega_t$$

$$\sum_{\forall ki \in \Omega_l} Q_{ki,t} - \sum_{\forall ij \in \Omega_l} \left(Q_{ij,t} + X_{ij} I^{sqr}_{ij,t} \right) + Q^{s}_{i,t} = Q^{d}_{i,t}; \quad \forall\, i \in \Omega_b,\ \forall\, t \in \Omega_t$$

$$V^{sqr}_{i,t} - 2\left(R_{ij} P_{ij,t} + X_{ij} Q_{ij,t} \right) - Z^{2}_{ij} I^{sqr}_{ij,t} - V^{sqr}_{j,t} - b_{ij,t} = 0; \quad \forall\, ij \in \Omega_l,\ \forall\, t \in \Omega_t$$

$$\left(\underline{V}^{2} + \frac{1}{2} \overline{\Delta}^{V} \right) I^{sqr}_{ij,t} + \sum_{s=1}^{S} P^{c}_{j,t,s} = \sum_{y=1}^{Y} m^{s}_{ij,t,y} \Delta P_{ij,t,y} + \sum_{y=1}^{Y} m^{s}_{ij,t,y} \Delta Q_{ij,t,y}; \quad \forall\, ij \in \Omega_l,\ \forall\, t \in \Omega_t$$

$$0 \leq I^{sqr}_{ij,t} \leq \overline{I_{ij}}^{2} \left(y^{+}_{ij,t} + y^{-}_{ij,t} \right); \quad \forall\, ij \in \Omega_l,\ \forall\, t \in \Omega_t$$

$$\underline{V}^{2} \leq V^{sqr}_{i,t} \leq \overline{V}^{2}; \quad \forall\, i \in \Omega_b,\ \forall\, t \in \Omega_t$$

$$\underline{V}^{2} + \overline{\Delta}^{V} \sum_{s=1}^{S} x^{V}_{i,t,s} \leq V^{sqr}_{i,t} \leq \underline{V}^{2} + \overline{\Delta}^{V} + \overline{\Delta}^{V} \sum_{s=1}^{S} x^{V}_{i,t,s}; \quad \forall\, i \in \Omega_b,\ \forall\, t \in \Omega_t$$

$$0 \leq \overline{\Delta}^{V} I^{sqr}_{ij,t} - P^{c}_{j,t,s} \leq \overline{\Delta}^{V} \overline{I_{ij}}^{2} \left(1 - x^{V}_{j,t,s} \right); \quad \forall\, ij \in \Omega_l,\ \forall\, t \in \Omega_t,\ \forall\, s \in 1...S$$

$$0 \leq P^{c}_{j,t,s} \leq \overline{\Delta}^{V} \overline{I_{ij}}^{2} x^{V}_{j,t,s}; \quad \forall\, ij \in \Omega_l,\ \forall\, t \in \Omega_t,\ \forall\, s \in 1...S$$

$$x^{V}_{i,t,s} \leq x^{V}_{i,t,s-1}; \quad \forall\, i \in \Omega_b,\ \forall\, t \in \Omega_t,\ \forall\, s \in 2...S$$

$$x^{V}_{i,t,s} \in \{0,1\}; \quad \forall\, i \in \Omega_b,\ \forall\, t \in \Omega_t,\ \forall\, s \in 1...S$$

$$\overline{\Delta}^{V} = \frac{\overline{V}^2 - \underline{V}^2}{S+1}$$

$$P^{+}_{ij,t} - P^{-}_{ij,t} = P_{ij,t}; \quad \forall\, ij \in \Omega_l,\ \forall\, t \in \Omega_t \tag{4.52}$$

$$Q^{+}_{ij,t} - Q^{-}_{ij,t} = Q_{ij,t}; \quad \forall\, ij \in \Omega_l,\ \forall\, t \in \Omega_t$$

$$P^{+}_{ij,t} + P^{-}_{ij,t} = \sum_{y=1}^{Y} \Delta P_{ij,t,y}; \quad \forall\, ij \in \Omega_l,\ \forall\, t \in \Omega_t$$

$$Q^{+}_{ij,t} + Q^{-}_{ij,t} = \sum_{y=1}^{Y} \Delta Q_{ij,t,y}; \quad \forall\, ij \in \Omega_l,\ \forall\, t \in \Omega_t$$

$$0 \leq \Delta P_{ij,t,y} \leq \Delta^{S}_{ij,t}; \quad \forall\, ij \in \Omega_l,\ \forall\, t \in \Omega_t,\ \forall\, y \in 1...Y$$

$$0 \leq \Delta Q_{ij,t,y} \leq \Delta^{S}_{ij,t}; \quad \forall\, ij \in \Omega_l,\ \forall\, t \in \Omega_t,\ \forall\, y \in 1...Y$$

$$Q^{+}_{ij,t};\ Q^{-}_{ij,t} \geq 0; \quad \forall\, ij \in \Omega_l,\ \forall\, t \in \Omega_t$$

$$\Delta^{S}_{ij,t} = \frac{\overline{V}\ \overline{I_{ij}}}{Y}; \quad \forall\, ij \in \Omega_l,\ \forall\, t \in \Omega_t$$

$$m^{s}_{ij,t,y} = (2y-1)\,\Delta^{S}_{ij,t}; \quad \forall\, ij \in \Omega_l,\ \forall\, t \in \Omega_t,\ \forall\, y \in 1...Y$$

$$0 \leq P^{+}_{ij,t} \leq \overline{V}\ \overline{I_{ij}} y^{+}_{ij,t}; \quad \forall\, ij \in \Omega_l,\ \forall\, t \in \Omega_t$$

$$0 \leq P^{-}_{ij,t} \leq \overline{V}\ \overline{I_{ij}} y^{-}_{ij,t}; \quad \forall\, ij \in \Omega_l,\ \forall\, t \in \Omega_t$$

$$|Q_{ij,t}| \leq \overline{V}\ \overline{I_{ij}} \left(y^{+}_{ij,t} + y^{-}_{ij,t}\right); \quad \forall\, ij \in \Omega_l,\ \forall\, t \in \Omega_t$$

$$|b_{ij,t}| \leq \left(\overline{V}^2 - \underline{V}^2\right)\left(1 - \left(y^{+}_{ij,t} + y^{-}_{ij,t}\right)\right); \quad \forall\, ij \in \Omega_l,\ \forall\, t \in \Omega_t$$

$$\sum_{\forall ij \in \Omega_l} \left(y^{+}_{ij,t} + y^{-}_{ij,t}\right) = N - 1; \quad \forall\, t \in \Omega_t$$

$$\sum_{\forall ij \in \Omega_l} \left(y^{+}_{ij,t}\right) + \sum_{\forall ki \in \Omega_l} \left(y^{-}_{ki,t}\right) \geq 1; \quad \forall\, i = Substation \in \Omega_b,\ \forall\, t \in \Omega_t$$

$$\sum_{\forall ij \in \Omega_l} \left(y^{-}_{ij,t}\right) + \sum_{\forall ki \in \Omega_l} \left(y^{+}_{ki,t}\right) = 1; \quad \forall\, i \neq Substation \in \Omega_b,\ \forall\, t \in \Omega_t$$

$$\left(y^{+}_{ij,t} + y^{-}_{ij,t}\right) \leq 1; \quad \forall\, ij \in \Omega_l,\ \forall\, t \in \Omega_t$$

$$y^{+}_{ij,t},\ y^{-}_{ij,t}\ \ binary; \quad \forall\, ij \in \Omega_l,\ \forall\, t \in \Omega_t$$

4.4 DSR with Placement of D-STATCOMs

With the modifications described in Equations (4.36), (4.37), (4.41), and (4.42), as well as the addition of Equations (4.38), (4.39) and (4.43) to (4.51) to the model given in (4.35), it is possible to obtain Model (4.53). This model addresses DSR while simultaneously locating D-STATCOM devices in radial PDS.

$$
\begin{aligned}
&Minimize\ f = f_1 + f_2 \\
&f_1 = \sum_{\forall ij \in \Omega_l} \sum_{\forall t \in \Omega_t} R_{ij} I_{ij,t}^{sqr} \\
&f_2 = \begin{cases} K_V \cdot \sum_{\forall i \in \Omega_b} \sum_{\forall t \in \Omega_t} \left(V_{i,t}^{sqr} - V_{nom}^2 \right) & V_{i,t}^{sqr} \geq V_{nom}^2 \\ 0 & V_{i,t}^{sqr} < V_{nom}^2 \end{cases} \\
&\sum_{\forall ki \in \Omega_l} P_{ki,t} - \sum_{\forall ij \in \Omega_l} \left(P_{ij,t} + R_{ij} I_{ij,t}^{sqr} \right) + P_{i,t}^{s} = P_{i,t}^{d}; \quad \forall\ i \in \Omega_b,\ \forall\ t \in \Omega_t \\
&\sum_{\forall ki \in \Omega_l} Q_{ki,t} - \sum_{\forall ij \in \Omega_l} \left(Q_{ij,t} + X_{ij} I_{ij,t}^{sqr} \right) + Q_{i,t}^{s} + Q_{i,t}^{STATCOM} = Q_{i,t}^{d}; \quad \forall\ i \in \Omega_b,\ \forall\ t \in \Omega_t \\
&V_{i,t}^{sqr} - 2\left(R_{ij} P_{ij,t} + X_{ij} Q_{ij,t} \right) - Z_{ij}^2 I_{ij,t}^{sqr} - V_{j,t}^{sqr} - b_{ij,t} = 0; \quad \forall\ ij \in \Omega_l,\ \forall\ t \in \Omega_t \\
&\left(\underline{V}^2 + \frac{1}{2}\overline{\Delta}^V \right) I_{ij,t}^{sqr} + \sum_{s=1}^{S} P_{j,t,s}^{c} = \sum_{y=1}^{Y} m_{ij,t,y}^{s} \Delta P_{ij,t,y} + \sum_{y=1}^{Y} m_{ij,t,y}^{s} \Delta Q_{ij,t,y}; \quad \forall\ ij \in \Omega_l,\ \forall\ t \in \Omega_t \\
&0 \leq I_{ij,t}^{sqr} \leq \overline{I_{ij}}^2 \left(y_{ij,t}^{+} + y_{ij,t}^{-} \right); \quad \forall\ ij \in \Omega_l,\ \forall\ t \in \Omega_t \\
&\underline{V}^2 \leq V_{i,t}^{sqr} \leq \overline{V}^2; \quad \forall\ i \in \Omega_b,\ \forall\ t \in \Omega_t \\
&\underline{V}^2 + \overline{\Delta}^V \sum_{s=1}^{S} x_{i,t,s}^{V} \leq V_{i,t}^{sqr} \leq \underline{V}^2 + \overline{\Delta}^V + \overline{\Delta}^V \sum_{s=1}^{S} x_{i,t,s}^{V}; \quad \forall\ i \in \Omega_b,\ \forall\ t \in \Omega_t \\
&0 \leq \overline{\Delta}^V I_{ij,t}^{sqr} - P_{j,t,s}^{c} \leq \overline{\Delta}^V \overline{I_{ij}}^2 \left(1 - x_{j,t,s}^{V} \right); \quad \forall\ ij \in \Omega_l,\ \forall\ t \in \Omega_t,\ \forall\ s \in 1...S \\
&0 \leq P_{j,t,s}^{c} \leq \overline{\Delta}^V \overline{I_{ij}}^2 x_{j,t,s}^{V}; \quad \forall\ ij \in \Omega_l,\ \forall\ t \in \Omega_t,\ \forall\ s \in 1...S \\
&x_{i,t,s}^{V} \leq x_{i,t,s-1}^{V}; \quad \forall\ i \in \Omega_b,\ \forall\ t \in \Omega_t,\ \forall\ s \in 2...S \\
&x_{i,t,s}^{V} \in \{0,1\}; \quad \forall\ i \in \Omega_b,\ \forall\ t \in \Omega_t,\ \forall\ s \in 1...S \\
&\overline{\Delta}^V = \frac{\overline{V}^2 - \underline{V}^2}{S+1} \\
&P_{ij,t}^{+} - P_{ij,t}^{-} = P_{ij,t}; \quad \forall\ ij \in \Omega_l,\ \forall\ t \in \Omega_t \\
&Q_{ij,t}^{+} - Q_{ij,t}^{-} = Q_{ij,t}; \quad \forall\ ij \in \Omega_l,\ \forall\ t \in \Omega_t \\
&P_{ij,t}^{+} + P_{ij,t}^{-} = \sum_{y=1}^{Y} \Delta P_{ij,t,y}; \quad \forall\ ij \in \Omega_l,\ \forall\ t \in \Omega_t \\
&Q_{ij,t}^{+} + Q_{ij,t}^{-} = \sum_{y=1}^{Y} \Delta Q_{ij,t,y}; \quad \forall\ ij \in \Omega_l,\ \forall\ t \in \Omega_t
\end{aligned}
\tag{4.53}
$$

$$0 \leq \Delta P_{ij,t,y} \leq \Delta^{S}_{ij,t}; \quad \forall\ ij \in \Omega_l,\ \forall\ t \in \Omega_t,\ \forall\ y \in 1...Y$$

$$0 \leq \Delta Q_{ij,t,y} \leq \Delta^{S}_{ij,t}; \quad \forall\ ij \in \Omega_l,\ \forall\ t \in \Omega_t,\ \forall\ y \in 1...Y$$

$$Q^{+}_{ij,t};\ Q^{-}_{ij,t} \geq 0; \quad \forall\ ij \in \Omega_l,\ \forall\ t \in \Omega_t$$

$$\Delta^{S}_{ij,t} = \frac{\overline{V}\ \overline{I_{ij}}}{Y}; \quad \forall\ ij \in \Omega_l,\ \forall\ t \in \Omega_t$$

$$m^{s}_{ij,t,y} = (2y-1)\,\Delta^{S}_{ij,t}; \quad \forall\ ij \in \Omega_l,\ \forall\ t \in \Omega_t,\ \forall\ y \in 1...Y$$

$$-w_i \cdot Q^{STATCOM}_{max} \leq Q^{STATCOM}_{i,t} \leq w_i \cdot Q^{STATCOM}_{max}; \quad \forall\ i \in \Omega_b,\ \forall\ t \in \Omega_t$$

$$\sum_{\forall i \in \Omega_i} w_i \leq N^{STATCOM}_{max}$$

$$0 \leq P^{+}_{ij,t} \leq \overline{V}\ \overline{I_{ij}} y^{+}_{ij,t}; \quad \forall\ ij \in \Omega_l,\ \forall\ t \in \Omega_t$$

$$0 \leq P^{-}_{ij,t} \leq \overline{V}\ \overline{I_{ij}} y^{-}_{ij,t}; \quad \forall\ ij \in \Omega_l,\ \forall\ t \in \Omega_t$$

$$|Q_{ij,t}| \leq \overline{V}\ \overline{I_{ij}} \left(y^{+}_{ij,t} + y^{-}_{ij,t}\right); \quad \forall\ ij \in \Omega_l,\ \forall\ t \in \Omega_t$$

$$|b_{ij,t}| \leq \left(\overline{V}^2 - \underline{V}^2\right)\left(1 - \left(y^{+}_{ij,t} + y^{-}_{ij,t}\right)\right); \quad \forall\ ij \in \Omega_l,\ \forall\ t \in \Omega_t$$

$$\sum_{\forall ij \in \Omega_l} \left(y^{+}_{ij,t} + y^{-}_{ij,t}\right) = N - 1; \quad \forall\ t \in \Omega_t$$

$$\sum_{\forall ij \in \Omega_l} \left(y^{+}_{ij,t}\right) + \sum_{\forall ki \in \Omega_l} \left(y^{-}_{ki,t}\right) \geq 1; \quad \forall\ i = Substation \in \Omega_b,\ \forall\ t \in \Omega_t$$

$$\sum_{\forall ij \in \Omega_l} \left(y^{-}_{ij,t}\right) + \sum_{\forall ki \in \Omega_l} \left(y^{+}_{ki,t}\right) = 1; \quad \forall\ i \neq Substation \in \Omega_b,\ \forall\ t \in \Omega_t$$

$$\left(y^{+}_{ij,t} + y^{-}_{ij,t}\right) \leq 1; \quad \forall\ ij \in \Omega_l,\ \forall\ t \in \Omega_t$$

$$y^{+}_{ij,t},\ y^{-}_{ij,t}\ \ binary; \quad \forall\ ij \in \Omega_l,\ \forall\ t \in \Omega_t$$

In this chapter, the nonlinear power flow model for radial PDS was presented. The necessary linearizations in the initial model to obtain a MILP model were discussed. Finally, the models for the placement of D-STATCOM devices, DSR, and both simultaneously were introduced. Since they are based on linear power flow, the presented models are also of the MILP type. The model for the placement of D-STATCOM devices is highlighted due to its mixed-integer linear nature, a type of model not found in the specialized literature. In these models, the subscript t can represent minutes, hours, days, or representative periods, such as maximum, medium and minimum demand periods. The meaning of the subscript is defined by the input data that specify the different model parameters.

5 TEST AND RESULTS

This chapter presents the results obtained from the application of the models from Chapter 4 to improve the HC in PDS. Firstly, the effectiveness of the proposed models is validated on the 136-bus test system, comparing the results obtained with the DSR, placement of D-STATCOMs, as well as both simultaneously, with the power flow of the base case. Then, the results obtained for the 33 and 69-bus systems are presented, applying the models to increase the HC in two applications: mapping and interconnection.

The analyses conducted did not consider the impact of DER on power quality and system protections, issues that also limit the hosting capacity [4, 8, 9]. In this case, the performance indices used were the maximum current of the conductors and a maximum voltage of 1,05 pu to ensure safe system operation. Additionally, reverse active power flow towards the substation was defined as the maximum limiting factor for the HC in the system, as this indicates that all the power demanded by the system, plus losses, is being supplied by DER. In this work, it is assumed that the DER installed in the system have a power factor of 1, meaning they are considered as an active power injection, such as solar PV DG.

To calculate the HC, the iterative method presented in Figure 5 was used. That is, the DER insertion level is gradually increased until a violation of one of the performance indices occurs. For each of the two applications, the iterative process is explained further below. To limit overvoltages, a K_V factor of 2 was used in the models that include it. This value was obtained experimentally, and its effect is detailed in the validation of the models. Additionally, three D-STATCOM devices are considered available for installation in all cases ($N_{max}^{STATCOM} = 3$). The mathematical models are implemented using the AMPL language but executed from Python using the amplpy library. The reason for executing the AMPL model from Python is that all the model generation and solver interaction are done through AMPL, while the modification of the DER insertion and subsequent results analysis are performed in Python. This approach optimizes the workflow by leveraging the advantages of both languages, the ease of modeling and solving in AMPL, and the input and output data handling capabilities of Python.

Table 2 presents the active and reactive power demand of the loads for a typical day, considering half-hour intervals. These demand profiles are used in the analyses conducted below.

Figure 10 shows the profiles from Table 2, where different combinations of active and reactive power are observed, as well as the variations that may occur from one period to another during a typical day of operation.

Table 2 – Profile of active and reactive power demand

Time period	**Active [pu]**	**Reactive [pu]**	**Time period**	**Active [pu]**	**Reactive [pu]**
1	0.28	0.2238	13	0.94	0.7228
2	0.22	0.1666	14	0.84	0.6868
3	0.20	0.1654	15	0.90	0.8538
4	0.18	0.1274	16	0.90	0.7294
5	0.20	0.1750	17	0.90	0.6162
6	0.26	0.2428	18	0.90	0.6672
7	0.34	0.2780	19	0.84	0.6798
8	0.50	0.3996	20	1.00	0.8122
9	0.68	0.6448	21	0.94	0.7640
10	0.78	0.7322	22	0.84	0.5502
11	0.86	0.6632	23	0.68	0.4710
12	0.92	0.7304	24	0.50	0.3636

Source: Created by the author

Figure 10 – Daily power demand profiles

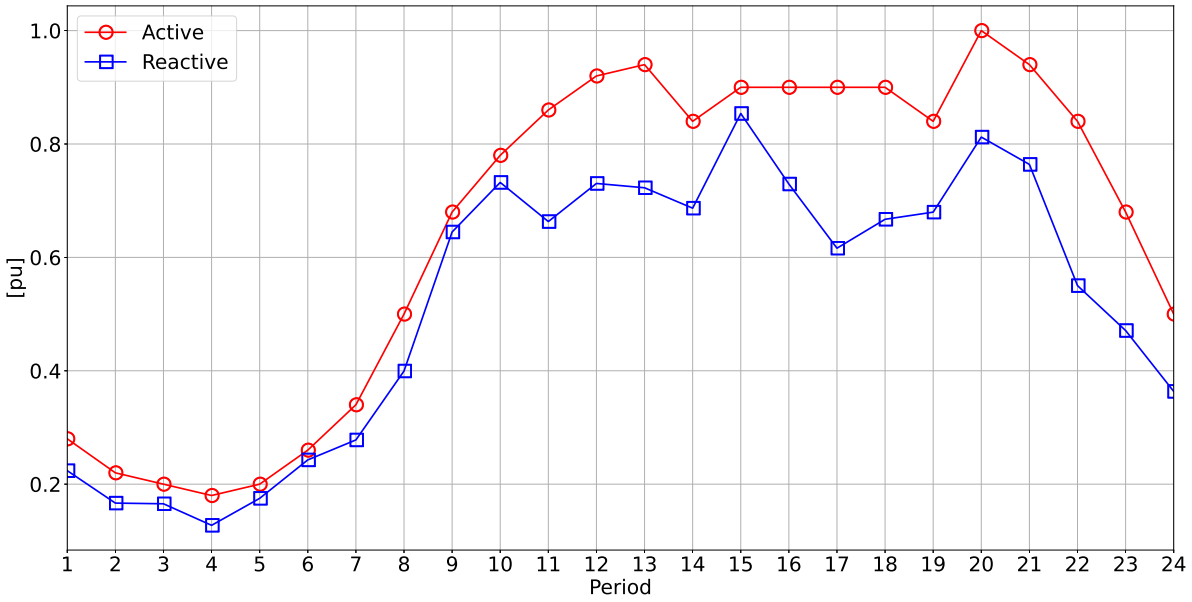

Source: Created by the author

5.1 Validation of the Models

The 136-bus test system is a radial network consisting of 136 buses, operating at 13,8 kV, 135 normally closed branches and 21 normally open branches. The system's peak demand is 18.313,809+j7.932,533 kVA, with the substation located at bus 0. The system data are presented in Appendix B. In this section, the 136-bus test system is used to validate the Models (4.40), (4.52) and (4.53) considering low, medium, and high load conditions, which correspond to periods 4, 9, and 20 in Table 2 and Figure 10. Additionally, a generator injecting 1.000, 3.000, and 4.000 kW respectively in each period is located at bus 117 to account for the DER integration in the system.

5.1.1 Placement of D-STATCOMs

In order to demonstrate the impact of the K_V factor on the results obtained, Figure 11 shows the outcomes when the Model (4.40) is executed with varying K_V values for the high load case. It can be observed that when K_V equals 0, voltages above 1 pu are disregarded, as the model prioritizes minimizing losses. Likewise, as the K_V value increases, voltages above 1 pu are gradually eliminated. A K_V value of 2 is selected because it strikes a balance between eliminating voltages above 1 pu and minimizing losses, as the losses can become excessively high if a larger value for this factor is considered.

Figure 11 – Effect of K_V factor variation on the voltage profile in the 136-bus system for high load

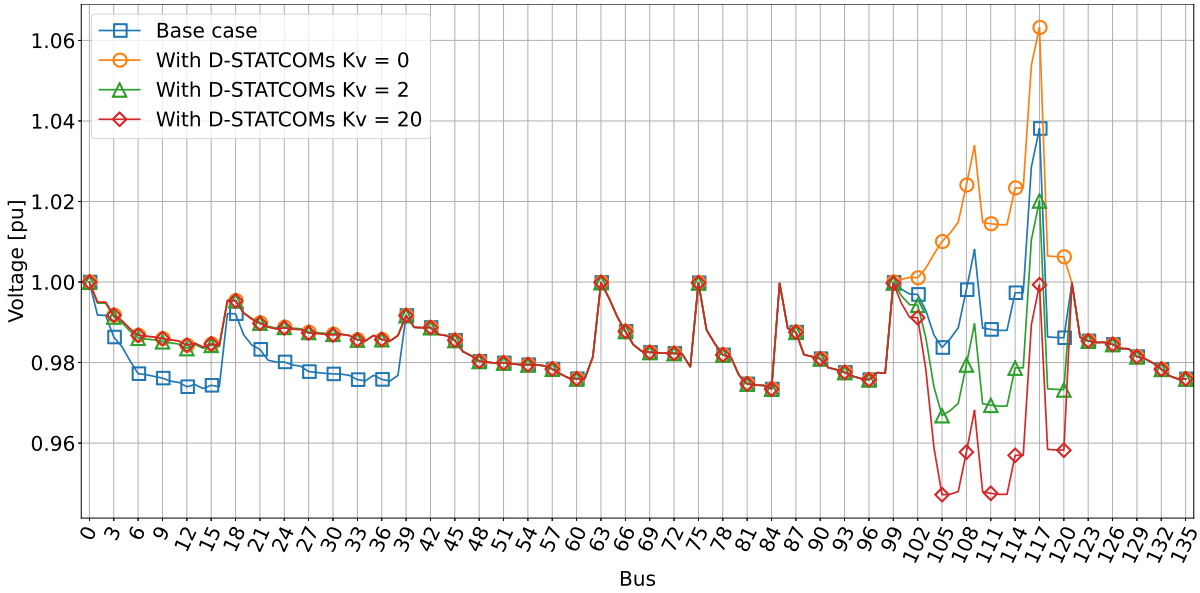

Source: Created by the author

Figure 12 shows the voltage profiles obtained after installing D-STATCOM devices compared to the base cases. It can be observed that in each of the three scenarios, voltages above 1 pu are reduced, and in the low load case, they are completely eliminated.

Figure 13 shows the reactive power injection or absorption of the installed D-STATCOM devices. It can be noted that there is a device located near bus 117 that absorbs reactive power to control the voltage, while the other two devices inject reactive power to reduce losses.

5.1.2 DSR

Figure 14 presents the comparison of voltage profiles for the three cases considering DSR and the base cases. It can be observed that voltages above 1 pu are completely eliminated. Additionally, some buses exhibit a reduction in voltage, likely as a result of the effort to eliminate voltages exceeding 1 pu.

Figure 12 – Voltage profile - Comparison between the base case and the case with D-STATCOMs in the 136-bus system for low, medium, and high load

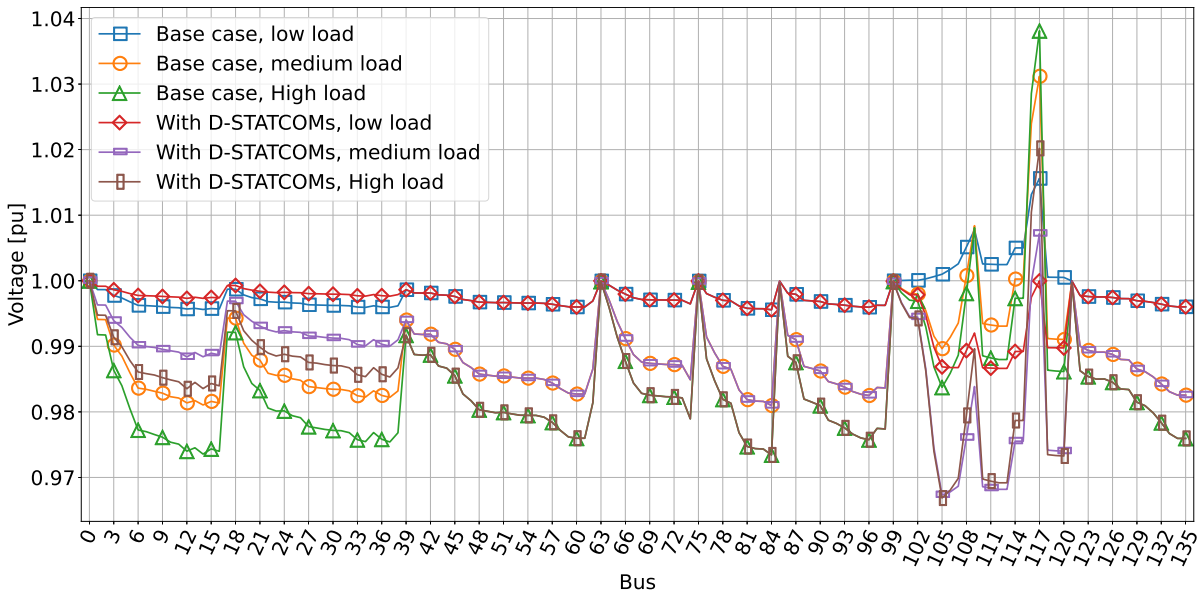

Source: Created by the author

Figure 13 – Reactive power of the D-STATCOMs in the 136-bus system for low, medium, and high load

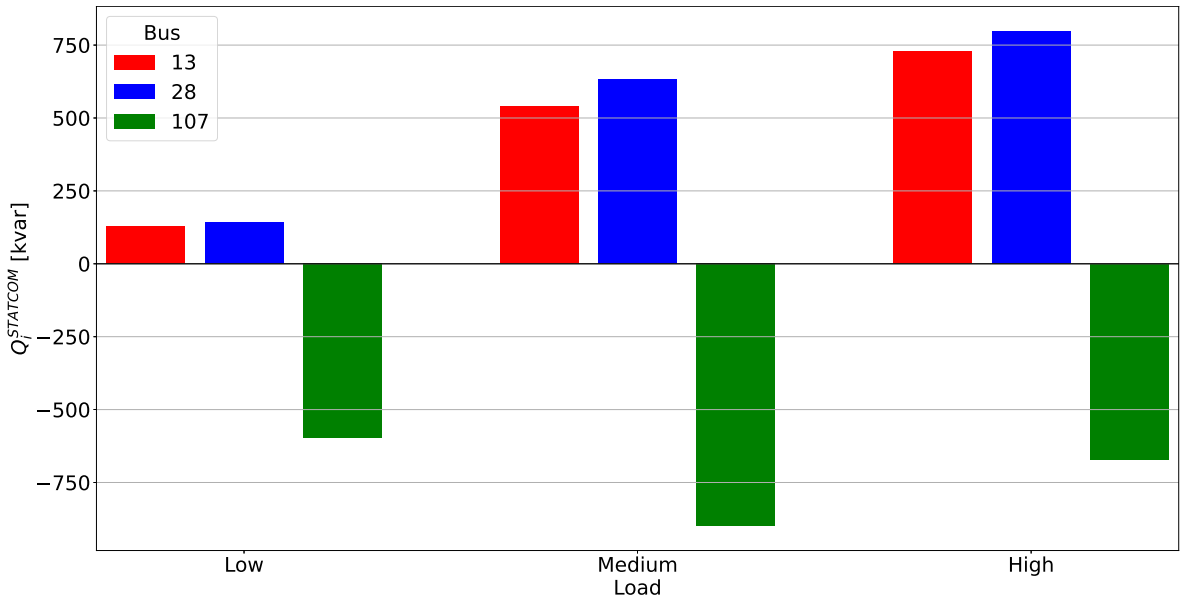

Source: Created by the author

5.1.3 DSR with Placement of D-STATCOMs

Figure 15 presents the voltage profiles considering both D-STATCOM devices and DSR. It is important to mention that in this work, when using Model (4.53), the locations of the D-STATCOM devices obtained with Model (4.40) are fixed to reduce computational time and enable a direct comparison of the techniques used separately or together. In this case, a similar result to the DSR scenario is observed in terms of reducing voltages

Figure 14 – Voltage profile - Comparison between the base case and the case with reconfiguration in the 136-bus system for low, medium, and high load

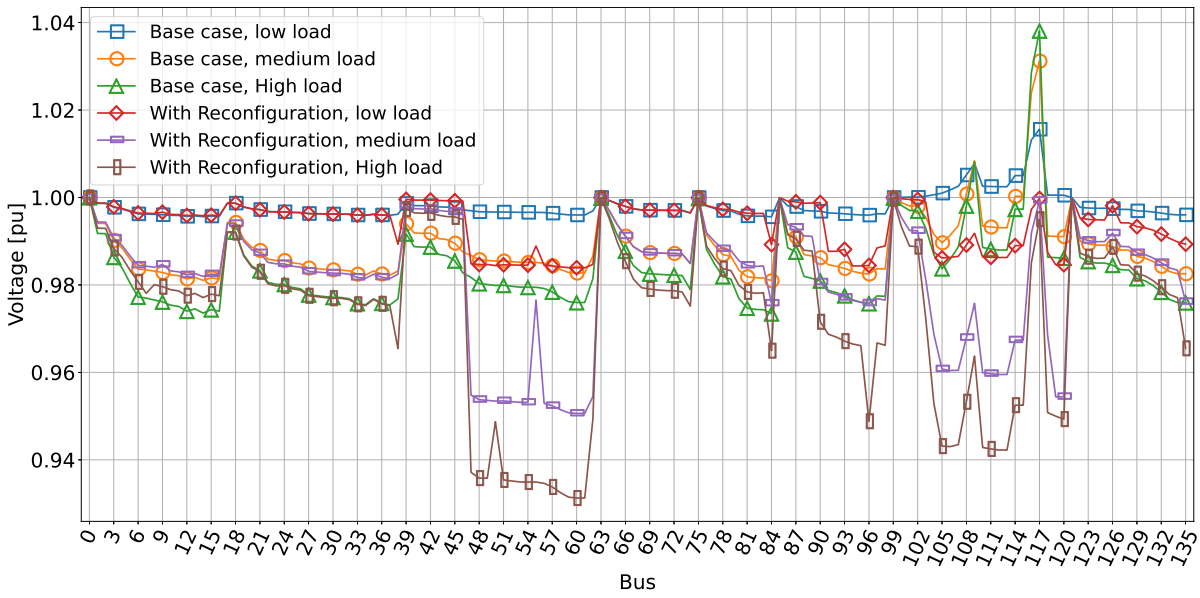

Source: Created by the author

above 1 pu. However, with the addition of D-STATCOMs, there is also an increase in the lower voltage levels within the system.

Figure 15 – Voltage profile - Comparison between the base case and the case with D-STATCOMs and reconfiguration in the 136-bus system for low, medium, and high load

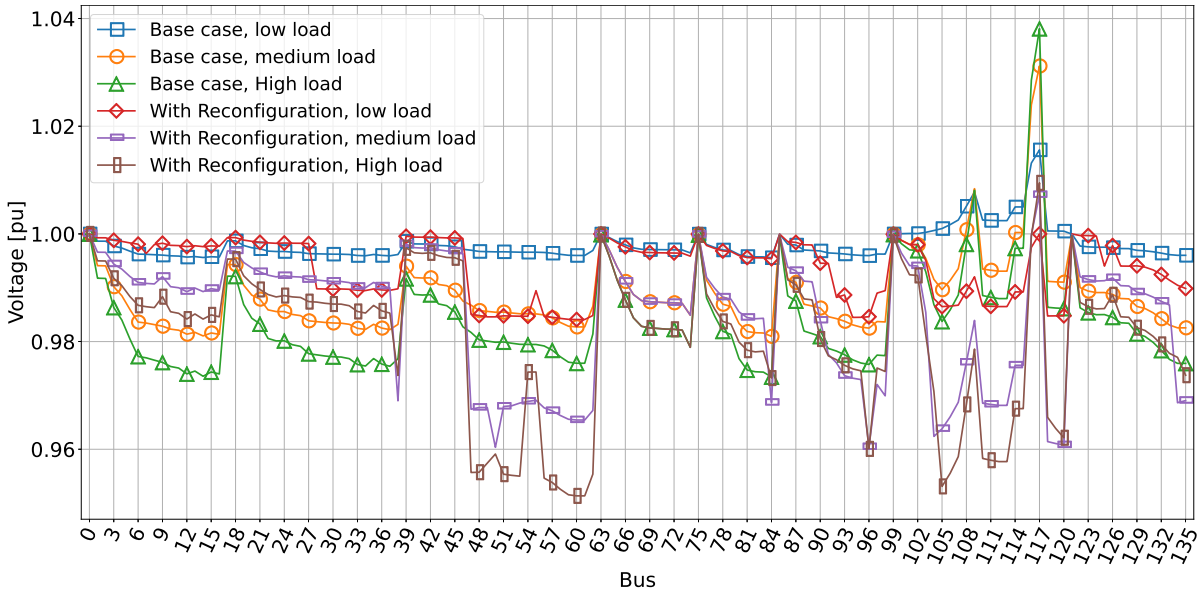

Source: Created by the author

Figure 16 shows the reactive power of the D-STATCOMs considering reconfiguration. It can be observed that the need to absorb reactive power for voltage control is almost entirely eliminated, and all the devices are utilized to minimize losses by injecting

reactive power.

Figure 16 – Reactive power of the D-STATCOMs considering reconfiguration in the 136-bus system for low, medium, and high load

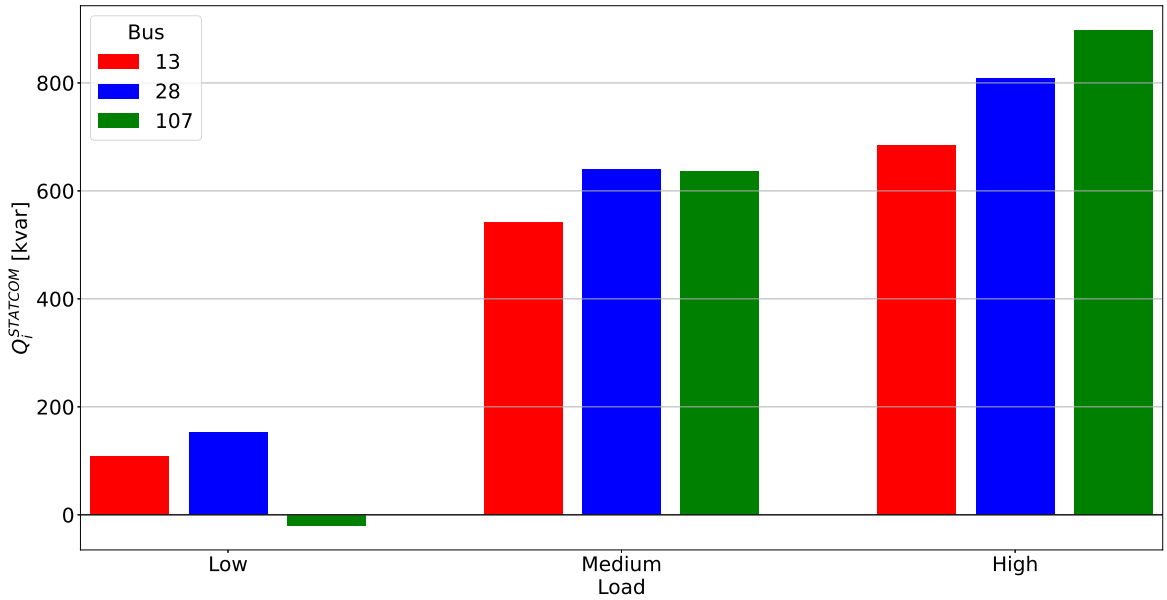

Source: Created by the author

5.1.4 Comparisons

Table 3 presents the comparison of open lines in the 136-bus system for each period. The variation in configuration between periods can be noted, as well as the effect of the D-STATCOM devices on the reconfiguration.

Table 3 – Comparison of open lines in the 136-bus system

Period	Reconfiguration	D-STATCOMs & Reconfiguration
Low	9 38 47 50 55 84 88 91 94 104 119 126 136 138 140 144 145 147 148 151 155	7 9 28 47 49 55 90 92 94 104 118 125 126 138 140 144 145 146 147 151 155
Medium	9 47 55 84 90 119 126 135 136 138 139 140 141 144 145 147 148 150 151 152 155	9 38 47 50 84 90 96 104 126 134 136 138 140 143 144 145 147 148 150 151 155
High	7 9 38 47 50 62 84 90 96 126 135 138 140 142 144 145 147 148 150 151 155	9 38 47 54 84 90 96 105 126 135 136 138 140 143 144 145 147 148 150 151 155

Source: Created by the author

Finally, Table 4 shows the comparison of total losses in the 136-bus system for the four considered cases. The base case exhibits total losses of 669,35 kW, which are exceeded in the case with D-STATCOM devices due to the reduction of voltages above 1 pu. The case considering DSR manages to reduce both the voltages and the losses, although the difference is not significant. The final case achieves a reduction in voltages

while significantly decreasing system losses by taking advantage of the combined benefits of DSR and D-STATCOM devices simultaneously.

Table 4 – Comparison of total losses for all cases in the 136-bus system

Case	**Total losses (kW)**
Base case	669.35
D-STATCOMs	728.28
Reconfiguration	657.61
D-STATCOMs and reconfiguration	597.34

Source: Created by the author

5.2 Mapping

For mapping, the HC is calculated at each bus considering each case separately, meaning that the HC value for one bus is not affected by the DER insertion or the HC of another bus. In this way, it would be possible to obtain a map like the one in Figure 3 to inform stakeholders interested in connecting DER to the system about potential attractive connection points. Four cases are considered to calculate the HC: the initial system, the system with D-STATCOMs installed, the system with DSR, and the system with both D-STATCOMs and reconfiguration.

In Figure 17, the diagram of the iterative method applied to mapping is presented. The process begins by selecting an analysis scenario, in this case, a maximum demand scenario corresponding to period 20 from Table 2 and Figure 10 is chosen. Subsequently, an iteration is performed over all buses in the system to determine the HC value, except for the substation bus. For each bus, the iterative process is executed by increasing the DER value until one of the considered conditions is violated. The complete process is carried out for the four models: the base case, the case considering D-STATCOMs, the case with reconfiguration, and the case considering both. As previously mentioned, mapping considers only one period; therefore, for this application t in the models corresponds to the selected single period. The choice of scenario or period will depend on the search for a more or less restrictive scenario for the integration of DER into the system.

5.2.1 33-Bus Test System

The 33-bus test system is a radial network consisting of 33 buses operating at 12.66 kV, 32 normally closed branches and 5 normally open branches. The system's peak demand is 3715+j2300 kVA, with the substation located at bus 1. Maximum currents in the branches are defined to account for the limitation of HC due to overcurrents in the system. The system data are presented in Appendix B.

The HC results per bus in the 33-bus system for the four considered cases are shown in Figure 18. In these figures, the black lines represent normally closed branches, while

Figure 17 – Diagram of the iterative method for mapping

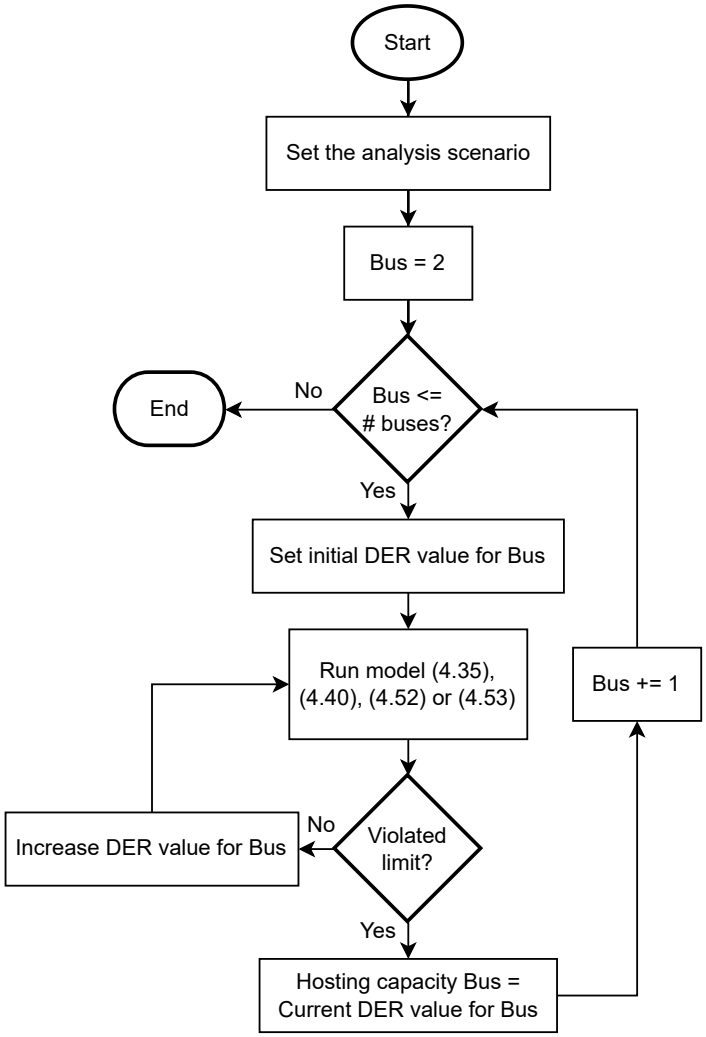

Source: Created by the author

the dotted lines represent normally open branches. It can be observed that in the base case (Figure 18 A), the system exhibits the lowest hosting capacity among the four cases, especially in buses located farther from the substation. The case with D-STATCOMs (Figure 18 B) slightly improves the system's hosting capacity; however, the improvement is more significant for the cases with DSR and simultaneous DSR with D-STATCOMs (Figure 18 C and D).

In this system, an interesting connection point would be bus 10, as it exhibits a high HC value across all cases, with the base case being the most limited. Conversely, buses that might be avoided, particularly in the base case and the case with D-STATCOM devices, would include buses 22, 25, 33, and 18.

Figure 18 – HC results for mapping in the 33-bus system - A) base case B) with D-STATCOMs C) with reconfiguration D) with D-STATCOMs and reconfiguration

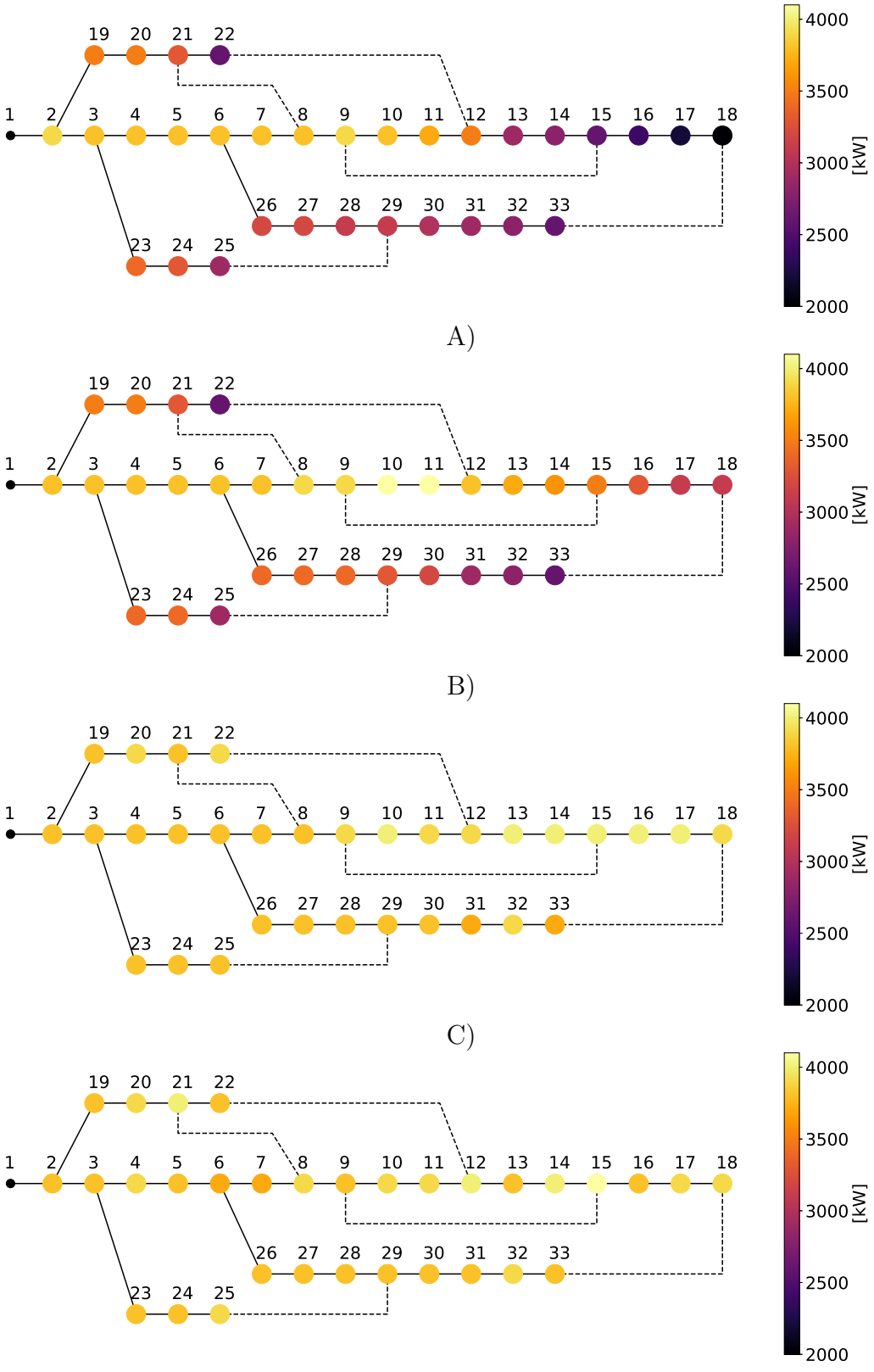

Source: Created by the author

5.2.1.1 Base Case

Figure 19 details the results for the base case of the 33-bus system. Part A shows the HC values for each bus, while Part B presents the losses, both classified according to the violated performance index. As shown in Figure 18 A, it can be observed that buses near the substation, which are connected by branches with high current capacity, are limited by reverse active power flow towards the substation. Additionally, buses farther from the substation tend to be limited by overvoltages, while lateral branches with lower current capacity are constrained by this limitation.

Figure 19 – Results of the base case for mapping in the 33-bus system - A) HC B) Losses

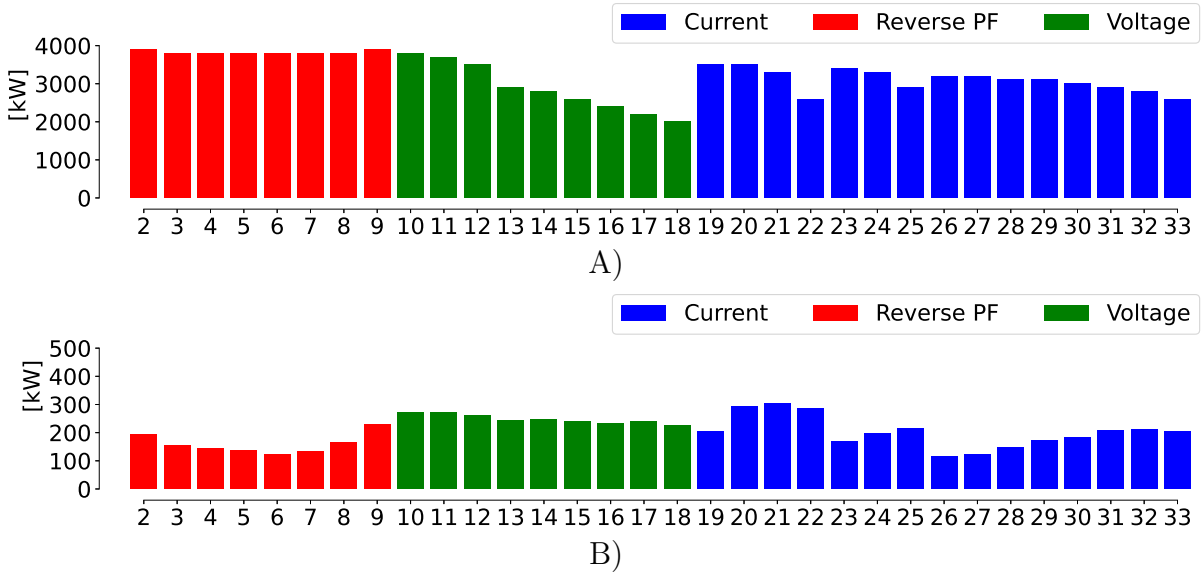

Source: Created by the author

5.2.1.2 Placement of D-STATCOMs

The detailed results for the case with D-STATCOMs in the 33-bus system are shown in Figure 20. As expected, the buses with voltage limitations see an increase in their HC value, at the expense of higher respective losses, even reaching other limits at buses 10, 11, and 12. On the other hand, the buses limited by current exhibit practically the same results as in the base case, as the D-STATCOM devices are unable to reduce the current in these cases.

5.2.1.3 DSR

The results for the DSR case in the 33-bus system are presented in Figure 21. A significant increase can be observed compared to the base case and the case with D-STATCOMs, with the main limitation being the reverse power flow towards the substation. Current limitations appear in a few buses, but in this case, voltage limitations are completely eliminated. This demonstrates the versatility of DSR in addressing constraints

Figure 20 – Results of the case with D-STATCOM for mapping in the 33-bus system - A) HC B) Losses

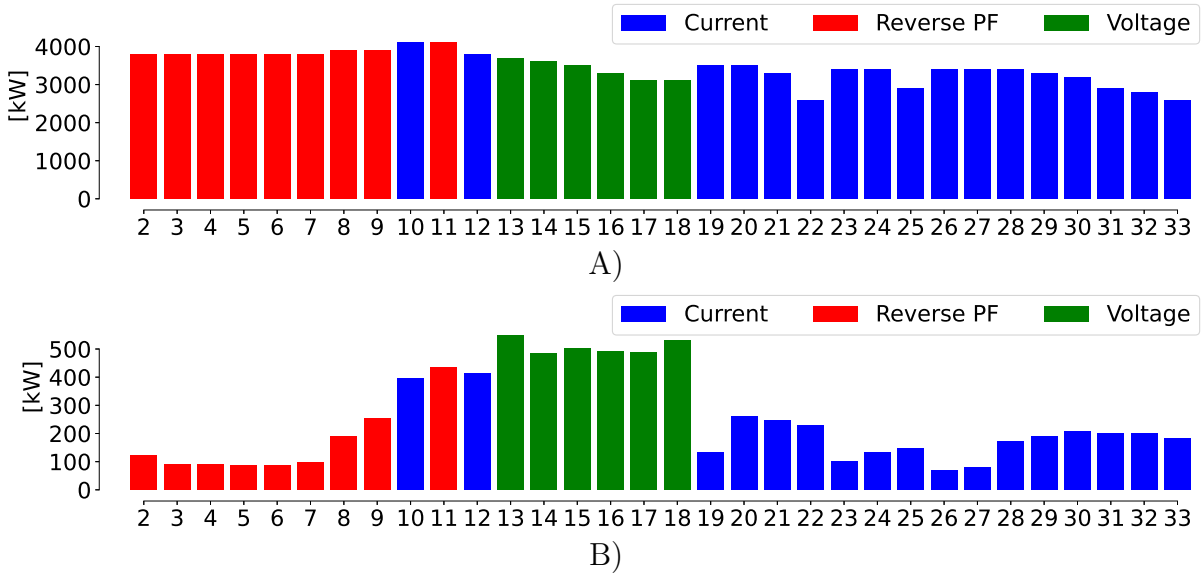

Source: Created by the author

in PDS. Regarding losses, a similarity is noted compared to the case with D-STATCOM devices, but the losses are higher than in the base case.

Figure 21 – Results of the case with reconfiguration for mapping in the 33-bus system - A) HC B) Losses

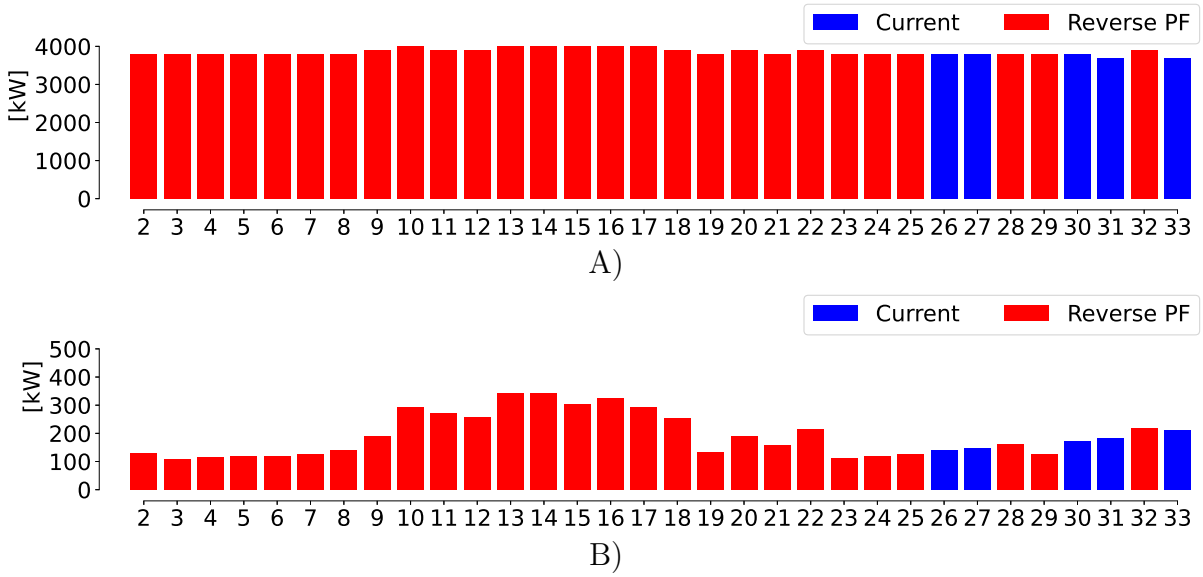

Source: Created by the author

5.2.1.4 DSR with Placement of D-STATCOMs

Finally, Figure 22 presents the results for the case that considers both DSR and D-STATCOM devices. In this scenario, following the results of DSR alone, voltage limitations are completely eliminated. Likewise, the number of current limitations is reduced

to only 2 out of the 33 buses. However, when compared to the reconfiguration case, where many buses are limited by reverse power flow, a slight decrease in HC is observed in some buses. This occurs due to losses, which as shown in Figure 22 B, generally exhibit lower values compared to the other cases. For this reason, less power from the DER is needed to supply the demand plus the losses before reverse power flow towards the substation occurs.

Figure 22 – Results of the case with D-STATCOM and reconfiguration for mapping in the 33-bus system - A) HC B) Losses

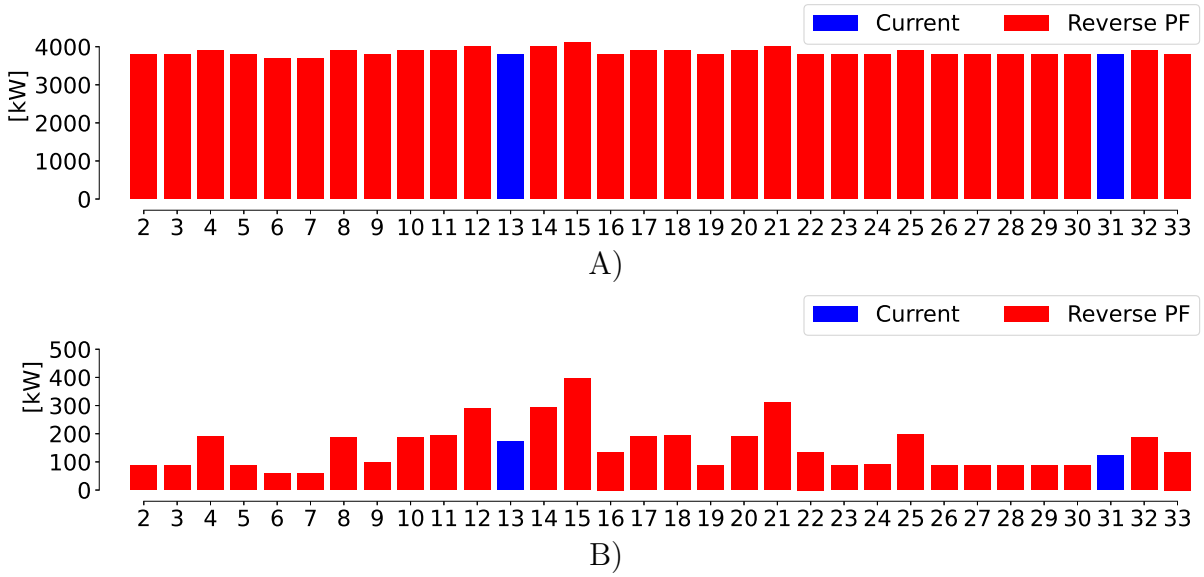

Source: Created by the author

Appendix A presents the mapping results for the 33-bus system in tabular form, detailing the HC value, the limiting factor, and the losses for each bus across all cases.

5.2.2 69-Bus Test System

The 69-bus test system is a radial network consisting of 69 buses operating at 12.66 kV, 68 normally closed branches and 5 normally open branches. The system's peak demand is 3802.19+j2694.6 kVA, with the substation located at bus 1. Maximum currents in the branches are defined to account for the limitation of HC due to overcurrents in the system. The system data are presented in Appendix B.

The HC results per bus in the 69-bus system for the four considered cases are shown in Figure 23. In the base case, the buses with the lowest HC values are observed among all cases, primarily at those farthest from the substation. The buses closer to the substation exhibit slightly higher values, constrained by the reverse power flow. In this system, the case with D-STATCOMs shows an increase in HC at some buses but a decrease at others. The reduction is attributed to the devices absorbing reactive power to control the voltage, which increases the current magnitude in the branches and thereby

limits the HC. Conversely, the DSR case displays the highest HC values overall, while the DSR combined with D-STATCOM devices yields similar results, although with slightly lower values for certain buses. In this latter case, the HC reduction is due to the decrease in losses, making less power necessary to induce a reverse power flow.

In the 69-bus system, promising connection points across all cases would be along the main branch up to bus 13 and buses 53 through 63. Conversely, buses that should be avoided include buses 34 and 35, as they consistently exhibit significantly low HC values across all scenarios. For these buses, the DSR is unable to significantly affect the voltage because the system lacks normally open branches connecting nearby buses.

Figure 23 – HC results for mapping in the 69-bus system - A) base case B) with D-STATCOMs C) with reconfiguration D) with D-STATCOMs and reconfiguration

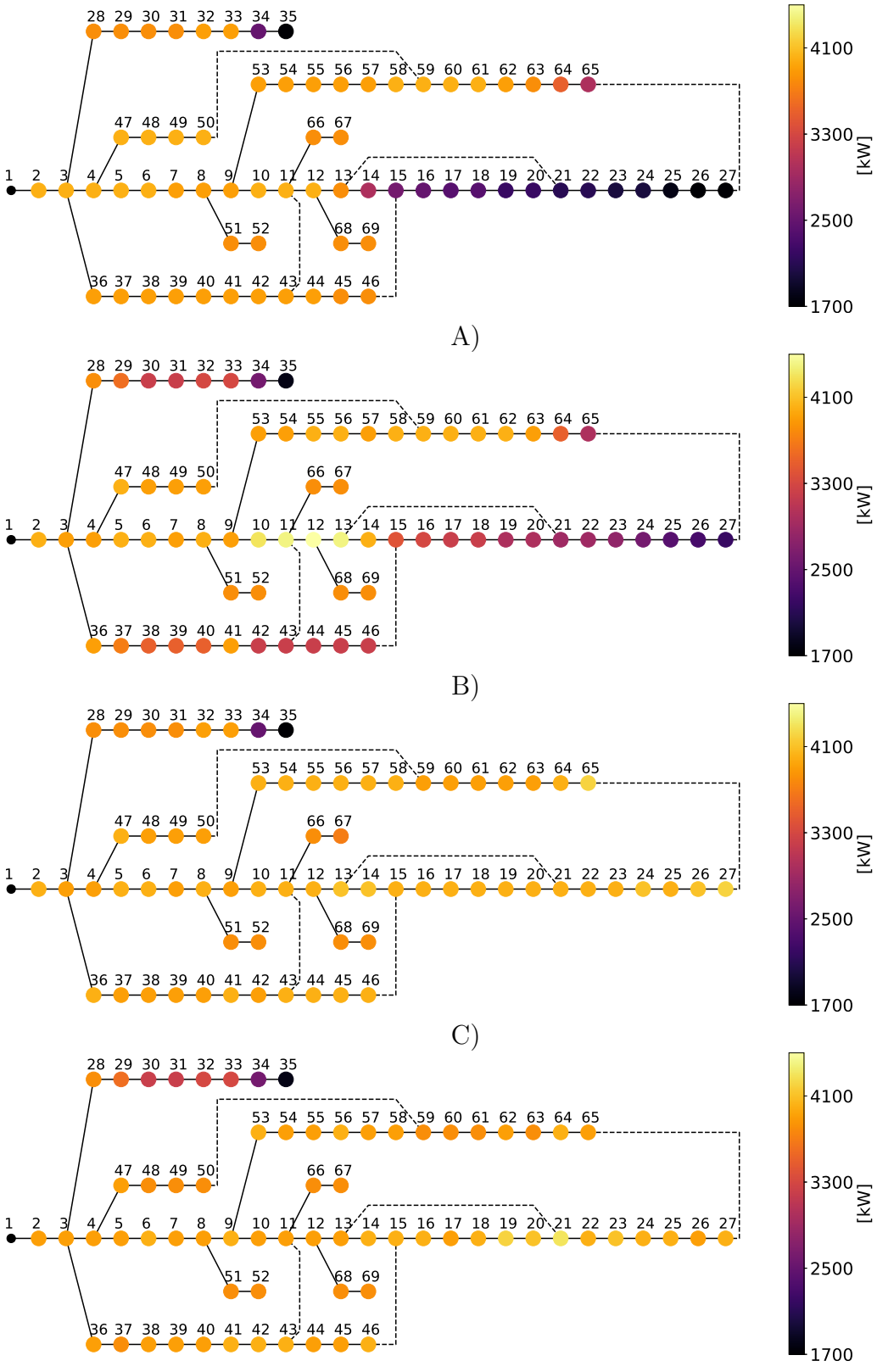

Source: Created by the author

5.2.2.1 Base Case

The results for the base case in the 69-bus system are detailed in Figure 24. The values of HC for each bus and the losses are classified according to the violated performance index. It can be observed that buses located near the substation are limited by the reverse power flow towards the substation, as the branches connecting them have higher current capacity. As the distance from the substation increases, overvoltage problems begin to appear. Similarly, the lateral branches of the system, due to their lower current capacity, present current-related limitations.

Figure 24 – Results of the base case for mapping in the 69-bus system - A) HC B) Losses

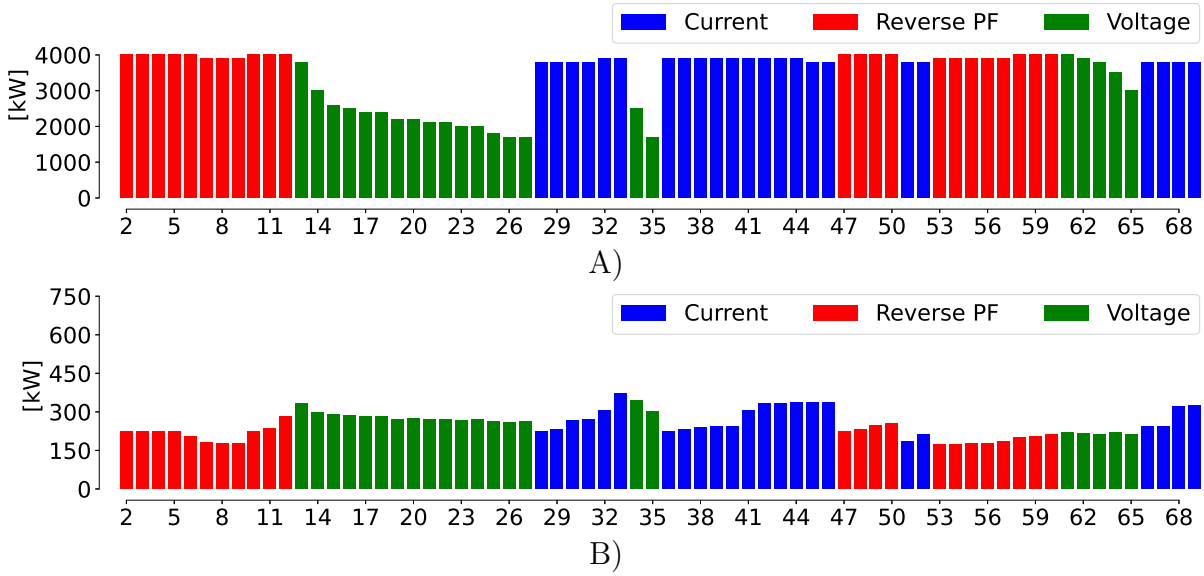

Source: Created by the author

5.2.2.2 Placement of D-STATCOMs

The results for the case considering D-STATCOMs in the 69-bus system are presented in Figure 25. In this case, an increase in HC is observed for buses 14 to 27, which were previously limited by voltage. However, a decrease is noticeable in some buses due to the D-STATCOMs absorbing reactive power to control the voltage. This absorption leads to an increase in current magnitude, which was already a limiting factor in the base case, causing an even greater limitation.

5.2.2.3 DSR

Figure 26 shows the results for the 69-bus system considering DSR. An increase in HC across the system's buses and a general reduction in losses can be observed. In this case, there are buses with voltage limitations that cannot be alleviated through DSR, as there are no normally open branches connected to nearby buses. However, most of the

Figure 25 – Results of the case with D-STATCOM for mapping in the 69-bus system - A) HC B) Losses

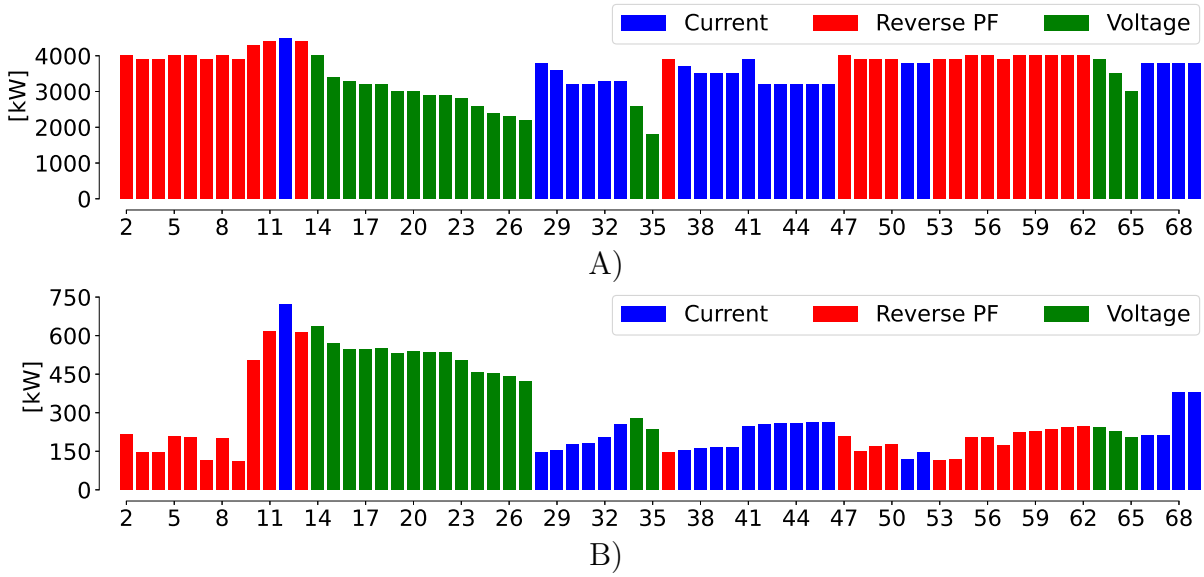

Source: Created by the author

buses are able to increase their HC value up to the maximum limit, which is constrained by the reverse power flow towards the substation.

Figure 26 – Results of the case with reconfiguration for mapping in the 69-bus system - A) HC B) Losses

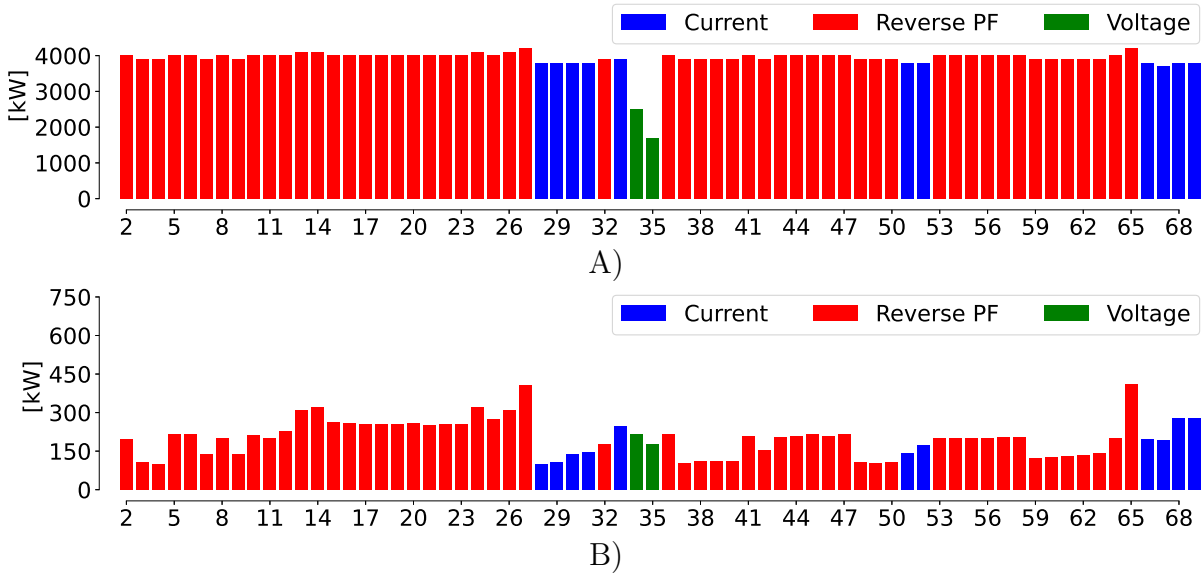

Source: Created by the author

5.2.2.4 DSR with Placement of D-STATCOMs

The results for the final case, considering both D-STATCOMs and DSR in the 69-bus system, are shown in Figure 27. A similar outcome to the DSR case is observed regarding the HC. There is a decrease in some buses, such as bus 32, where the D-

STATCOMs attempt to control the voltage by absorbing reactive power, which increases the current magnitude and consequently limits the HC value at that bus. When examining the losses, a general decrease can be observed, with a noticeable increase only in some cases where the HC value was raised.

Figure 27 – Results of the case with D-STATCOM and reconfiguration for mapping in the 69-bus system - A) HC B) Losses

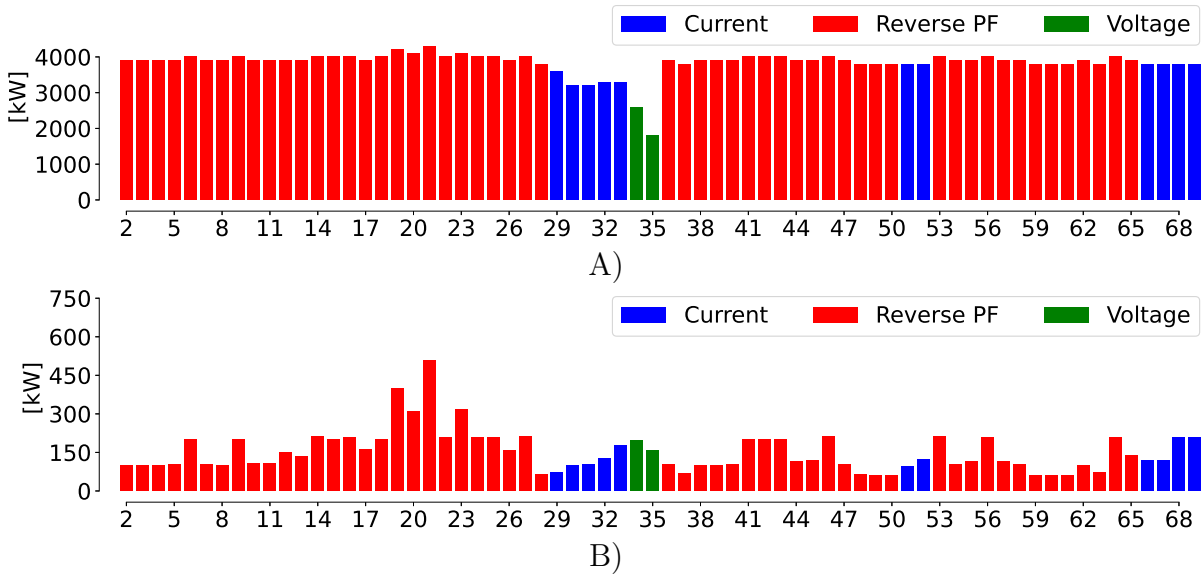

Source: Created by the author

Appendix A presents the mapping results for the 69-bus system in tabular form, detailing the HC value, the limiting factor, and the losses for each bus across all cases.

5.3 Interconnection

For interconnection, the HC is calculated for each of the 24 periods of a typical operational day, providing indications of the maximum DER insertion the system can support at a connection point during each period. In this case, the models are applied to improve the operation considering the maximum DER insertion that the system in its initial state can accommodate.

In Figure 28, the diagram of the iterative method applied to interconnection is presented. The process begins by selecting a bus to analyze the impact of connecting DER to it. Subsequently, an iteration is performed over all the considered periods; in this case, the 24 periods of a typical operational day from Table 2 and Figure 10 are analyzed. For each period, the iterative process is executed by increasing the DER value until one of the considered conditions is violated. The complete process is carried out only for the base case, resulting in the HC value for each period at the selected bus. This result provides an approximation of the maximum DER value that an interested party could connect to the analyzed bus for each of the considered periods.

However, the HC values found push the system's operating conditions to the considered limits. Therefore, Models (4.40), (4.52) and (4.53) are used to improve the system's operating conditions, considering the integration of the HC value found for each period at the bus of interest. In this application, t in the models corresponds to the hourly periods of a typical operational day.

This application corresponds to a process that can be carried out by an entity interested in connecting DER to a distribution system. By seeking to maximize the amount of DER without compromising the system's conditions, the entity evaluates different alternatives; hence its name, interconnection.

Figure 28 – Diagram of the iterative method for interconnection

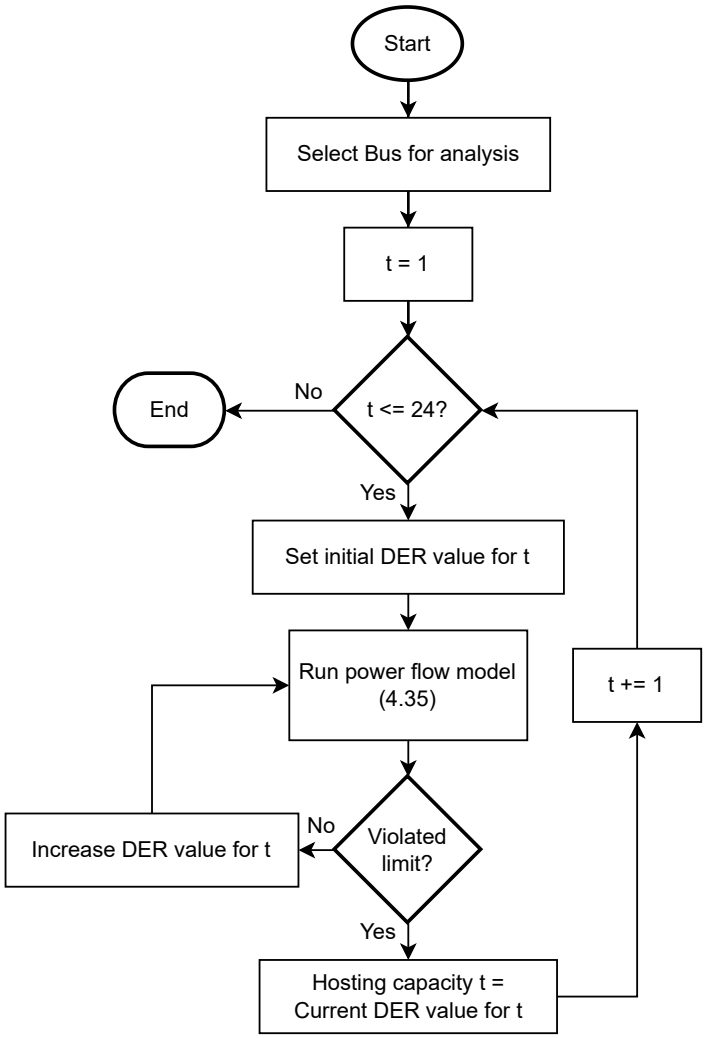

Source: Created by the author

5.3.1 33-Bus Test System

Bus 18 is selected because, as observed in mapping, it presents a voltage limitation and is one of the buses with the lowest HC values. The objective is to analyze how the HC varies across each period, its limiting factor, and how the proposed solutions can improve system operation. Table 5 shows the HC results obtained for the 33-bus system when considering bus 18 for DER integration. It can be observed that during periods 1 to 5, where the load is low, the limitation is the reverse power flow to the substation since the DER injection is sufficient to supply the entire system's power demand without significantly increasing the voltage at the bus. Starting from period 6, voltage limitation appears, with different HC values for each period. In this interconnection scenario, the goal is to expand the system's operational margin during these periods, specifically by increasing the maximum voltage margin, which translates into the possibility of enhancing DER integration.

Table 5 – HC results for interconnection at bus 18 in the 33-bus system

Period	**HC (kW)**	**Limit**	**Losses (kW)**
1	1000	Reverse PF	45.67
2	800	Reverse PF	29.47
3	700	Reverse PF	22.91
4	600	Reverse PF	16.5
5	700	Reverse PF	23.11
6	1000	Voltage	47.06
7	1100	Voltage	54.84
8	1300	Voltage	76.73
9	1600	Voltage	126.72
10	1700	Voltage	148.13
11	1800	Voltage	155.53
12	1800	Voltage	164.27
13	1900	Voltage	176.68
14	1700	Voltage	145.12
15	1900	Voltage	190.03
16	1800	Voltage	163.36
17	1800	Voltage	152.52
18	1800	Voltage	157.19
19	1700	Voltage	144.45
20	2000	Voltage	202.15
21	1900	Voltage	181.07
22	1700	Voltage	133.22
23	1500	Voltage	101.88
24	1300	Voltage	74.87

Source: Created by the author

5.3.1.1 Placement of D-STATCOMs

In Figure 29, the comparison of the voltage profile between the base case in Table 5 and the case with D-STATCOMs is presented, considering the integration of DER for each period. It can be observed that the voltage at bus 18 decreases significantly, thus

widening the margin with respect to the maximum operating voltage considered (1.05 pu). Likewise, the voltage profile is improved in the buses that exhibited low voltage levels, enhancing the overall condition of the system.

Figure 29 – Voltage profile - Comparison between the base case and the case with D-STATCOMs in the 33-bus system

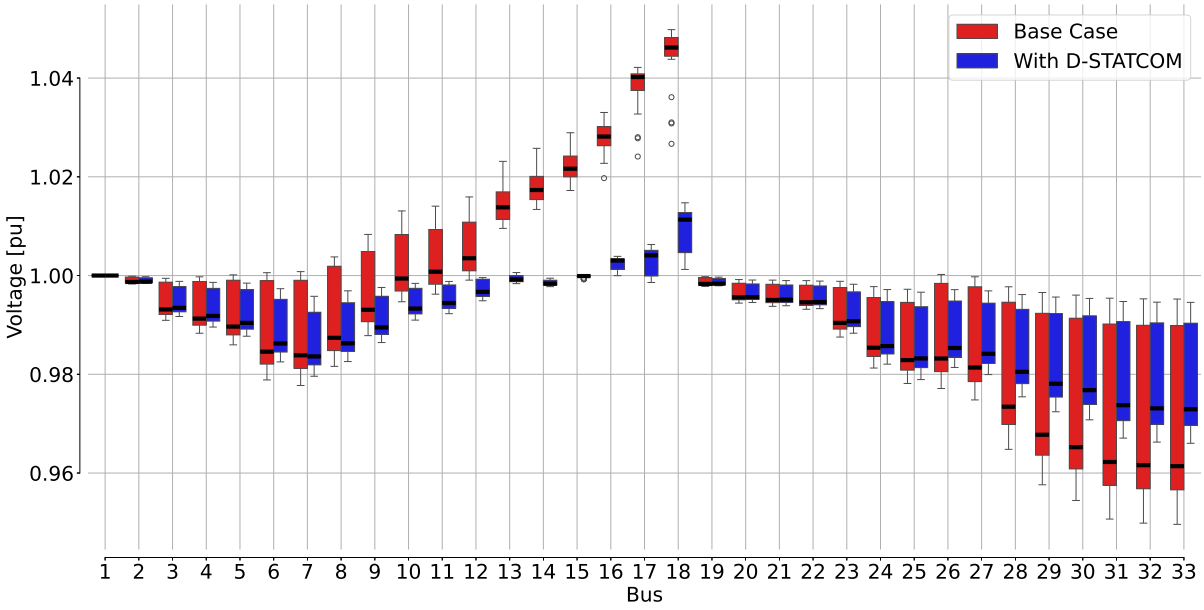

Source: Created by the author

The reactive power of the D-STATCOM devices located in this case is presented in Figure 30. It can be observed that at bus 17, which is close to bus 18, there is a device that absorbs reactive power during all periods to reduce the voltage. The devices located at buses 12 and 30 supply reactive power to enhance the voltage profile in the rest of the system and to reduce losses.

5.3.1.2 DSR

Figure 31 presents the comparison of the voltage profile of the base case with the voltage profile when considering DSR with the insertion of DER. It can be observed that DSR successfully eliminates voltages above 1 pu and improves the overall voltage profile.

5.3.1.3 DSR with Placement of D-STATCOMs

The comparison between the base case and the case considering both DSR and the placement of D-STATCOM devices simultaneously is shown in Figure 32. In this case, the results obtained with DSR alone are improved, as the voltage profile is very close to 1 pu across all buses. Additionally, a smaller variation between periods can be observed for all buses.

For the DSR and the placement of D-STATCOM devices, the same locations as in the case with D-STATCOMs alone were considered. Thus, Figure 33 presents the

Figure 30 – Reactive power of the D-STATCOMs in the 33-bus system

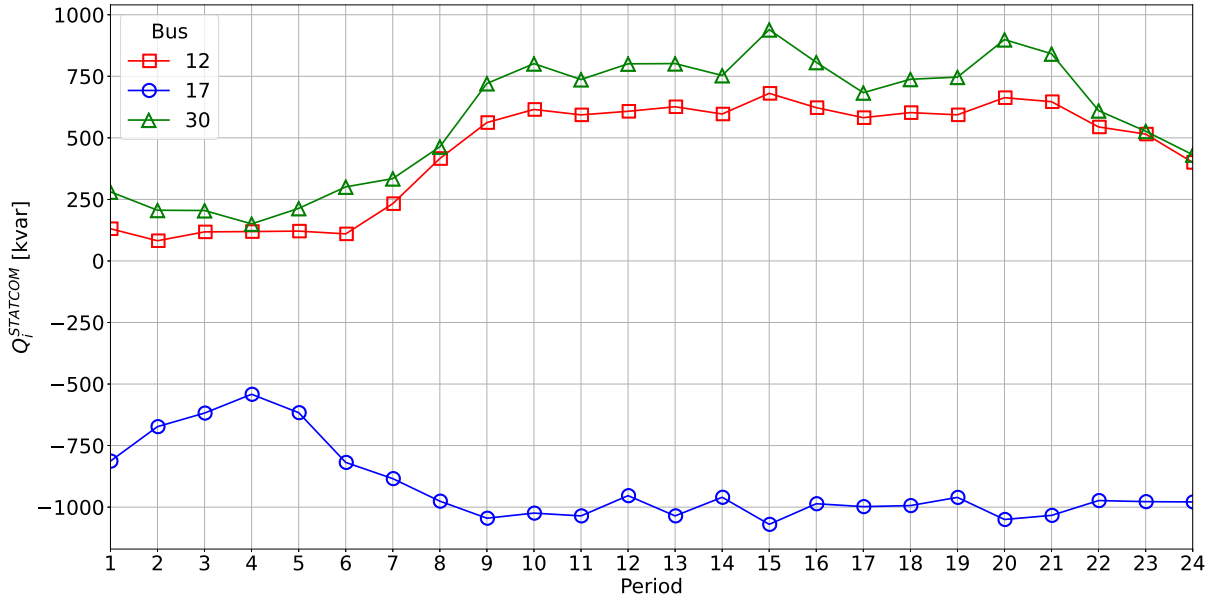

Source: Created by the author

Figure 31 – Voltage profile - Comparison between the base case and the case with reconfiguration in the 33-bus system

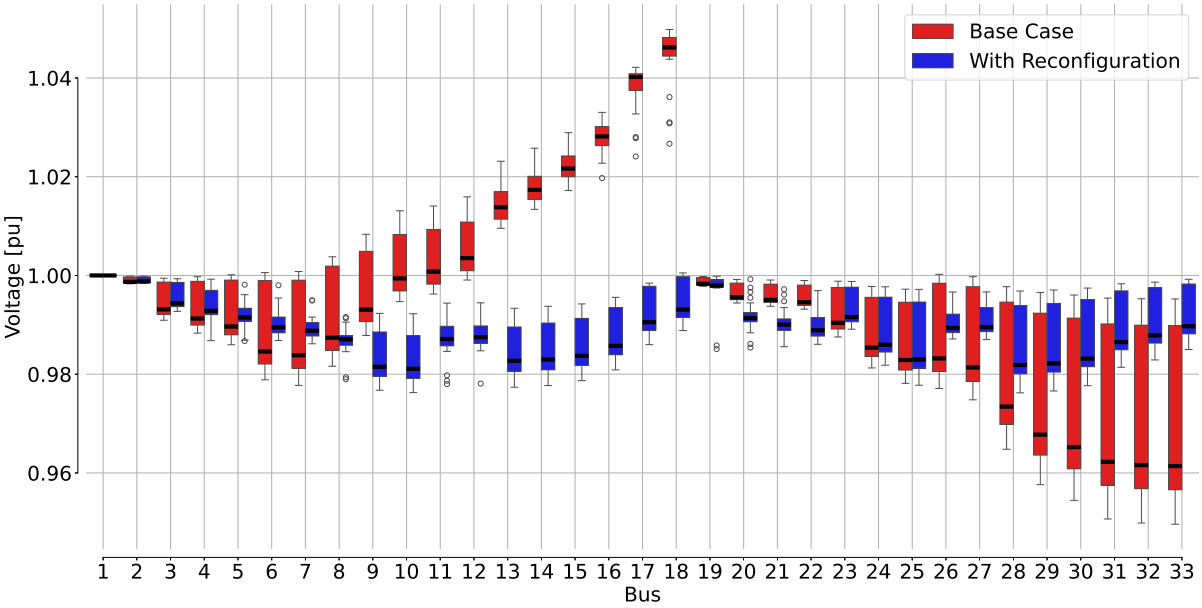

Source: Created by the author

reactive power of the devices. It can be observed that, except in a few periods, it is not necessary to absorb reactive power to decrease the voltage, as the DSR is capable of doing so on its own. Therefore, the D-STATCOM devices serve the purpose of injecting reactive power to improve the voltage profile and reduce losses. As a result, devices with a lower capacity are required compared to the case using D-STATCOMs alone, which translates into savings in investment.

Figure 32 – Voltage profile - Comparison between the base case and the case with D-STATCOMs and reconfiguration in the 33-bus system

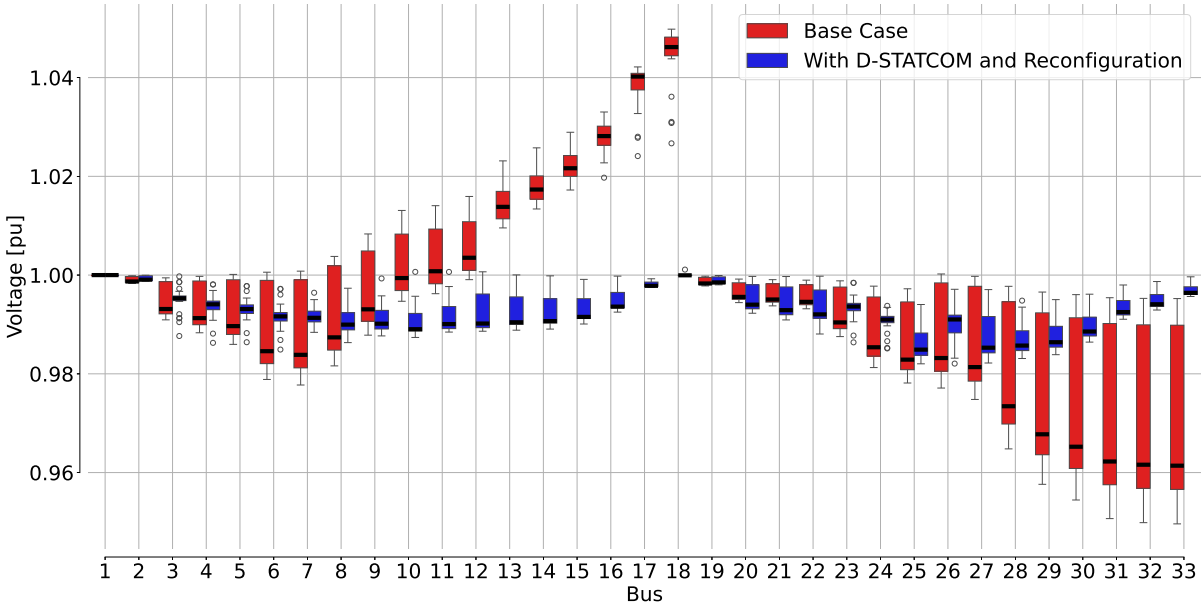

Source: Created by the author

Figure 33 – Reactive power of the D-STATCOMs considering reconfiguration in the 33-bus system

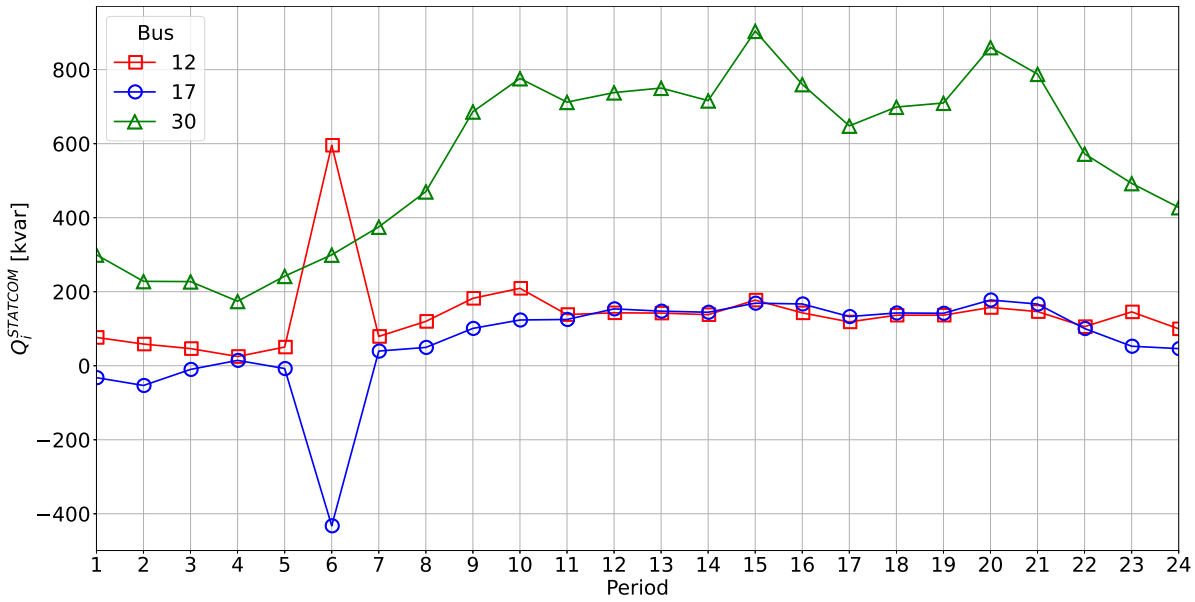

Source: Created by the author

5.3.1.4 Comparisons

In Table 6, the total losses for all periods across the four considered cases are presented. In the case with D-STATCOM devices, a decrease in voltage is achieved at the expense of increasing losses. The DSR has the capability to reduce both voltage and losses simultaneously compared to the base case. Finally, the case with both techniques applied simultaneously significantly outperforms all previous cases in terms of loss reduction.

Table 6 – Comparison of total losses for all cases in the 33-bus system

Case	**Total losses (kW)**
Base case	2733.47
D-STATCOMs	3540.92
Reconfiguration	1029.69
D-STATCOMs and reconfiguration	523.06

Source: Created by the author

In Table 7, the comparison of the topology chosen for the system for each period by the DSR, with and without D-STATCOM devices, is presented. It can be observed that there is a dominant topology in most periods, varying only in a few cases where there may be a change in demand. Additionally, it is noted that the D-STATCOM devices influence the optimal topology, as the configurations differ across all periods.

Table 7 – Comparison of open lines in the 33-bus system

Period	**Reconfiguration**	**D-STATCOMs & Reconfiguration**
1	4 6 11 18 33	2 3 6 11 33
2	3 9 19 26 33	2 3 6 11 33
3	4 9 19 25 33	2 3 6 11 33
4	4 10 19 25 33	2 6 10 22 33
5	4 6 11 19 33	2 3 6 11 33
6	4 9 18 25 33	2 14 23 26 33
7	6 9 20 25 33	3 6 10 22 33
8	7 10 12 25 33	6 9 21 23 27
9	7 10 13 27 33	5 6 9 21 24
10	7 8 10 12 27	7 9 24 25 33
11	7 8 11 12 27	7 9 24 25 35
12	7 8 10 12 27	7 10 24 27 35
13	7 8 10 12 27	7 10 24 26 35
14	7 8 10 12 27	7 9 24 26 35
15	7 8 10 12 27	7 9 24 25 35
16	7 8 10 12 27	7 10 24 26 35
17	7 8 11 12 27	7 10 24 26 35
18	7 8 10 12 27	7 10 24 26 35
19	7 8 10 12 27	7 9 24 26 35
20	7 8 10 12 27	7 10 24 26 35
21	7 8 10 12 27	7 10 24 26 35
22	7 8 10 27 35	7 10 24 26 35
23	7 10 12 27 33	7 10 24 25 33
24	7 9 25 33 35	6 9 21 23 27

Source: Created by the author

5.3.2 69-Bus Test System

For the 69-bus system, bus 27 is selected to evaluate the variation in HC during the periods of a typical day of operation. Table 8 presents the HC value, losses, and the performance index limiting the HC for the 24 periods of a typical day. During the low-load periods (2-6), the system can supply the entire load plus losses without exceeding the voltage limit. For the remaining periods, the violated performance index is the voltage.

This section evaluates the proposed techniques to expand the operational margin when connecting DER to bus 27 in the 69-bus system.

Table 8 – HC results for interconnection at bus 27 in the 69-bus system

Period	**HC (kW)**	**Limit**	**Losses (kW)**
1	1100	Voltage	56.81
2	800	Reverse PF	30.85
3	700	Reverse PF	24.25
4	700	Reverse PF	23.35
5	700	Reverse PF	24.47
6	1000	Reverse PF	48.5
7	1100	Voltage	59.82
8	1300	Voltage	91.16
9	1400	Voltage	135.12
10	1500	Voltage	166.62
11	1500	Voltage	171.88
12	1600	Voltage	199.28
13	1600	Voltage	202.2
14	1500	Voltage	170.97
15	1600	Voltage	210.58
16	1600	Voltage	195.52
17	1500	Voltage	174.3
18	1600	Voltage	188.88
19	1500	Voltage	170.25
20	1600	Voltage	225.09
21	1600	Voltage	206.92
22	1500	Voltage	158.2
23	1400	Voltage	120.94
24	1300	Voltage	89.21

Source: Created by the author

5.3.2.1 Placement of D-STATCOMs

Figure 34 shows the comparison of the voltage profile between the base case presented in Table 8 and the case considering D-STATCOM devices. It can be observed that the voltage is reduced in buses with voltages exceeding 1 pu. Additionally, one device is used to increase the voltage profile in other buses, reducing losses and improving the overall system condition.

Figure 35 shows the reactive power of the three devices located in the case considering only D-STATCOMs. It is evident that two of the three devices are absorbing reactive power, positioned near bus 27 to reduce the voltage. The other device is supplying reactive power to improve the voltage profile and reduce losses.

5.3.2.2 DSR

The comparison of the voltage profile between the base case and the case considering DSR is shown in Figure 36. It can be observed that DSR successfully eliminates voltages above 1 pu while simultaneously improving the overall condition of the system

Figure 34 – Voltage profile - Comparison between the base case and the case with D-STATCOMs in the 69-bus system

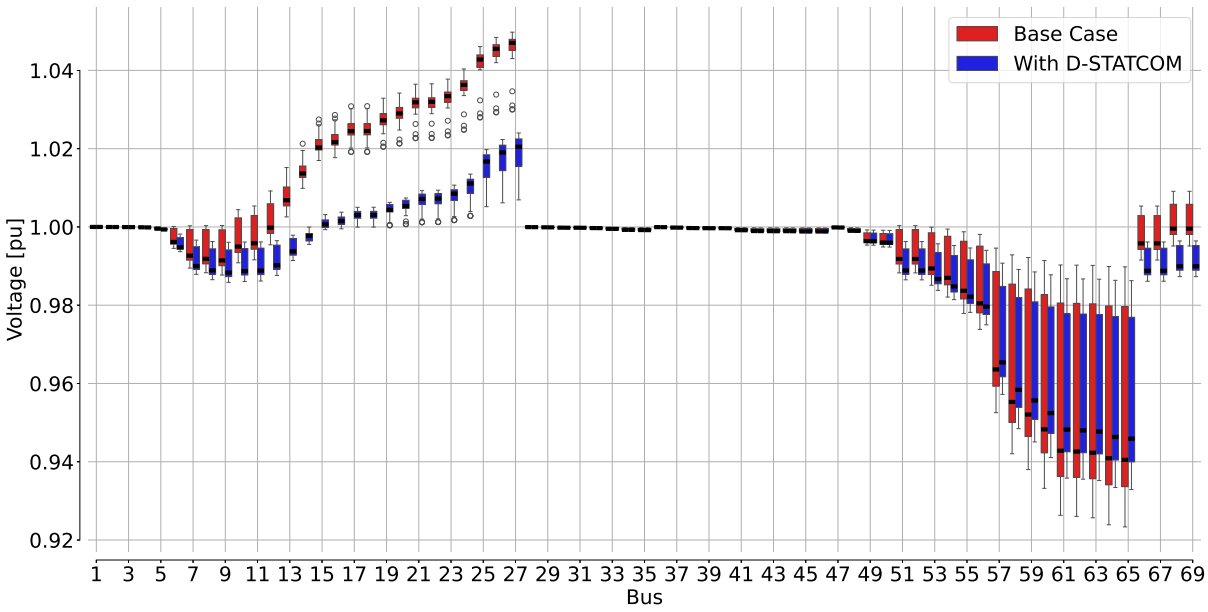

Source: Created by the author

Figure 35 – Reactive power of the D-STATCOMs in the 69-bus system

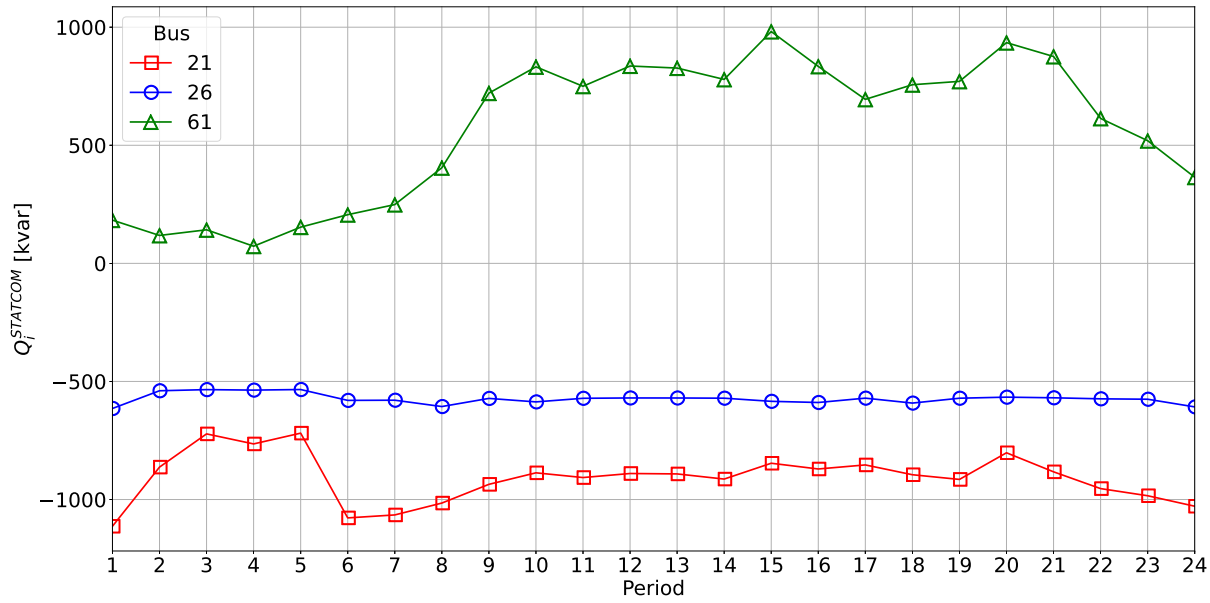

Source: Created by the author

by increasing the voltage at low-voltage buses. This results in improved system operation and a reduction in losses.

5.3.2.3 DSR with Placement of D-STATCOMs

Finally, for the case considering both DSR and D-STATCOM devices simultaneously, the same locations identified in the case with only D-STATCOMs are used. The comparison of the voltage profiles between this case and the base case is shown in Fig-

Figure 36 – Voltage profile - Comparison between the base case and the case with reconfiguration in the 69-bus system

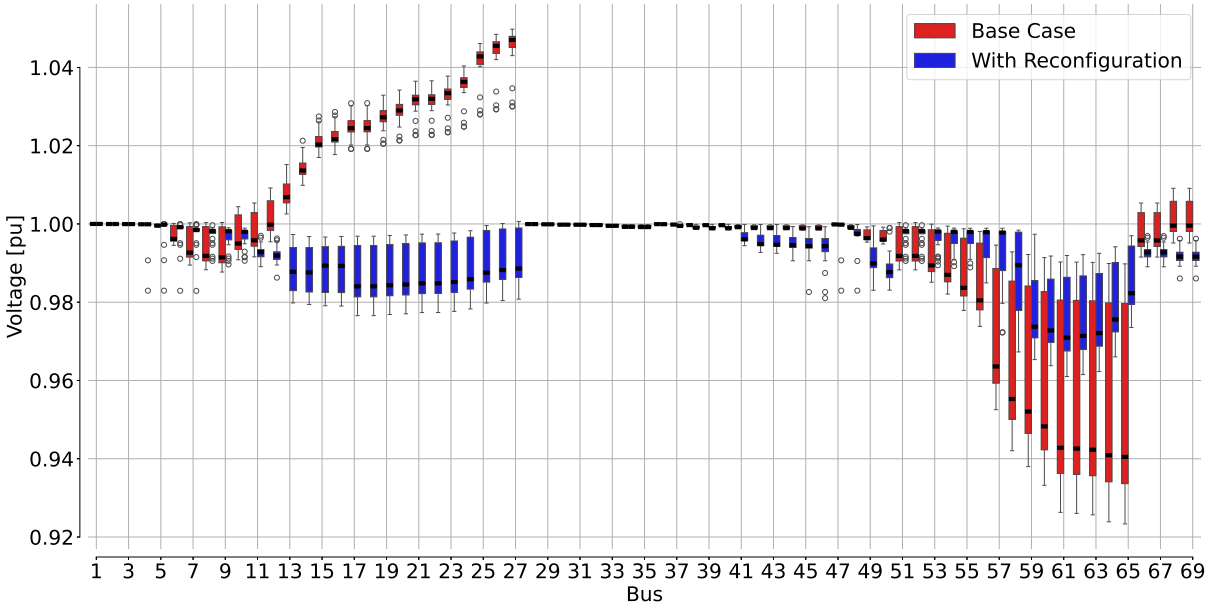

Source: Created by the author

ure 37. It can be observed that the results obtained with DSR alone are improved, as the voltages above 1 pu are eliminated and the variation in voltages across all buses is reduced.

Figure 37 – Voltage profile - Comparison between the base case and the case with D-STATCOMs and reconfiguration in the 69-bus system

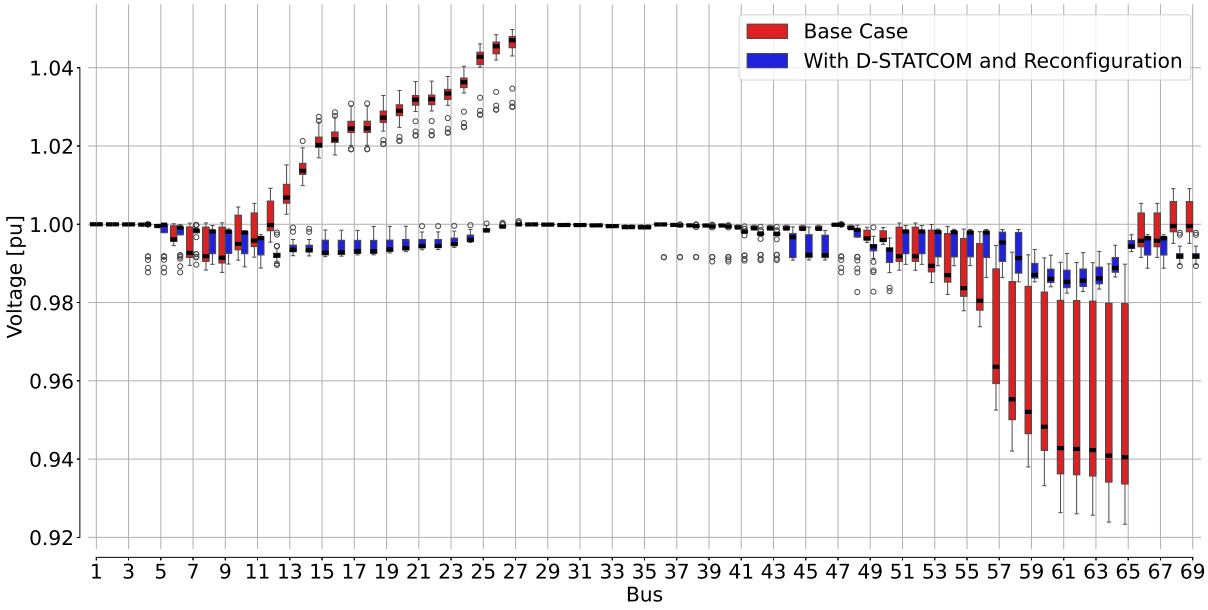

Source: Created by the author

Figure 38 presents the reactive power of the devices. The main difference in this case is that the use of D-STATCOMs to absorb reactive power and reduce voltage is hardly necessary, as the DSR is capable of eliminating voltages above 1 pu on its own.

The device at bus 26 is primarily used to control voltage during period 1, as it remains close to 0 in the subsequent periods. The other two devices are responsible for injecting reactive power to enhance the voltage profile and reduce losses.

Figure 38 – Reactive power of the D-STATCOMs considering reconfiguration in the 69-bus system

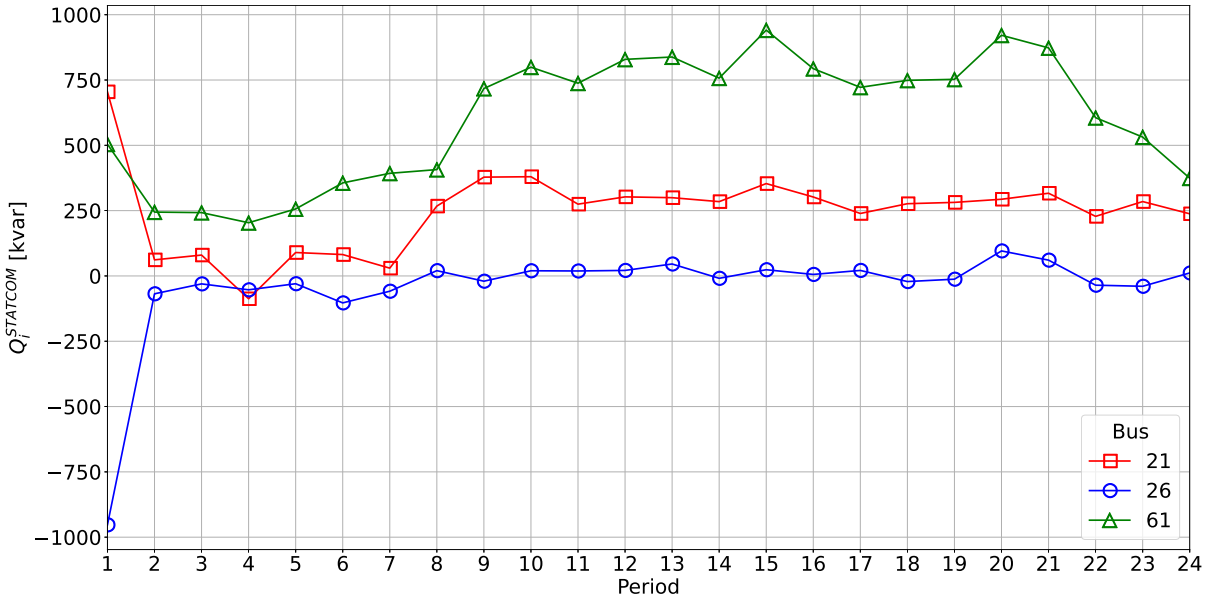

Source: Created by the author

5.3.2.4 Comparisons

The Table 9 presents a comparison of total losses among the four cases considered. The base case exhibits total losses of 3145.17 kW across all periods. The case including D-STATCOMs manages to expand the operational voltage margin at the expense of significantly increasing losses. The DSR eliminates voltages above 1 pu while simultaneously reducing losses compared to the base case. However, the best results are achieved in the case that simultaneously considers both the DSR and D-STATCOM devices, showing improvements in both the voltage profile and total losses.

Table 9 – Comparison of total losses for all cases in the 69-bus system

Case	**Total Losses (kW)**
Base case	3145.17
D-STATCOMs	5817.02
Reconfiguration	1017.78
D-STATCOMs and reconfiguration	519.54

Source: Created by the author

In Table 10, the comparison of the topology chosen for the system for each period by the DSR, with and without D-STATCOM devices, is presented. It can be observed that there is a dominant topology in most periods, varying only in a few cases where there may

be a change in demand. Additionally, it is noted that the D-STATCOM devices influence the optimal topology, as the configurations differ across all periods.

Table 10 – Comparison of open lines in the 69-bus system

Period	**Reconfiguration**	**D-STATCOMs & Reconfiguration**
1	3 14 15 49 55	8 17 45 47 56
2	7 13 49 60 69	3 14 49 52 69
3	5 14 52 69 72	3 14 49 52 69
4	3 7 12 15 58	3 6 15 55 71
5	4 14 53 69 72	3 14 49 52 69
6	8 14 49 59 69	3 14 49 52 69
7	7 13 58 59 69	4 14 49 55 69
8	10 13 55 69 71	7 14 35 59 69
9	10 12 15 45 58	9 14 39 55 69
10	10 12 16 58 71	10 14 45 56 69
11	10 12 16 58 71	10 11 14 44 56
12	10 12 16 58 71	10 11 14 43 58
13	10 12 16 58 71	10 11 14 43 57
14	10 12 16 57 71	10 11 14 44 58
15	10 12 16 57 70	10 11 14 43 58
16	10 12 16 57 71	10 11 14 43 58
17	10 12 16 56 71	10 11 15 45 58
18	10 12 15 45 58	10 11 14 44 57
19	10 12 16 56 71	10 11 14 43 58
20	10 12 16 58 70	10 11 14 57 71
21	10 12 14 16 57	10 11 14 43 58
22	10 12 15 44 58	10 11 14 43 57
23	10 11 14 56 71	9 14 38 58 69
24	10 14 43 57 69	7 14 35 59 69

Source: Created by the author

5.4 Final Remarks of the Chapter

In this chapter, the models presented in Chapter 4 were employed to calculate and enhance the HC in benchmark distribution systems available in the specialized literature. The advantages of DSR in improving the operational condition of a system were evident, such as minimizing losses and improving the voltage profile. On the other hand, the results with D-STATCOM devices, when compared to DSR, may seem less favorable. However, it is crucial to emphasize the aspect mentioned in the mathematical model formulation: in this work, D-STATCOM devices are considered solely for voltage control by injecting or absorbing reactive power. For this reason, it is important to take into account the additional benefits that this type of device can offer to a system.

6 CONCLUSIONS

A detailed review on HC was conducted, highlighting the lack of a standard for its definition and calculation. Similarly, a review of the techniques used to increase HC in PDS was carried out, with particular attention given to D-STATCOM devices for their voltage control capability and DSR for its versatility in improving the operational conditions of a system.

An iterative method was implemented to calculate the HC in PDS, which allowed not only the determination of the maximum value but also the corresponding losses and the HC limit. The employed method was evaluated using two applications, mapping and interconnection. The first aims to assess the HC of PDS at each connection point separately, thereby providing information to potential stakeholders interested in connecting DER to the system. The interconnection application seeks to determine the maximum amount of DER that a connection point can accommodate without violating any operational limit in a given scenario, providing information on the potential operation of new DER that may be connected to PDS.

D-STATCOM devices proved to be an effective option for voltage control, specifically for mitigating overvoltages or reducing losses, two objectives that inherently oppose each other and are balanced through a factor that can vary depending on the requirements of each case. These advantages make D-STATCOM devices a viable option for increasing HC in PDS, particularly in scenarios where voltage constraints are the primary limitation. The placement of D-STATCOM devices have been primarily addressed in the specialized literature using analytical and metaheuristic techniques; with some references employing classical optimization methods but of the nonlinear type. In this work, a linear optimization model was presented to solve this problem, contributing to the study of the application of such devices in PDS.

A MILP model was implemented to solve the DSR problem. This model allows for determining the optimal configuration of PDS given specific operating conditions. Additionally, a factor was considered to reduce the overvoltages caused by the integration of DER into the system. The results presented in this work demonstrate the great versatility of DSR in improving operational conditions in PDS and, in this case, enhancing HC.

A model that simultaneously considers the placement of D-STATCOMs and DSR was proposed. This model leverages the advantages of both techniques to increase HC and improve the overall system conditions. The results demonstrate that using both techniques together outperforms the other cases in effectively and safely expanding the integration of DER into PDS.

The models presented and used in this work, as well as the iterative method, were implemented in benchmark systems available in the specialized literature, demonstrating their effectiveness in increasing and calculating the HC in PDS.

Although the HC is improved in all cases, the results obtained with D-STATCOM devices alone appear to be of lower quality. However, it is important to note that the model only considers the injection or absorption of reactive power by the D-STATCOMs to control voltage in steady state, limiting its ability to represent the additional advantages of these devices. Furthermore, for the case of DSR, it was assumed that all branches can be opened or closed without regard to the number of operations. In reality, this may not be the case, and this should be considered in future work.

Finally, the computational time for large-scale PDS can be significantly elevated due to the complexity of the proposed models and the strategy employed to calculate the HC through the iterative method. Future work could focus on utilizing alternative methods for calculating HC, such as stochastic or streamlined approaches. Additionally, incorporating uncertainty in the integration of DER and demand could help obtain a range of possible HC values. Furthermore, it is also posible to explore solutions to the models presented in this study using other techniques, such as metaheuristics or analytical methods, as well as novel approaches that leverage artificial intelligence and operational historical data.

BIBLIOGRAPHY

[1] UNITED NATIONS. *Transforming our world: the 2030 Agenda for Sustainable Development*. New York, NY, 2015. A/RES/70/1. Available at: <https://documents.un.org/doc/undoc/gen/n15/291/89/pdf/n1529189.pdf>.

[2] EMPRESA DE PESQUISA ENERGÉTICA (EPE). *Balanço Energético Nacional 2024*. Rio de Janeiro – RJ – CEP: 20091-040, 2024. Available at: <https://www.epe.gov.br/sites-pt/publicacoes-dados-abertos/publicacoes/PublicacoesArquivos/publicacao-819/topico-723/BEN2024.pdf>.

[3] EMPRESA DE PESQUISA ENERGÉTICA (EPE). *Anuário Estatístico de Energia Elétrica 2024*. Rio de Janeiro – RJ – CEP: 20091-040, 2024. Available at: <https://www.epe.gov.br/pt/publicacoes-dados-abertos/publicacoes/anuario-estatistico-de-energia-eletrica>.

[4] ISMAEL, S. M. et al. State-of-the-art of hosting capacity in modern power systems with distributed generation. *Renewable Energy*, v. 130, p. 1002–1020, 2019. ISSN 0960-1481. Available at: <https://www.sciencedirect.com/science/article/pii/S0960148118307936>.

[5] EPRI. *Defining a Roadmap for Successful Implementation of a Hosting Capacity Method for New York State*. Palo Alto, CA, 2016. 3002008848.

[6] ARSHAD, A.; LEHTONEN, M. A stochastic assessment of PV hosting capacity enhancement in distribution network utilizing voltage support techniques. *IEEE Access*, v. 7, p. 46461–46471, 2019.

[7] ISMAEL, S. M. et al. Practical considerations for optimal conductor reinforcement and hosting capacity enhancement in radial distribution systems. *IEEE Access*, v. 6, p. 27268–27277, 2018.

[8] SAKAR, S. et al. Increasing PV hosting capacity in distorted distribution systems using passive harmonic filtering. *Electric Power Systems Research*, v. 148, p. 74–86, 2017. ISSN 0378-7796. Available at: <https://www.sciencedirect.com/science/article/pii/S0378779617301207>.

[9] ZHAN, H. et al. Relay protection coordination integrated optimal placement and sizing of distributed generation sources in distribution networks. *IEEE Transactions on Smart Grid*, v. 7, n. 1, p. 55–65, 2016.

[10] DAVIDSON, C.; OLIVEIRA, M. M. de. Technical description of static compensators (STATCOM). In: ANDERSEN, B. R.; NILSSON, S. L. (Ed.). *Flexible AC Transmission Systems : FACTS*. Cham: Springer International Publishing, 2020. p. 207–251. ISBN 978-3-030-35386-5. Available at: <https://doi.org/10.1007/978-3-030-35386-5_8>.

[11] CAPITANESCU, F. et al. Assessing the potential of network reconfiguration to improve distributed generation hosting capacity in active distribution systems. *IEEE Transactions on Power Systems*, v. 30, n. 1, p. 346–356, 2015.

[12] SCHWAEGERL, C. et al. Voltage control in distribution systems as a limitation of the hosting capacity for distributed energy resources. In: *CIRED 2005 - 18th International Conference and Exhibition on Electricity Distribution*. [S.l.: s.n.], 2005. p. 1–5.

[13] EPRI. *Impact Factors, Methods, and Considerations for Calculating and Applying Hosting Capacity*. Palo Alto, CA, 2018. 3002011009.

[14] EPRI. *The Hosting Capacity Process*. Palo Alto, CA, 2020. 3002019750.

[15] New York State Electric & Gas (NYSEG) and Rochester Gas and Electric (RG&E). *NYSEG/RGE Hosting Capacity Portal*. 2022. Available at: <https://www.arcgis.com/apps/instant/portfolio/index.html?appid=5fc7fc4820af48838cb5bdfd54e5baad>.

[16] CONGRESO DE COLOMBIA. *Ley 1715*. Bogotá DC, 2014. Available at: <https://www.funcionpublica.gov.co/eva/gestornormativo/norma_pdf.php?i=57353>.

[17] MINISTÉRIO DE MINAS E ENERGIA. *Ley 14300*. Brasília, 2022. Available at: <https://www.planalto.gov.br/ccivil_03/_ato2019-2022/2022/lei/l14300.htm>.

[18] KARIMI, M. et al. Photovoltaic penetration issues and impacts in distribution network – a review. *Renewable and Sustainable Energy Reviews*, v. 53, p. 594–605, 2016. ISSN 1364-0321. Available at: <https://www.sciencedirect.com/science/article/pii/S136403211500903X>.

[19] CIGRE WORKING GROUP C6.24. *Capacity of Distribution Feeders for Hosting DER*. Paris, 2014. Technical Brochure 586.

[20] EPRI. *Distribution Resource Integration and Value Estimation (DRIVE) Tool: Advancing Hosting Capacity Methods to Include Existing DER and Reactive Power Control*. Palo Alto, CA, 2016. 3002008293.

[21] IEEE TASK FORCE. Proposed terms and definitions for flexible ac transmission system (FACTS). *IEEE Transactions on Power Delivery*, v. 12, n. 4, p. 1848–1853, 1997.

[22] HINGORANI, N. G. Introducing custom power. *IEEE Spectrum*, v. 32, n. 6, p. 41–48, 1995.

[23] HINGORANI, N. G.; GYUGYI, L. FACTS concept and general system considerations. In: *Understanding FACTS*. John Wiley & Sons, Ltd, 1999. cap. 1, p. 1–35. ISBN 9780470546802. Available at: <https://onlinelibrary.wiley.com/doi/abs/10.1002/9780470546802.ch1>.

[24] MAROUANI, I. et al. Optimized FACTS devices for power system enhancement: Applications and solving methods. *Sustainability*, v. 15, p. 9348, 06 2023.

[25] KRONEBERG, A. A. Expansion of the system of the Southern California Edison Company. *Transactions of the American Institute of Electrical Engineers*, v. 69, n. 2, p. 861–864, 1950.

[26] JOLLIFFE, J. P. Pacific Northwest 1952 power shortage. *Electrical Engineering*, v. 73, n. 2, p. 111–115, 1954.

[27] GYUGYI, L. Reactive power generation and control by thyristor circuits. *IEEE Transactions on Industry Applications*, IA-15, n. 5, p. 521–532, 1979.

[28] GYUGYI, L.; TAYLOR, E. R. Characteristics of static, thyristor-controlled shunt compensators for power transmission system applications. *IEEE Transactions on Power Apparatus and Systems*, PAS-99, n. 5, p. 1795–1804, 1980.

[29] HINGORANI, N. G. Power electronics in electric utilities: role of power electronics in future power systems. *Proceedings of the IEEE*, v. 76, n. 4, p. 481–482, 1988.

[30] SCHAUDER, C. et al. Operation of ±100 MVAr TVA STATCON. *IEEE Transactions on Power Delivery*, v. 12, n. 4, p. 1805–1811, 1997.

[31] SCHAUDER, C. et al. AEP UPFC project: installation, commissioning and operation of the ±160 MVA STATCOM (phase i). *IEEE Transactions on Power Delivery*, v. 13, n. 4, p. 1530–1535, 1998.

[32] VENKATASUBRAMANIAN, V.; TAYLOR, C. Improving pacific intertie stability using slatt thyristor controlled series compensation. In: *2000 IEEE Power Engineering Society Winter Meeting. Conference Proceedings (Cat. No.00CH37077)*. [S.l.: s.n.], 2000. v. 2, p. 1468–1470 vol.2.

[33] CHEN, J. et al. Application of FACTS devices for the interconnected line between fujian network and huadong network. In: *2000 Power Engineering Society Summer Meeting (Cat. No.00CH37134)*. [S.l.: s.n.], 2000. v. 3, p. 1612–1617 vol. 3.

[34] SHAOPING, X. et al. The application of modern power electronics technology in power system-the feasibility study using phase-shifter in north-west power system. In: *POWERCON '98. 1998 International Conference on Power System Technology. Proceedings (Cat. No.98EX151)*. [S.l.: s.n.], 1998. v. 1, p. 677–681 vol.1.

[35] ALHASAWI, F. B.; MILANOVIC, J. V. Techno-economic contribution of FACTS devices to the operation of power systems with high level of wind power integration. *IEEE Transactions on Power Systems*, v. 27, n. 3, p. 1414–1421, 2012.

[36] ADAPA, R. et al. Technical description of the unified power flow controller (UPFC) and its potential variations. In: ANDERSEN, B. R.; NILSSON, S. L. (Ed.). *Flexible AC Transmission Systems : FACTS*. Cham: Springer International Publishing, 2020. p. 299–351. ISBN 978-3-030-35386-5. Available at: <https://doi.org/10.1007/978-3-030-35386-5_10>.

[37] GONG, C.; SOU, W.-K.; LAM, C.-S. Reinforcement learning based sliding mode control for a Hybrid-STATCOM. *IEEE Transactions on Power Electronics*, v. 38, n. 6, p. 6795–6800, 2023.

[38] MITRA, P. et al. Simulations and field experience of Opladen STATCOM with grid-forming behavior. In: CIGRE NATIONAL COMMITTEE. *B4 International SC Meeting and Colloquium*. [S.l.], 2023.

[39] MOHANTY, A.; BARIK, A. Power system stability improvement using FACTS devices. *International Journal of Modern Engineering Research (IJMER)*, v. 1, n. 2, p. 666–672, 2011. ISSN 2249-6645.

[40] AHMAD, A. A.; SIRJANI, R. Optimal placement and sizing of multi-type FACTS devices in power systems using metaheuristic optimisation techniques: An updated review. *Ain Shams Engineering Journal*, v. 11, n. 3, p. 611–628, 2020. ISSN 2090-4479. Available at: <https://www.sciencedirect.com/science/article/pii/S2090447919301510>.

[41] PADIYAR, K. R. Load compensation and distribution STATCOM. In: *FACTS Controllers in Power Transmission and Distribution*. 4835/24, Ansari Road, Daryaganj, New Delhi - 110002: New Age International (P) Ltd., Publishers, 2007. cap. 13, p. 433–465. ISBN 978-81-224-2541-3.

[42] LIU, J. et al. Review and prospect of active distribution system planning. *Journal of Modern Power Systems and Clean Energy*, v. 3, n. 4, p. 457–467, 2015.

[43] ANDERSEN, B. R.; WOODFORD, D.; LOVE, G. FACTS planning studies. In: ANDERSEN, B. R.; NILSSON, S. L. (Ed.). *Flexible AC Transmission Systems : FACTS*. Cham: Springer International Publishing, 2020. p. 753–785. ISBN 978-3-030-35386-5. Available at: <https://doi.org/10.1007/978-3-030-35386-5_17>.

[44] MONTOYA, O. D. et al. Genetic-convex model for dynamic reactive power compensation in distribution networks using d-statcoms. *Applied Sciences*, v. 11, n. 8, 2021. ISSN 2076-3417. Available at: <https://www.mdpi.com/2076-3417/11/8/3353>.

[45] SIRJANI, R.; Rezaee Jordehi, A. Optimal placement and sizing of distribution static compensator (d-statcom) in electric distribution networks: A review. *Renewable and Sustainable Energy Reviews*, v. 77, p. 688–694, 2017. ISSN 1364-0321. Available at: <https://www.sciencedirect.com/science/article/pii/S1364032117305415>.

[46] SINHA, S. et al. Optimal placement of D-STATCOM for reduction of power loss and improvement of voltage profile using power stability and power loss indices in a radial distribution system. In: *2019 IEEE 5th International Conference for Convergence in Technology (I2CT)*. [S.l.: s.n.], 2019. p. 1–4.

[47] GUPTA, A. R.; KUMAR, A. Optimal placement of D-STATCOM using sensitivity approaches in mesh distribution system with time variant load models under load growth. *Ain Shams Engineering Journal*, v. 9, n. 4, p. 783–799, 2018. ISSN 2090-4479. Available at: <https://www.sciencedirect.com/science/article/pii/S2090447916300855>.

[48] HUSSAIN, S. Identification of weak buses using voltage stability indicator and its voltage profile improvement by using DSTATCOM in radial distribution systems. *IOSR Journal of Electrical and Electronics Engineering*, v. 2, p. 17–23, 01 2012.

[49] GUPTA, A. R.; KUMAR, A. Reactive power deployment and cost benefit analysis in DNO operated distribution electricity markets with D-STATCOM. *Frontiers in Energy*, v. 13, n. 1, p. 86–98, 2019. ISSN 2095-1698. Available at: <https://doi.org/10.1007/s11708-017-0456-8>.

[50] ARYA, A. K.; KUMAR, A.; CHANANA, S. Analysis of distribution system with D-STATCOM by gravitational search algorithm (GSA). *Journal of The Institution of Engineers (India): Series B*, v. 100, n. 3, p. 207–215, 2019. ISSN 2250-2114. Available at: <https://doi.org/10.1007/s40031-019-00383-2>.

[51] SHAHRYARI, H. S. E.; MORADZADEH, M. Probabilistic and multi-objective placement of D-STATCOM in distribution systems considering load uncertainty. *Electric Power Components and Systems*, Taylor & Francis, v. 46, n. 1, p. 27–42, 2018. Available at: <https://doi.org/10.1080/15325008.2018.1431819>.

[52] THANGARAJ, Y.; KUPPAN, R. Multi-objective simultaneous placement of DG and DSTATCOM using novel lightning search algorithm. *Journal of Applied Research and Technology*, v. 15, n. 5, Jun. 2019. Available at: <https://jart.icat.unam.mx/index.php/jart/article/view/692>.

[53] GHATAK, S. R.; SANNIGRAHI, S.; ACHARJEE, P. Comparative performance analysis of DG and DSTATCOM using improved PSO based on success rate for deregulated environment. *IEEE Systems Journal*, v. 12, n. 3, p. 2791–2802, 2018.

[54] MONTOYA, O. D.; GIL-GONZÁLEZ, W.; HERNÁNDEZ, J. C. Efficient operative cost reduction in distribution grids considering the optimal placement and sizing of D-STATCOMs using a discrete-continuous VSA. *Applied Sciences*, v. 11, n. 5, 2021. ISSN 2076-3417. Available at: <https://www.mdpi.com/2076-3417/11/5/2175>.

[55] GARCÍA-PINEDA, L. P.; MONTOYA, O. D. Optimal reactive power compensation via D-STATCOMs in electrical distribution systems by applying the generalized normal distribution optimizer. *Algorithms*, v. 16, n. 1, 2023. ISSN 1999-4893. Available at: <https://www.mdpi.com/1999-4893/16/1/29>.

[56] BARRETO-PARRA, G. F.; CORTÉS-CAICEDO, B.; MONTOYA, O. D. Optimal integration of D-STATCOMs in radial and meshed distribution networks using a MATLAB-GAMS interface. *Algorithms*, v. 16, n. 3, 2023. ISSN 1999-4893. Available at: <https://www.mdpi.com/1999-4893/16/3/138>.

[57] ISMAIL, B. et al. A comprehensive review on optimal location and sizing of reactive power compensation using hybrid-based approaches for power loss reduction, voltage stability improvement, voltage profile enhancement and loadability enhancement. *IEEE Access*, v. 8, p. 222733–222765, 2020.

[58] DEVABALAJI, K.; RAVI, K. Optimal size and siting of multiple DG and DSTATCOM in radial distribution system using bacterial foraging optimization algorithm. *Ain Shams Engineering Journal*, v. 7, n. 3, p. 959–971, 2016. ISSN 2090-4479. Available at: <https://www.sciencedirect.com/science/article/pii/S2090447915001069>.

[59] ABDRABO, M. et al. Optimal allocation of multiple D-STATCOM in distribution system using PSO. *Mansoura Engineering Journal*, v. 44, n. 2, 2020. Available at: <https://doi.org/10.21608/bfemu.2020.95020>.

[60] SELIM, A.; KAMEL, S.; JURADO, F. Hybrid optimization technique for optimal placement of DG and D-STATCOM in distribution networks. In: *2018 Twentieth International Middle East Power Systems Conference (MEPCON)*. [S.l.: s.n.], 2018. p. 689–693.

[61] YUVARAJ, T.; RAVI, K.; DEVABALAJI, K. DSTATCOM allocation in the radial distribution networks with different stability indices using bat algorithm. *Gazi University Journal of Science*, Gazi University, v. 30, n. 4, p. 314–328, 2017.

[62] MONTOYA, O. D.; ALVARADO-BARRIOS, L.; HERNÁNDEZ, J. C. An approximate mixed-integer convex model to reduce annual operating costs in radial distribution networks using STATCOMs. *Electronics*, v. 10, n. 24, 2021. ISSN 2079-9292. Available at: <https://www.mdpi.com/2079-9292/10/24/3102>.

[63] GARRIDO, V. M. et al. Optimal reactive power compensation in distribution networks with radial and meshed structures using D-STATCOMs: A mixed-integer convex approach. *Sensors*, v. 22, n. 22, 2022. ISSN 1424-8220. Available at: <https://www.mdpi.com/1424-8220/22/22/8676>.

[64] MONTOYA, O. D.; GARCES, A.; GIL-GONZÁLEZ, W. Minimization of the distribution operating costs with D-STATCOMS: A mixed-integer conic model. *Electric Power Systems Research*, v. 212, p. 108346, 2022. ISSN 0378-7796. Available at: <https://www.sciencedirect.com/science/article/pii/S037877962200520X>.

[65] GIL-GONZÁLEZ, W. Optimal placement and sizing of D-STATCOMs in electrical distribution networks using a stochastic mixed-integer convex model. *Electronics*, v. 12, n. 7, 2023. ISSN 2079-9292. Available at: <https://www.mdpi.com/2079-9292/12/7/1565>.

[66] LAVORATO, M. et al. Imposing radiality constraints in distribution system optimization problems. *IEEE Transactions on Power Systems*, v. 27, n. 1, p. 172–180, 2012.

[67] AMINI, M.; JALILIAN, A.; BEHBAHANI, M. R. P. A new method for evaluation of harmonic distortion in reconfiguration of distribution network. *International Transactions on Electrical Energy Systems*, v. 30, n. 6, p. e12370, 2020. Available at: <https://onlinelibrary.wiley.com/doi/abs/10.1002/2050-7038.12370>.

[68] HONG, H. et al. Directed graph-based distribution network reconfiguration for operation mode adjustment and service restoration considering distributed generation. *Journal of Modern Power Systems and Clean Energy*, v. 5, n. 1, p. 142–149, 2017.

[69] GEREZ, C. et al. Distribution network reconfiguration using selective firefly algorithm and a load flow analysis criterion for reducing the search space. *IEEE Access*, v. 7, p. 67874–67888, 2019.

[70] BEHBAHANI, M. R. et al. Comprehensive review on static and dynamic distribution network reconfiguration methodologies. *IEEE Access*, v. 12, p. 9510–9525, 2024.

[71] MERLIN, A.; BACK, H. Search for a minimal loss operating spanning tree configuration in an urban power distribution system. In: *Power Systems Computation Conference*. Cambridge, UK: [s.n.], 1975. p. 1–18.

[72] CIVANLAR, S. et al. Distribution feeder reconfiguration for loss reduction. *IEEE Transactions on Power Delivery*, v. 3, n. 3, p. 1217–1223, 1988.

[73] BARAN, M.; WU, F. Network reconfiguration in distribution systems for loss reduction and load balancing. *IEEE Transactions on Power Delivery*, v. 4, n. 2, p. 1401–1407, 1989.

[74] SHIRMOHAMMADI, D.; HONG, H. Reconfiguration of electric distribution networks for resistive line losses reduction. *IEEE Transactions on Power Delivery*, v. 4, n. 2, p. 1492–1498, 1989.

[75] NARA, K. et al. Implementation of genetic algorithm for distribution systems loss minimum re-configuration. *IEEE Transactions on Power Systems*, v. 7, n. 3, p. 1044–1051, 1992.

[76] WU, W.; TSAI, M. Application of enhanced integer coded particle swarm optimization for distribution system feeder reconfiguration. *IEEE Transactions on Power Systems*, v. 26, n. 3, p. 1591–1599, 2011.

[77] WU, Y. et al. Study of reconfiguration for the distribution system with distributed generators. *IEEE Transactions on Power Delivery*, v. 25, n. 3, p. 1678–1685, 2010.

[78] JEON, Y. et al. An efficient simulated annealing algorithm for network reconfiguration in large-scale distribution systems. *IEEE Transactions on Power Delivery*, v. 17, n. 4, p. 1070–1078, 2002.

[79] JABR, R. A.; SINGH, R.; PAL, B. C. Minimum loss network reconfiguration using mixed-integer convex programming. *IEEE Transactions on Power Systems*, v. 27, n. 2, p. 1106–1115, 2012.

[80] BORGES, M. C. O.; FRANCO, J. F.; RIDER, M. J. Optimal reconfiguration of electrical distribution systems using mathematical programming. *Journal of Control, Automation and Electrical Systems*, v. 25, n. 1, p. 103–111, 2014.

[81] ZHAI, H. et al. Dynamic reconfiguration of three-phase unbalanced distribution networks. *International Journal of Electrical Power & Energy Systems*, v. 99, p. 1–10, 2018. ISSN 0142-0615. Available at: <https://www.sciencedirect.com/science/article/pii/S0142061517321555>.

[82] GALLEGO, L. A.; LÓPEZ-LEZAMA, J. M.; CARMONA, O. G. A mixed-integer linear programming model for simultaneous optimal reconfiguration and optimal placement of capacitor banks in distribution networks. *IEEE Access*, v. 10, p. 52655–52673, 2022.

[83] SEREETER, B.; VUIK, C.; WITTEVEEN, C. On a comparison of newton–raphson solvers for power flow problems. *Journal of Computational and Applied Mathematics*, v. 360, p. 157–169, 2019. ISSN 0377-0427. Available at: <https://www.sciencedirect.com/science/article/pii/S0377042719301876>.

[84] SHIRMOHAMMADI, D. et al. A compensation-based power flow method for weakly meshed distribution and transmission networks. *IEEE Transactions on Power Systems*, v. 3, n. 2, p. 753–762, 1988.

Appendix

APPENDIX A – DETAILED RESULTS FOR MAPPING

A.1 33-Bus Test System

Table 11 – HC results for mapping in the 33-bus system - Base case

Bus	**HC (kW)**	**Limit**	**Losses (kW)**
2	3900	Reverse PF	192.85
3	3800	Reverse PF	152.84
4	3800	Reverse PF	142.74
5	3800	Reverse PF	135.28
6	3800	Reverse PF	124.0
7	3800	Reverse PF	131.88
8	3800	Reverse PF	163.82
9	3900	Reverse PF	227.7
10	3800	Voltage	272.8
11	3700	Voltage	270.12
12	3500	Voltage	262.56
13	2900	Voltage	242.71
14	2800	Voltage	247.27
15	2600	Voltage	238.96
16	2400	Voltage	232.93
17	2200	Voltage	238.62
18	2000	Voltage	226.68
19	3500	Current	202.98
20	3500	Current	294.35
21	3300	Current	304.64
22	2600	Current	285.8
23	3400	Current	167.51
24	3300	Current	195.49
25	2900	Current	214.4
26	3200	Current	114.4
27	3200	Current	122.28
28	3100	Current	149.02
29	3100	Current	173.19
30	3000	Current	181.42
31	2900	Current	208.08
32	2800	Current	209.79
33	2600	Current	203.68

Source: Created by the author

Table 12 – HC results for mapping in the 33-bus system - With D-STATCOMs

Bus	**HC (kW)**	**Limit**	**Losses (kW)**	**D-STATCOM [Bus (kvar)]**
2	3800	Reverse PF	123.09	13 (375.24), 24 (525.0), 30 (1016.19)
3	3800	Reverse PF	89.65	2 (837.09), 13 (357.09), 30 (1001.35)
4	3800	Reverse PF	88.97	2 (1288.51), 14 (192.92), 30 (714.9)
5	3800	Reverse PF	87.97	2 (1392.4), 4 (-369.46), 30 (1006.68)
6	3800	Reverse PF	87.5	7 (-503.3), 24 (509.35), 30 (854.28)
7	3800	Reverse PF	97.83	7 (-634.83), 24 (537.75), 30 (910.04)

Continued on next page

Bus	**HC (kW)**	**Limit**	**Losses (kW)**	**D-STATCOM [Bus (kvar)]**
8	3900	Reverse PF	188.94	3 (2000.0), 7 (-2000.0), 30 (1096.78)
9	3900	Reverse PF	253.29	5 (967.12), 10 (-1262.49), 30 (819.63)
10	4100	Current	395.44	5 (897.58), 14 (-1330.51), 30 (681.72)
11	4100	Reverse PF	435.77	7 (-663.13), 15 (-1213.69), 30 (1380.04)
12	3800	Current	414.4	11 (-835.37), 12 (2000.0), 15 (-1748.88)
13	3700	Voltage	548.41	11 (-1002.2), 13 (1887.98), 17 (-1841.89)
14	3600	Voltage	485.64	5 (1770.23), 10 (-1964.14), 30 (967.58)
15	3500	Voltage	501.42	10 (-839.45), 14 (-750.84), 30 (1295.6)
16	3300	Voltage	491.14	14 (-526.94), 18 (-702.52), 30 (1072.07)
17	3100	Voltage	488.87	5 (1192.74), 17 (-1134.15), 30 (831.23)
18	3100	Voltage	531.5	5 (1355.95), 17 (-1198.56), 30 (932.13)
19	3500	Current	133.1	13 (375.24), 24 (525.0), 30 (1016.19)
20	3500	Current	259.34	20 (2000.0), 22 (-1888.99), 30 (1227.67)
21	3300	Current	247.13	12 (459.17), 22 (-553.32), 30 (1044.12)
22	2600	Current	230.2	12 (459.17), 21 (-683.33), 30 (1044.12)
23	3400	Current	101.39	13 (375.24), 25 (247.33), 30 (1016.19)
24	3400	Current	132.05	13 (347.68), 24 (383.17), 30 (989.17)
25	2900	Current	147.78	7 (394.21), 14 (275.29), 30 (903.21)
26	3400	Current	67.94	16 (147.8), 25 (367.26), 30 (676.08)
27	3400	Current	80.42	17 (94.88), 25 (340.98), 30 (644.42)
28	3400	Current	172.41	27 (-383.79), 28 (2000.0), 31 (-1110.74)
29	3300	Current	189.9	28 (-431.45), 29 (1621.29), 33 (-958.72)
30	3200	Current	207.71	29 (-699.16), 30 (2000.0), 33 (-1202.57)
31	2900	Current	199.61	5 (1039.51), 14 (273.21), 33 (-360.22)
32	2800	Current	202.21	5 (1235.86), 14 (315.13), 31 (-424.67)
33	2600	Current	183.34	5 (1178.14), 14 (333.69), 32 (-275.18)

Source: Created by the author

Table 13 – HC results for mapping in the 33-bus system - With reconfiguration

Bus	**HC (kW)**	**Limit**	**Losses (kW)**	**Open Lines**
2	3800	Reverse PF	130.38	7 9 14 32 37
3	3800	Reverse PF	106.7	9 14 28 32 33
4	3800	Reverse PF	116.03	10 14 28 31 33
5	3800	Reverse PF	118.7	11 14 32 33 37
6	3800	Reverse PF	118.85	11 13 20 32 37
7	3800	Reverse PF	124.43	11 13 20 32 37
8	3800	Reverse PF	141.33	14 18 31 35 37
9	3900	Reverse PF	188.65	14 18 24 30 33
10	4000	Reverse PF	293.91	3 30 33 34 37
11	3900	Reverse PF	271.25	4 30 33 34 37
12	3900	Reverse PF	257.67	5 30 33 34 37
13	4000	Reverse PF	343.36	5 9 29 33 37
14	4000	Reverse PF	344.41	4 9 29 33 37
15	4000	Reverse PF	302.26	9 18 25 33 37
16	4000	Reverse PF	323.26	3 9 18 28 33
17	4000	Reverse PF	292.51	4 9 18 27 33
18	3900	Reverse PF	253.05	5 10 19 25 33
19	3800	Reverse PF	134.49	7 9 14 32 37
20	3900	Reverse PF	190.45	5 8 14 31 37
21	3800	Reverse PF	158.34	3 11 28 30 34
22	3900	Reverse PF	215.29	4 28 30 33 34
23	3800	Reverse PF	110.63	9 14 28 32 33
24	3800	Reverse PF	117.23	11 14 25 33 34

Continued on next page

Bus	**HC (kW)**	**Limit**	**Losses (kW)**	**Open Lines**
25	3800	Reverse PF	125.77	5 10 14 33 34
26	3800	Current	140.53	11 12 15 24 33
27	3800	Current	148.5	14 24 33 34 35
28	3800	Reverse PF	163.08	11 13 15 23 33
29	3800	Reverse PF	127.71	5 11 14 33 34
30	3800	Current	171.87	5 7 10 21 33
31	3700	Current	183.78	4 7 9 33 35
32	3900	Reverse PF	217.8	4 6 9 21 33
33	3700	Current	211.09	5 6 9 21 33

Source: Created by the author

Table 14 – HC results for mapping in the 33-bus system - With D-STATCOMs and reconfiguration

Bus	**HC (kW)**	**Limit**	**Losses (kW)**	**D-STATCOM [Bus (kvar)]**	**Open Lines**
2	3800	Reverse PF	86.94	8 (572.21), 25 (673.91), 30 (1119.4)	7 9 14 36 37
3	3800	Reverse PF	86.97	2 (1130.29), 25 (808.96), 33 (426.33)	26 33 34 35 36
4	3900	Reverse PF	190.49	2 (888.93), 4 (1557.45)	11 15 18 24 35
5	3800	Reverse PF	88.71	2 (975.21), 12 (264.1), 30 (800.82)	14 18 35 36 37
6	3700	Reverse PF	58.19	9 (354.12), 24 (505.47), 30 (936.04)	2 13 17 21 37
7	3700	Reverse PF	58.6	11 (316.56), 23 (428.33), 30 (1070.26)	2 14 24 32 35
8	3900	Reverse PF	185.78	2 (1980.45), 25 (395.14), 30 (95.31)	4 9 32 35 37
9	3800	Reverse PF	97.78	3 (571.66), 25 (375.58), 30 (867.84)	2 14 24 29 33
10	3900	Reverse PF	187.14	2 (629.64), 4 (820.62), 30 (994.08)	2 32 33 34 37
11	3900	Reverse PF	192.97	2 (1050.73), 12 (-54.67), 28 (1452.16)	5 22 31 33 34
12	4000	Reverse PF	290.17	2 (2000.0), 11 (-615.95), 30 (1175.79)	3 12 28 30 33
13	3800	Current	171.24	7 (434.74), 12 (-380.65), 30 (1100.12)	3 9 24 28 33
14	4000	Reverse PF	292.32	2 (1981.04), 30 (1111.59), 32 (-508.0)	7 9 23 28 33
15	4100	Reverse PF	395.94	2 (1701.01), 5 (1473.37), 15 (-515.01)	10 14 20 24 26
16	3800	Reverse PF	135.02	6 (544.8), 24 (335.19), 30 (957.5)	2 11 23 28 33
17	3900	Reverse PF	189.49	2 (1055.64), 17 (80.1), 25 (1347.38)	3 7 11 22 33
18	3900	Reverse PF	193.62	2 (802.1), 21 (373.85), 29 (1305.64)	2 7 9 28 35
19	3800	Reverse PF	88.6	8 (332.79), 24 (649.44), 30 (988.35)	7 9 14 32 37
20	3900	Reverse PF	188.95	2 (1969.04), 20 (-801.16), 30 (1303.83)	3 14 34 35 37
21	4000	Reverse PF	311.15	2 (318.77), 24 (1452.72), 33 (782.07)	2 11 15 28 34
22	3800	Reverse PF	134.96	24 (278.68), 25 (369.72), 30 (883.67)	4 8 24 29 34
23	3800	Reverse PF	87.92	2 (1961.83), 23 (-942.58), 30 (1177.64)	11 13 15 26 33
24	3800	Reverse PF	89.42	7 (373.25), 24 (-452.53), 30 (1128.1)	5 11 13 33 34
25	3900	Reverse PF	197.04	2 (1517.71), 6 (409.17), 8 (535.91)	6 9 13 20 23
26	3800	Reverse PF	87.66	2 (889.87), 15 (388.7), 25 (1092.84)	14 18 21 22 31
27	3800	Reverse PF	86.54	2 (886.66), 7 (573.9), 30 (910.16)	2 14 17 21 24
28	3800	Reverse PF	87.12	6 (-1108.08), 7 (1577.7), 30 (1311.93)	2 3 12 21 34
29	3800	Reverse PF	87.3	2 (710.28), 21 (823.05), 23 (838.51)	3 13 20 21 34
30	3800	Reverse PF	87.45	7 (498.07), 14 (366.41), 24 (679.45)	3 8 11 18 21
31	3800	Current	121.63	7 (431.23), 16 (359.32), 25 (894.05)	2 4 11 33 34
32	3900	Reverse PF	188.11	3 (706.03), 19 (1184.54), 33 (462.77)	2 3 7 14 35
33	3800	Reverse PF	135.31	13 (346.21), 24 (568.23), 30 (732.63)	2 4 7 11 33

Source: Created by the author

A.2 69-Bus Test System

Table 15 – HC results for mapping in the 69-bus system - Base case

Bus	**HC (kW)**	**Limit**	**Losses (kW)**
2	4000	Reverse PF	224.94
3	4000	Reverse PF	224.88
4	4000	Reverse PF	224.73
5	4000	Reverse PF	223.27
6	4000	Reverse PF	202.81
7	3900	Reverse PF	182.08
8	3900	Reverse PF	177.55
9	3900	Reverse PF	175.45
10	4000	Reverse PF	224.42
11	4000	Reverse PF	235.28
12	4000	Reverse PF	281.13
13	3800	Voltage	331.32
14	3000	Voltage	299.21
15	2600	Voltage	290.42
16	2500	Voltage	284.85
17	2400	Voltage	283.23
18	2400	Voltage	283.34
19	2200	Voltage	270.48
20	2200	Voltage	274.93
21	2100	Voltage	271.46
22	2100	Voltage	271.76
23	2000	Voltage	264.92
24	2000	Voltage	271.7
25	1800	Voltage	264.39
26	1700	Voltage	258.99
27	1700	Voltage	261.55
28	3800	Current	225.26
29	3800	Current	230.81
30	3800	Current	265.06
31	3800	Current	270.97
32	3900	Current	303.98
33	3900	Current	373.3
34	2500	Voltage	343.17
35	1700	Voltage	303.04
36	3900	Current	225.26
37	3900	Current	230.82
38	3900	Current	240.03
39	3900	Current	242.67
40	3900	Current	242.83
41	3900	Current	305.68
42	3900	Current	331.3
43	3900	Current	334.64
44	3900	Current	335.39
45	3800	Current	338.22
46	3800	Current	338.29
47	4000	Reverse PF	224.92
48	4000	Reverse PF	229.79
49	4000	Reverse PF	247.4
50	4000	Reverse PF	253.9
51	3800	Current	184.81
52	3800	Current	213.97

Continued on next page

Bus	**HC (kW)**	**Limit**	**Losses (kW)**
53	3900	Reverse PF	175.08
54	3900	Reverse PF	174.87
55	3900	Reverse PF	175.2
56	3900	Reverse PF	176.14
57	3900	Reverse PF	185.85
58	4000	Reverse PF	202.11
59	4000	Reverse PF	205.88
60	4000	Reverse PF	212.5
61	4000	Voltage	221.61
62	3900	Voltage	216.14
63	3800	Voltage	213.73
64	3500	Voltage	218.9
65	3000	Voltage	212.84
66	3800	Current	242.51
67	3800	Current	242.9
68	3800	Current	322.86
69	3800	Current	323.21

Source: Created by the author

Table 16 – HC results for mapping in the 69-bus system - With D-STATCOMs

Bus	**HC (kW)**	**Limit**	**Losses (kW)**	**D-STATCOM [Bus (kvar)]**
2	4000	Reverse PF	215.56	67 (1656.86), 68 (325.62), 69 (20.0)
3	3900	Reverse PF	145.08	11 (383.38), 21 (231.05), 61 (1199.5)
4	3900	Reverse PF	144.94	11 (383.38), 21 (231.05), 61 (1199.5)
5	4000	Reverse PF	209.88	67 (237.08), 68 (1023.58), 69 (20.0)
6	4000	Reverse PF	203.53	4 (1734.37), 6 (-96.87), 48 (957.55)
7	3900	Reverse PF	113.98	18 (292.6), 51 (-475.44), 61 (1193.04)
8	4000	Reverse PF	199.1	4 (2000.0), 60 (-204.74)
9	3900	Reverse PF	110.41	8 (-669.76), 18 (292.6), 61 (1186.85)
10	4300	Reverse PF	504.94	4 (2000.0), 10 (-2000.0), 11 (-1695.84)
11	4400	Reverse PF	618.2	11 (-2000.0), 12 (-398.64), 66 (-1845.97)
12	4500	Current	720.66	14 (-1159.21), 66 (-1158.4), 68 (-1625.17)
13	4400	Reverse PF	613.53	9 (-1109.62), 23 (-2000.0), 61 (1194.79)
14	4000	Voltage	635.61	9 (-1101.65), 23 (-2000.0), 61 (1194.79)
15	3400	Voltage	570.18	5 (-2000.0), 23 (-2000.0), 61 (1100.62)
16	3300	Voltage	547.47	5 (-2000.0), 23 (-1921.24), 61 (1119.25)
17	3200	Voltage	548.66	5 (-2000.0), 23 (-1916.61), 61 (1119.25)
18	3200	Voltage	548.85	5 (-2000.0), 23 (-1916.53), 61 (1119.25)
19	3000	Voltage	529.96	5 (-2000.0), 23 (-1892.22), 61 (1115.74)
20	3000	Voltage	537.88	5 (-2000.0), 23 (-1889.07), 61 (1115.74)
21	2900	Voltage	536.22	5 (-2000.0), 23 (-1885.89), 61 (1115.74)
22	2900	Voltage	536.76	5 (-2000.0), 23 (-1885.7), 61 (1115.74)
23	2800	Voltage	502.94	5 (-2000.0), 23 (-1767.5), 61 (1145.04)
24	2600	Voltage	457.05	5 (-2000.0), 24 (-1590.81), 61 (1157.55)
25	2400	Voltage	451.79	22 (-963.9), 26 (-657.15), 61 (1157.21)
26	2300	Voltage	441.99	5 (-2000.0), 23 (-1592.34), 61 (1157.55)
27	2200	Voltage	421.75	5 (-2000.0), 23 (-1535.48), 61 (1157.55)
28	3800	Current	145.46	11 (383.38), 21 (231.05), 61 (1199.5)
29	3600	Current	152.44	17 (350.68), 29 (-1234.75), 61 (1244.72)
30	3200	Current	176.84	17 (350.68), 29 (-2000.0), 61 (1244.72)
31	3200	Current	181.07	17 (350.68), 29 (-2000.0), 61 (1244.72)
32	3300	Current	205.27	17 (350.68), 29 (-2000.0), 61 (1244.72)
33	3300	Current	255.81	17 (350.68), 29 (-2000.0), 61 (1244.72)
34	2600	Voltage	276.39	17 (350.68), 29 (-2000.0), 61 (1244.72)

Continued on next page

Bus	**HC (kW)**	**Limit**	**Losses (kW)**	**D-STATCOM [Bus (kvar)]**
35	1800	Voltage	235.93	17 (350.68), 29 (-2000.0), 61 (1244.72)
36	3900	Reverse PF	145.46	11 (383.38), 21 (231.05), 61 (1199.5)
37	3700	Current	152.41	17 (350.68), 37 (-1139.98), 61 (1244.72)
38	3500	Current	161.49	17 (350.68), 38 (-1538.83), 61 (1244.72)
39	3500	Current	164.46	17 (350.68), 39 (-1614.91), 61 (1244.72)
40	3500	Current	164.67	17 (350.68), 39 (-1633.79), 61 (1244.72)
41	3900	Current	245.42	41 (1712.96), 45 (-2000.0), 61 (1312.47)
42	3200	Current	254.96	17 (350.68), 44 (-2000.0), 61 (1244.72)
43	3200	Current	257.4	17 (350.68), 44 (-2000.0), 61 (1244.72)
44	3200	Current	257.96	17 (350.68), 44 (-2000.0), 61 (1244.72)
45	3200	Current	264.48	17 (350.68), 44 (-2000.0), 61 (1244.72)
46	3200	Current	264.54	17 (350.68), 44 (-2000.0), 61 (1244.72)
47	4000	Reverse PF	209.35	67 (1178.85), 68 (468.31), 69 (20.0)
48	3900	Reverse PF	149.66	11 (383.38), 21 (231.05), 61 (1199.5)
49	3900	Reverse PF	169.89	17 (350.68), 49 (-568.03), 61 (1244.72)
50	3900	Reverse PF	176.98	17 (350.68), 50 (-641.89), 61 (1244.72)
51	3800	Current	117.07	18 (292.6), 51 (-477.84), 61 (1193.04)
52	3800	Current	145.73	18 (292.6), 51 (-463.32), 61 (1193.04)
53	3900	Reverse PF	113.93	8 (-853.91), 18 (292.6), 61 (1157.55)
54	3900	Reverse PF	120.47	8 (-1133.91), 18 (286.83), 61 (1111.15)
55	4000	Reverse PF	204.65	55 (-2000.0), 56 (-500.82), 61 (1161.07)
56	4000	Reverse PF	203.4	55 (-871.11), 56 (-1499.42), 61 (1161.07)
57	3900	Reverse PF	175.01	18 (306.7), 56 (-772.69), 61 (385.61)
58	4000	Reverse PF	224.69	5 (-2000.0), 17 (325.42), 56 (-698.83)
59	4000	Reverse PF	228.43	5 (-2000.0), 17 (325.42), 56 (-697.4)
60	4000	Reverse PF	234.68	5 (-2000.0), 17 (325.42), 56 (-689.17)
61	4000	Reverse PF	242.74	5 (-2000.0), 17 (325.42), 56 (-666.58)
62	4000	Reverse PF	248.78	5 (-2000.0), 17 (325.42), 56 (-650.04)
63	3900	Voltage	242.37	5 (-2000.0), 17 (336.84), 56 (-577.34)
64	3500	Voltage	226.64	5 (-2000.0), 17 (341.89), 56 (-396.63)
65	3000	Voltage	203.6	5 (-2000.0), 17 (325.42), 50 (507.44)
66	3800	Current	212.93	11 (-655.61), 14 (-390.38), 61 (1151.22)
67	3800	Current	213.29	11 (-656.26), 14 (-389.61), 61 (1151.22)
68	3800	Current	379.17	9 (-1057.39), 18 (-1190.74), 61 (1194.79)
69	3800	Current	379.45	9 (-1055.8), 18 (-1190.62), 61 (1194.79)

Source: Created by the author

Table 17 – HC results for mapping in the 69-bus system - With reconfiguration

Bus	**HC (kW)**	**Limit**	**Losses (kW)**	**Open Lines**
2	4000	Reverse PF	198.27	14 39 62 70 72
3	3900	Reverse PF	106.14	10 12 13 55 63
4	3900	Reverse PF	100.5	14 58 63 69 70
5	4000	Reverse PF	214.72	10 13 17 49 61
6	4000	Reverse PF	216.87	13 23 38 45 72
7	3900	Reverse PF	139.23	13 20 61 69 72
8	4000	Reverse PF	199.92	13 18 37 49 61
9	3900	Reverse PF	139.68	13 20 41 61 72
10	4000	Reverse PF	211.2	5 62 70 71 72
11	4000	Reverse PF	199.93	4 12 19 63 72
12	4000	Reverse PF	226.23	8 17 43 61 72
13	4100	Reverse PF	309.18	4 15 56 59 69
14	4100	Reverse PF	319.19	6 11 19 59 72
15	4000	Reverse PF	263.14	9 11 57 59 70
16	4000	Reverse PF	260.36	9 11 55 59 70

Continued on next page

Bus	**HC (kW)**	**Limit**	**Losses (kW)**	**Open Lines**
17	4000	Reverse PF	256.55	9 11 56 60 70
18	4000	Reverse PF	256.52	9 11 58 60 70
19	4000	Reverse PF	256.48	8 11 58 60 70
20	4000	Reverse PF	257.47	8 11 13 60 72
21	4000	Reverse PF	252.11	9 14 56 60 69
22	4000	Reverse PF	254.15	8 14 56 60 69
23	4000	Reverse PF	255.2	8 14 55 59 69
24	4100	Reverse PF	321.47	7 13 49 59 69
25	4000	Reverse PF	275.55	7 14 60 69 72
26	4100	Reverse PF	309.75	7 9 14 69 72
27	4200	Reverse PF	405.81	5 10 14 43 49
28	3800	Current	99.9	14 56 61 69 70
29	3800	Current	105.44	14 58 61 69 70
30	3800	Current	139.69	14 55 61 69 70
31	3800	Current	145.61	14 58 61 69 70
32	3900	Reverse PF	178.62	14 57 61 69 70
33	3900	Current	247.93	14 58 61 69 70
34	2500	Voltage	217.8	14 58 61 69 70
35	1700	Voltage	177.67	14 55 61 69 70
36	4000	Reverse PF	216.41	9 14 49 62 70
37	3900	Reverse PF	103.28	12 57 61 69 70
38	3900	Reverse PF	110.99	10 14 56 61 70
39	3900	Reverse PF	112.02	10 14 55 61 70
40	3900	Reverse PF	112.09	10 14 57 61 70
41	4000	Reverse PF	209.84	8 12 20 61 72
42	3900	Reverse PF	155.54	4 17 43 56 61
43	4000	Reverse PF	205.05	7 12 20 62 72
44	4000	Reverse PF	208.95	5 12 19 63 72
45	4000	Reverse PF	216.02	6 12 15 61 72
46	4000	Reverse PF	208.83	4 12 13 61 72
47	4000	Reverse PF	214.89	10 12 20 49 61
48	3900	Reverse PF	105.44	10 14 19 56 62
49	3900	Reverse PF	102.54	10 14 17 55 62
50	3900	Reverse PF	105.1	14 54 64 69 70
51	3800	Current	142.86	13 20 61 69 72
52	3800	Current	171.83	13 20 61 69 72
53	4000	Reverse PF	198.81	13 17 39 49 62
54	4000	Reverse PF	201.76	19 39 45 49 62
55	4000	Reverse PF	199.57	13 20 35 49 62
56	4000	Reverse PF	199.72	13 20 35 49 62
57	4000	Reverse PF	204.33	4 14 20 23 69
58	4000	Reverse PF	205.16	8 16 39 45 62
59	3900	Reverse PF	122.4	8 12 24 69 70
60	3900	Reverse PF	126.65	7 10 12 17 70
61	3900	Reverse PF	129.2	7 10 12 16 71
62	3900	Reverse PF	135.06	7 10 12 16 71
63	3900	Reverse PF	143.05	8 10 12 15 45
64	4000	Reverse PF	201.1	8 11 14 16 41
65	4200	Reverse PF	409.66	3 11 15 49 56
66	3800	Current	197.05	8 13 20 61 72
67	3700	Current	194.5	8 13 20 61 72
68	3800	Current	278.45	8 17 43 61 72
69	3800	Current	278.84	8 17 43 61 72

Source: Created by the author

Table 18 – HC results for mapping in the 69-bus system - With D-STATCOMs and reconfiguration

Bus	**HC (kW)**	**Limit**	**Losses (kW)**	**D-STATCOM [Bus (kvar)]**	**Open Lines**
2	3900	Reverse PF	98.31	4 (1078.61), 61 (1330.95), 66 (400.28)	8 9 11 15 21
3	3900	Reverse PF	98.85	38 (1015.34), 61 (1794.54)	8 10 20 71 73
4	3900	Reverse PF	99.72	61 (1489.57), 68 (1099.19), 69 (20.0)	19 52 69 71 73
5	3900	Reverse PF	102.18	2 (2000.0), 5 (-582.44), 59 (1117.24)	13 19 35 54 61
6	4000	Reverse PF	200.84	40 (508.68), 50 (381.42), 61 (1819.72)	3 11 45 52 70
7	3900	Reverse PF	101.83	49 (421.7), 61 (888.14), 64 (256.09)	3 14 19 61 72
8	3900	Reverse PF	101.13	3 (1022.38), 61 (1268.32), 64 (455.16)	3 13 19 62 72
9	4000	Reverse PF	200.04	50 (1296.74), 67 (598.31)	3 4 17 43 61
10	3900	Reverse PF	107.58	49 (856.29), 61 (1013.54), 64 (359.31)	3 13 20 61 72
11	3900	Reverse PF	107.33	11 (-285.75), 61 (996.07), 64 (309.51)	5 14 18 61 72
12	3900	Reverse PF	149.56	26 (227.31), 49 (697.03), 61 (1043.97)	3 20 60 71 72
13	3900	Reverse PF	134.59	11 (484.34), 49 (697.88), 61 (1127.69)	3 16 59 69 72
14	4000	Reverse PF	211.73	3 (1378.89), 50 (400.33), 61 (1020.28)	6 18 49 59 69
15	4000	Reverse PF	200.78	2 (2000.0), 20 (-794.77), 63 (1125.72)	10 11 13 54 60
16	4000	Reverse PF	207.45	36 (1181.18), 48 (610.99), 61 (940.91)	3 4 11 14 59
17	3900	Reverse PF	160.98	11 (553.52), 15 (-647.24), 61 (1124.01)	5 13 60 69 72
18	4000	Reverse PF	201.31	40 (1545.07), 51 (230.04), 63 (871.75)	3 11 14 57 72
19	4200	Reverse PF	399.94	19 (-1048.17), 50 (1460.3), 64 (627.66)	3 13 17 47 52
20	4100	Reverse PF	307.64	29 (101.42), 50 (1090.12), 61 (8.67)	9 13 47 59 69
21	4300	Reverse PF	508.96	2 (1080.91), 4 (2000.0), 69 (-71.2)	5 13 38 60 69
22	4000	Reverse PF	207.54	3 (1992.7), 40 (-112.9), 61 (782.03)	3 16 45 52 60
23	4100	Reverse PF	318.81	2 (1362.25), 4 (1164.81), 27 (360.51)	8 14 18 49 57
24	4000	Reverse PF	209.79	40 (404.93), 50 (733.26), 61 (811.01)	3 6 20 59 69
25	4000	Reverse PF	207.9	15 (-341.37), 37 (1115.31), 61 (1836.15)	5 14 48 54 69
26	3900	Reverse PF	159.45	15 (-447.56), 48 (627.0), 61 (1442.12)	3 14 49 53 69
27	4000	Reverse PF	210.18	2 (1209.0), 61 (1619.23)	3 6 15 58 69
28	3800	Reverse PF	65.92	11 (387.81), 61 (1047.26), 64 (347.71)	14 58 61 69 70
29	3600	Current	73.41	29 (-1232.19), 61 (1047.26), 64 (347.71)	14 56 61 69 70
30	3200	Current	97.81	29 (-2000.0), 61 (1047.26), 64 (347.71)	14 57 61 69 70
31	3200	Current	102.03	29 (-2000.0), 61 (1047.26), 64 (347.71)	14 56 61 69 70
32	3300	Current	126.23	29 (-2000.0), 61 (1047.26), 64 (347.71)	14 57 61 69 70
33	3300	Current	176.77	29 (-2000.0), 61 (1047.26), 64 (347.71)	14 58 61 69 70
34	2600	Voltage	197.36	29 (-2000.0), 61 (1047.26), 64 (347.71)	14 57 61 69 70
35	1800	Voltage	156.89	29 (-2000.0), 61 (1047.26), 64 (347.71)	14 56 61 69 70
36	3900	Reverse PF	104.33	2 (94.93), 63 (1113.42), 69 (-114.31)	9 14 56 69 73
37	3800	Reverse PF	69.05	11 (387.81), 61 (1037.38), 64 (297.12)	14 56 61 69 70
38	3900	Reverse PF	98.58	3 (2000.0), 38 (-1019.69), 61 (1463.56)	8 12 14 26 55
39	3900	Reverse PF	98.73	3 (2000.0), 40 (-1360.01), 60 (1710.69)	12 14 58 63 69
40	3900	Reverse PF	103.2	4 (2000.0), 40 (-1326.96), 61 (1381.98)	10 13 20 21 57
41	4000	Reverse PF	201.96	36 (1555.42), 41 (-1606.46), 61 (1887.36)	4 11 19 61 69
42	4000	Reverse PF	198.89	40 (846.38), 42 (-1652.4), 61 (2000.0)	5 11 20 24 58
43	4000	Reverse PF	202.16	5 (307.27), 43 (-1534.91), 60 (1820.07)	6 13 17 21 55
44	3900	Reverse PF	113.8	44 (-381.86), 61 (1009.54), 64 (310.16)	8 12 61 70 72
45	3900	Reverse PF	120.29	45 (-380.32), 61 (1005.42), 64 (310.91)	8 11 61 70 72
46	4000	Reverse PF	211.66	2 (1412.5), 61 (1408.03)	5 12 19 49 60
47	3900	Reverse PF	103.65	13 (408.7), 53 (269.69), 61 (1432.36)	4 25 53 69 70
48	3800	Reverse PF	63.91	11 (387.81), 61 (997.17), 64 (347.71)	14 55 61 69 70
49	3800	Reverse PF	60.03	11 (387.81), 61 (952.82), 65 (350.14), 66 (0.0)	14 56 63 69 70
50	3800	Reverse PF	60.55	11 (387.81), 61 (911.0), 65 (350.14)	14 57 63 69 70
51	3800	Current	96.55	49 (556.56), 61 (950.91), 64 (280.66)	3 13 20 61 72
52	3800	Current	124.51	49 (573.4), 61 (963.58), 64 (289.77)	3 13 20 61 72
53	4000	Reverse PF	210.84	36 (1104.23), 61 (1687.38)	3 5 12 16 64

Continued on next page

Bus	**HC (kW)**	**Limit**	**Losses (kW)**	**D-STATCOM [Bus (kvar)]**	**Open Lines**
54	3900	Reverse PF	103.03	50 (446.9), 61 (904.32), 64 (224.26)	3 13 20 63 72
55	3900	Reverse PF	115.66	37 (-1111.93), 50 (534.68), 61 (1068.45)	3 14 19 64 72
56	4000	Reverse PF	206.54	4 (1790.08), 56 (-838.7), 61 (1729.81)	12 14 20 37 48
57	3900	Reverse PF	114.49	21 (202.64), 50 (556.73), 61 (1029.39)	3 17 48 70 71
58	3900	Reverse PF	101.28	11 (662.68), 47 (1305.73), 61 (618.94)	7 14 35 69 73
59	3800	Reverse PF	59.36	11 (477.75), 21 (249.06), 61 (847.05)	4 12 14 16 41
60	3800	Reverse PF	59.69	11 (450.22), 21 (332.7), 61 (824.24)	5 12 15 36 43
61	3800	Reverse PF	61.71	11 (323.03), 21 (475.56), 61 (544.47)	4 11 14 35 44
62	3900	Reverse PF	100.15	11 (755.77), 47 (1606.6), 50 (116.4)	9 15 37 57 71
63	3800	Reverse PF	73.06	11 (232.65), 21 (533.78), 61 (548.33)	4 11 14 35 69
64	4000	Reverse PF	206.7	21 (124.22), 48 (1958.7), 61 (-127.33)	7 12 18 42 44
65	3900	Reverse PF	138.4	8 (279.42), 50 (586.89), 61 (932.15)	3 14 48 52 69
66	3800	Current	120.23	50 (507.44), 61 (910.66), 64 (206.09)	5 14 19 61 72
67	3800	Current	120.62	50 (507.44), 61 (911.11), 64 (206.09)	4 14 19 61 72
68	3800	Current	209.31	49 (697.88), 61 (915.91), 64 (271.01)	3 14 20 60 72
69	3800	Current	209.7	49 (697.88), 61 (915.91), 64 (271.01)	3 14 20 59 72

Source: Created by the author

APPENDIX B – DATA OF THE SYSTEMS USED

NO: Normally Open

B.1 33-Bus Test System

Table 19 – Electrical data of the 33-bus test system

#	Branch		R	X	I_{max}	P_j	Q_j	#	Branch		R	X	I_{max}	P_j	Q_j
	i	j	[Ω]	[Ω]	[A]	[kW]	[kvar]		i	j	[Ω]	[Ω]	[A]	[kW]	[kvar]
1	1	2	0.0922	0.0470	400	100	60	20	20	21	0.4095	0.4784	250	90	40
2	2	3	0.4930	0.2511	400	90	40	21	21	22	0.7089	0.9373	200	90	40
3	3	4	0.3660	0.1864	400	120	80	22	3	23	0.4512	0.3083	200	90	50
4	4	5	0.3811	0.1941	400	60	30	23	23	24	0.8980	0.7091	200	420	200
5	5	6	0.8190	0.7070	400	60	20	24	24	25	0.8960	0.7011	200	420	200
6	6	7	0.1872	0.6188	300	200	100	25	6	26	0.2030	0.1034	200	60	25
7	7	8	0.7114	0.2351	300	200	100	26	26	27	0.2842	0.1447	200	60	25
8	8	9	1.0300	0.7400	300	60	20	27	27	28	1.0590	0.9337	200	60	20
9	9	10	1.0440	0.7400	300	60	20	28	28	29	0.8042	0.7006	200	120	70
10	10	11	0.1966	0.0650	300	45	30	29	29	30	0.5075	0.2585	200	200	600
11	11	12	0.3744	0.1238	250	60	35	30	30	31	0.9744	0.9630	200	150	70
12	12	13	1.4680	1.1550	250	60	35	31	31	32	0.3105	0.3619	200	210	100
13	13	14	0.5416	0.7129	250	120	80	32	32	33	0.3410	0.5302	200	60	40
14	14	15	0.5910	0.5260	250	60	10	33	8	21	2.0000	2.0000	400	NO	NO
15	15	16	0.7463	0.5450	250	60	20	34	9	15	2.0000	2.0000	400	NO	NO
16	16	17	1.2890	1.7210	250	60	20	35	12	22	2.0000	2.0000	400	NO	NO
17	17	18	0.7320	0.5740	250	90	40	36	18	33	0.5000	0.5000	400	NO	NO
18	2	19	0.1640	0.1565	250	90	40	37	25	29	0.5000	0.5000	400	NO	NO
19	19	20	1.5042	1.3554	250	90	40	-	-	-	-	-	-	-	-

Source: Created by the author

B.2 69-Bus Test System

Table 20 – Electrical data of the 69-bus test system

#	Branch		R	X	I_{max}	P_j	Q_j	#	Branch		R	X	I_{max}	P_j	Q_j
	i	j	[Ω]	[Ω]	[A]	[kW]	[kvar]		i	j	[Ω]	[Ω]	[A]	[kW]	[kvar]
1	1	2	0.0005	0.0012	600	0.00	0.00	38	38	39	0.0304	0.0355	300	24.00	17.00
2	2	3	0.0005	0.0012	600	0.00	0.00	39	39	40	0.0018	0.0021	300	24.00	17.00
3	3	4	0.0015	0.0036	600	0.00	0.00	40	40	41	0.7283	0.8509	300	1.20	1.00
4	4	5	0.0251	0.0294	600	0.00	0.00	41	41	42	0.3100	0.3623	300	0.00	0.00
5	5	6	0.3660	0.1864	600	2.60	2.20	42	42	43	0.0410	0.0478	300	6.00	4.30
6	6	7	0.3811	0.1941	600	40.40	30.00	43	43	44	0.0092	0.0116	300	0.00	0.00
7	7	8	0.0922	0.0470	600	75.00	54.00	44	44	45	0.1089	0.1373	300	39.22	26.30
8	8	9	0.0493	0.0251	600	30.00	22.00	45	45	46	0.0009	0.0012	300	39.22	26.30
9	9	10	0.8190	0.2707	600	28.00	19.00	46	4	47	0.0034	0.0084	300	0.00	0.00
10	10	11	0.1872	0.0619	600	145.00	104.00	47	47	48	0.0851	0.2083	300	79.00	56.40
11	11	12	0.7114	0.2351	400	145.00	104.00	48	48	49	0.2898	0.7091	300	384.70	274.50
12	12	13	1.0300	0.3400	400	8.00	5.50	49	49	50	0.0822	0.2011	300	384.70	274.50
13	13	14	1.0440	0.3400	400	8.00	5.50	50	8	51	0.0928	0.0473	300	40.50	28.30
14	14	15	1.0580	0.3496	400	0.00	0.00	51	51	52	0.3319	0.1114	300	3.60	2.70
15	15	16	0.1966	0.0650	400	45.50	30.00	52	9	53	0.1740	0.0886	300	4.35	3.50
16	16	17	0.3744	0.1238	400	60.00	35.00	53	53	54	0.2030	0.1034	300	26.40	19.00
17	17	18	0.0047	0.0016	400	60.00	35.00	54	54	55	0.2842	0.1447	300	24.00	17.20
18	18	19	0.3276	0.1083	400	0.00	0.00	55	55	56	0.2813	0.1433	300	0.00	0.00
19	19	20	0.2106	0.0696	400	1.00	0.60	56	56	57	1.5900	0.5337	300	0.00	0.00
20	20	21	0.3416	0.1129	400	114.00	81.00	57	57	58	0.7837	0.2630	300	0.00	0.00
21	21	22	0.0140	0.0046	300	5.30	3.50	58	58	59	0.3042	0.1006	300	100.00	72.00
22	22	23	0.1591	0.0526	300	0.00	0.00	59	59	60	0.3861	0.1172	300	0.00	0.00
23	23	24	0.3463	0.1145	300	28.00	20.00	60	60	61	0.5075	0.2555	300	1244.00	888.00
24	24	25	0.7488	0.2475	300	0.00	0.00	61	61	62	0.0974	0.0496	300	32.00	23.00
25	25	26	0.3089	0.1021	300	14.00	10.00	62	62	63	0.1450	0.0738	300	0.00	0.00
26	26	27	0.1732	0.0572	300	14.00	10.00	63	63	64	0.7105	0.3619	300	227.00	162.00
27	3	28	0.0044	0.0108	300	26.00	18.60	64	64	65	1.0410	0.5302	300	59.00	42.00
28	28	29	0.0640	0.1565	300	26.00	18.60	65	11	66	0.2012	0.0611	300	18.00	13.00
29	29	30	0.3978	0.1351	300	0.00	0.00	66	66	67	0.0047	0.0014	300	18.00	13.00
30	30	31	0.0702	0.0232	300	0.00	0.00	67	12	68	0.7394	0.2444	300	28.00	20.00
31	31	32	0.3510	0.1160	300	0.00	0.00	68	68	69	0.0047	0.0016	300	28.00	20.00
32	32	33	0.8390	0.2816	300	14.00	10.00	69	11	43	0.5000	0.5000	600	NO	NO
33	33	34	1.7080	0.5646	300	19.50	14.00	70	13	21	0.5000	0.5000	600	NO	NO
34	34	35	1.4740	0.4873	300	6.00	4.00	71	15	46	1.0000	1.0000	600	NO	NO
35	3	36	0.0044	0.0108	300	26.00	18.55	72	50	59	2.0000	2.0000	600	NO	NO
36	36	37	0.0640	0.1565	300	26.00	18.55	73	27	65	1.0000	1.0000	600	NO	NO
37	37	38	0.1053	0.1230	300	0.00	0.00	-	-	-	-	-	-	-	-

Source: Created by the author

B.3 136-Bus Test System

Table 21 – Electrical data of the 136-bus test system

#	Branch		R	X	P_j	Q_j	#	Branch		R	X	P_j	Q_j
	i	j	[Ω]	[Ω]	[kW]	[kvar]		i	j	[Ω]	[Ω]	[kW]	[kvar]
1	0	1	0.33205	0.76653	0.0	0.0	79	78	79	0.04690	0.10827	300.454	127.366
2	1	2	0.00188	0.00433	47.780	19.009	80	79	80	0.61950	0.61857	141.238	59.873
3	2	3	0.22324	0.51535	42.551	16.929	81	80	81	0.34049	0.33998	279.847	118.631
4	3	4	0.09943	0.22953	87.022	34.622	82	81	82	0.56862	0.29911	87.312	37.013
5	4	5	0.15571	0.35945	311.310	123.855	83	81	83	0.10877	0.10860	243.849	103.371
6	5	6	0.16321	0.37677	148.869	59.228	84	83	84	0.56862	0.29911	247.750	105.025
7	6	7	0.11444	0.26417	238.672	94.956	85	0	85	0.01126	0.02598	0.0	0.0
8	6	8	0.05675	0.05666	62.299	24.786	86	85	86	0.41835	0.96575	89.878	38.101
9	8	9	0.52124	0.27418	124.598	49.571	87	86	87	0.10499	0.13641	1137.280	482.108
10	8	10	0.10877	0.10860	140.175	55.768	88	86	88	0.43898	1.01338	458.339	194.296
11	10	11	0.39803	0.20937	116.813	46.474	89	88	89	0.07520	0.02579	385.197	163.290
12	10	12	0.91744	0.31469	249.203	99.145	90	89	90	0.07692	0.17756	0.0	0.0
13	10	13	0.11823	0.11805	291.447	115.952	91	90	91	0.33205	0.76653	79.608	33.747
14	13	14	0.50228	0.26421	303.720	120.835	92	91	92	0.08442	0.19488	87.312	37.013
15	13	15	0.05675	0.05666	215.396	85.695	93	92	93	0.13320	0.30748	0.0	0.0
16	15	16	0.29379	0.15454	198.586	79.007	94	93	94	0.29320	0.29276	74.001	31.370
17	0	17	0.33205	0.76653	0.0	0.0	95	94	95	0.21753	0.21721	232.050	98.369
18	17	18	0.00188	0.00433	0.0	0.0	96	95	96	0.26482	0.26443	141.819	60.119
19	18	19	0.22324	0.51535	0.0	0.0	97	93	97	0.10318	0.23819	0.0	0.0
20	19	20	0.10881	0.25118	30.127	14.729	98	97	98	0.13507	0.31181	76.449	32.408
21	20	21	0.71078	0.37388	230.972	112.920	99	0	99	0.00938	0.02165	0.0	0.0
22	20	22	0.18197	0.42008	60.256	29.458	100	99	100	0.16884	0.38976	51.322	21.756
23	22	23	0.30326	0.15952	230.972	112.920	101	100	101	0.11819	0.27283	59.874	25.381
24	22	24	0.02439	0.05630	120.507	58.915	102	101	102	2.28608	0.78414	9.065	3.843
25	24	25	0.04502	0.10394	0.0	0.0	103	101	103	0.45587	1.05236	2.092	0.887
26	25	26	0.01876	0.04331	56.981	27.857	104	103	104	0.69600	1.60669	16.735	7.094
27	26	27	0.11823	0.11805	364.665	178.281	105	104	105	0.45774	1.05669	1506.522	638.634
28	27	28	0.02365	0.02361	0.0	0.0	106	105	106	0.20298	0.26373	313.023	132.694
29	28	29	0.18954	0.09970	124.647	60.939	107	106	107	0.21348	0.27737	79.831	33.842
30	29	30	0.39803	0.20937	56.981	27.857	108	107	108	0.54967	0.28914	51.322	21.756
31	28	31	0.05675	0.05666	0.0	0.0	109	108	109	0.54019	0.28415	0.0	0.0
32	31	32	0.09477	0.04985	85.473	41.787	110	107	110	0.04550	0.05911	202.435	85.815
33	32	33	0.41699	0.21934	0.0	0.0	111	110	111	0.47385	0.24926	60.823	25.784
34	33	34	0.11372	0.05982	396.735	193.960	112	111	112	0.86241	0.45364	45.618	19.338
35	31	35	0.07566	0.07555	0.0	0.0	113	112	113	0.56862	0.29911	0.0	0.0
36	35	36	0.36960	0.19442	181.152	88.563	114	108	114	0.77711	0.40878	157.070	66.584
37	36	37	0.26536	0.13958	242.172	118.395	115	114	115	1.08038	0.56830	0.0	0.0
38	35	38	0.05675	0.05666	75.316	36.821	116	109	116	1.09933	0.57827	250.148	106.041
39	0	39	0.33205	0.76653	0.0	0.0	117	116	117	0.47385	0.24926	0.0	0.0
40	39	40	0.11819	0.27283	1.254	0.531	118	104	118	0.32267	0.74488	69.809	29.593
41	40	41	2.96288	1.01628	6.274	2.660	119	118	119	0.14633	0.33779	32.072	13.596
42	40	42	0.00188	0.00433	0.0	0.0	120	119	120	0.12382	0.28583	61.084	25.894
43	42	43	0.06941	0.16024	117.880	49.971	121	0	121	0.01126	0.02598	0.0	0.0
44	43	44	0.81502	0.42872	62.668	26.566	122	121	122	0.64910	1.49842	94.622	46.260
45	43	45	0.06378	0.14724	172.285	73.034	123	122	123	0.04502	0.10394	49.858	24.375
46	45	46	0.13132	0.30315	458.556	194.388	124	123	124	0.52640	0.18056	123.164	60.214
47	46	47	0.06191	0.14291	262.962	111.473	125	123	125	0.02064	0.04764	78.350	38.304
48	47	48	0.11444	0.26417	235.761	99.942	126	125	126	0.53071	0.27917	145.475	71.121
49	48	49	0.28374	0.28331	0.0	0.0	127	125	127	0.09755	0.22520	21.369	10.447
50	49	50	0.28374	0.28331	109.215	46.298	128	127	128	0.11819	0.27283	74.789	36.564
51	48	51	0.04502	0.10394	0.0	0.0	129	127	129	0.13882	0.32047	227.926	111.431

Continued on next page

#	Branch		R	X	P_j	Q_j	#	Branch		R	X	P_j	Q_j
	i	j	[Ω]	[Ω]	[kW]	[kvar]		i	j	[Ω]	[Ω]	[kW]	[kvar]
52	51	52	0.02626	0.06063	72.809	30.865	130	129	130	0.04315	0.09961	35.614	17.411
53	52	53	0.06003	0.13858	258.473	109.570	131	130	131	0.09192	0.21220	249.295	121.877
54	53	54	0.03002	0.06929	69.169	29.322	132	131	132	0.16134	0.37244	316.722	154.842
55	54	55	0.02064	0.04764	21.843	9.260	133	132	133	0.37832	0.37775	333.817	163.199
56	52	56	0.10881	0.25118	0.0	0.0	134	133	134	0.39724	0.39664	249.295	121.877
57	56	57	0.25588	0.13460	20.527	8.702	135	134	135	0.29320	0.29276	0.0	0.0
58	57	58	0.41699	0.21934	150.548	63.819	136	7	73	0.13132	0.30315	NO	NO
59	58	59	0.50228	0.26421	220.687	93.552	137	9	24	0.26536	0.13958	NO	NO
60	59	60	0.33170	0.17448	92.384	39.163	138	15	83	0.14187	0.14166	NO	NO
61	60	61	0.20849	0.10967	0.0	0.0	139	38	135	0.08512	0.08499	NO	NO
62	47	62	0.13882	0.32047	226.693	96.098	140	25	51	0.04502	0.10394	NO	NO
63	0	63	0.00750	0.01732	0.0	0.0	141	50	96	0.14187	0.14166	NO	NO
64	63	64	0.27014	0.62362	294.016	116.974	142	55	98	0.14187	0.14166	NO	NO
65	64	65	0.38270	0.88346	83.015	33.028	143	62	120	0.03940	0.09094	NO	NO
66	65	66	0.33018	0.76220	83.015	33.028	144	66	79	0.12944	0.29882	NO	NO
67	66	67	0.32830	0.75787	103.770	41.285	145	79	131	0.01688	0.03898	NO	NO
68	67	68	0.17072	0.39409	176.408	70.184	146	84	135	0.33170	0.17448	NO	NO
69	68	69	0.55914	0.29412	83.015	33.028	147	91	104	0.14187	0.14166	NO	NO
70	68	70	0.05816	0.13425	217.917	86.698	148	90	129	0.07692	0.17756	NO	NO
71	70	71	0.70130	0.36890	23.294	9.267	149	90	103	0.07692	0.17756	NO	NO
72	71	72	1.02352	0.53839	5.075	2.019	150	92	104	0.07692	0.17756	NO	NO
73	70	73	0.06754	0.15591	72.638	28.899	151	92	132	0.07692	0.17756	NO	NO
74	73	74	1.32352	0.45397	405.990	161.5235	152	96	120	0.26482	0.26443	NO	NO
75	0	75	0.01126	0.02598	0.0	0.0	153	110	47	0.49696	0.64567	NO	NO
76	75	76	0.72976	1.68464	100.182	42.468	154	126	76	0.17059	0.08973	NO	NO
77	76	77	0.22512	0.51968	142.523	60.417	155	128	77	0.05253	0.12126	NO	NO
78	77	78	0.20824	0.48071	96.042	40.713	156	135	98	0.29320	0.29276	NO	NO

Source: Created by the author

WORKS PUBLISHED BY THE AUTHOR

Works published by the author during the program.

Paper presented at a conference.

- Juan Esteban Suarez Patiño, Juliani Chico Piai Paiva, José Fernando Mangili Júnior, Luis Alfonso Gallego Pareja. **Impacto da Geração Solar Distribuída no Problema da Reconfiguração de Redes de Distribuição de Energia Elétrica**. XIV Congresso Brasileiro de Planejamento Energético – XIV CBPE. Manaus-AM, Outubro/2024.

Manuscript submitted to a journal.

- Juan Esteban Suarez Patiño, Oscar Gómez Carmona, Luis Alfonso Gallego Pareja. **Optimal Placement, Sizing and Operation of D-STATCOMs in Power Distribution Systems Using a Mixed-Integer Linear Programming Model**. Results in Engineering. ISSN 2590-1230.

IMPACTO DA GERAÇÃO SOLAR DISTRIBUÍDA NO PROBLEMA DA RECONFIGURAÇÃO DE REDES DE DISTRIBUIÇÃO DE ENERGIA ELÉTRICA

RESUMO

Neste artigo estuda-se o impacto das fontes de geração distribuída (GD) solar fotovoltaica (PV) no problema de reconfiguração dos sistemas de distribuição de energia elétrica (RSDEE). Assim, o objetivo principal deste trabalho é identificar a melhor topologia proposta pela RSDEE para a rede a medida que aumenta a inserção da GD solar PV. Para representar o problema da RSDEE, neste artigo é apresentado um modelo linear inteiro misto que é obtido através do modelo do fluxo de potência não linear para sistemas de distribuição de energia (SDE). O modelo proposto pode ser escrito em qualquer linguagem de programação matemática e pode ser solucionado com qualquer software comercial. Neste caso, a implementação computacional foi realizada na linguagem de programação AMPL e foi usado o CPLEX. Para determinar o impacto da GD na RSDEE e com o propósito de avaliar a eficácia do modelo, foram empregados os sistemas de 69 y 136 barras. O modelo proposto oferece uma implementação simples além de obter a solução ótima para o problema da RSDEE. Da mesma forma, o modelo proposto demonstra sua eficácia independentemente do tipo de sistema utilizado. A RSDEE demonstrou ser uma estratégia que promove a inserção de GD solar PV nos SDE aportando nos Objetivos de Desenvolvimento Sustentável (ODS) das Nações Unidas.

Palavras-Chave: Sistemas de Distribuição. Perdas de Potência. Otimização. Energias Renováveis. Transição Energética.

ABSTRACT

This article examines the impact of photovoltaic (PV) solar distributed generation (DG) sources on the reconfiguration of electric power distribution networks (REPDN) problem. Thus, the main objective of this work is to identify the best topology proposed by REPDN for the network as the insertion of PV solar DG increases. To represent the REPDN problem, a mixed-integer linear model obtained through the nonlinear power flow model for power distribution systems (PDS) is presented in this article. The proposed model can be written in any mathematical programming language and can be solved with any commercial software. In this case, computational implementation was performed in the AMPL programming language, and CPLEX was used. To determine the impact of DG on REPDN and to assess the effectiveness of the model, the 69 and 136 buses test systems were employed. The proposed model offers a simple implementation and achieves the optimal solution to the REPDN problem. Likewise, the proposed model demonstrates its effectiveness regardless of the type of system used. REPDN has proven to be a strategy that promotes the integration of PV solar DG into PDS, contributing to the United Nations' Sustainable Development Goals (SDGs).

Keywords: Distribution Systems. Power Losses. Optimization. Renewable Energies. Energy Transition.

1. INTRODUÇÃO

Os ODS das Nações Unidas são um conjunto de objetivos globais destinados a enfrentar vários desafios sociais, econômicos e ambientais para alcançar um futuro mais sustentável até 2030 (Nações Unidas, 2015). Esses objetivos são adaptados ao contexto e às prioridades locais, com um foco particular na promoção de fontes de energia renovável, como a energia solar PV.

O Brasil possui uma abundância de luz solar e vastas extensões de terra, tornando-o adequado para o desenvolvimento de projetos de energia solar. O país tem investido ativamente em infraestrutura solar, incluindo usinas solares PV, instalações solares em telhados e iniciativas solares comunitárias, com o objetivo de diversificar sua matriz energética e reduzir sua dependência de combustíveis fósseis (MME; EPE, 2019).

Particularmente, a inserção de energia solar PV distribuída nos SDE é uma prioridade para alcançar as metas da transição energética no setor elétrico. No entanto, existem efeitos adversos decorrentes da alta inserção de GD, como problemas nas proteções do sistema devido a fluxos reversos ou sobretensões. Para enfrentar esses desafios, diferentes técnicas têm sido estudadas, como as propostas por Hill *et al.* (2012), Hasheminamin *et al.* (2015) e Mortazavi *et al.* (2015).

O problema da RSDEE consiste em realizar uma alteração na topologia da rede. Inicialmente o problema foi solucionado por Merlin e Pack (1975) por um modelo de otimização não linear inteiro misto, empregando com um algoritmo Branch and Bound e com o objetivo de reduzir as perdas de energia.

Recentemente, diversas técnicas ou metodologias têm sido desenvolvidas para abordar simultaneamente os desafios da GD solar PV e o problema da RSDEE. Os métodos de solução podem ser exatos, aproximados tais como heurísticos ou metaheurísticos.

Os métodos exatos garantem uma solução ótima, mas devido à sua alta complexidade, podem ter um alto custo computacional. Os autores Mahdavi, Schmitt e Jurado (2023) apresentaram um modelo de otimização robusto para RSDEE com incerteza em cargas e GD. O modelo de programação cônica inteira mista é implementado em AMPL e resolvido com CPLEX. O objetivo do modelo é minimizar as perdas e evitar os problemas de uma má localização de GD. Os autores Hong *et al*. (2017) descreveram um método baseado em

grafos direcionados para o problema da RSDEE considerando GD. É considerado o caso de ajuste de modo de operação buscando minimizar as perdas de potência ativa e o caso de restauração do sistema buscando aumentar a carga restaurada. Ambas as situações são modeladas como problema de programação quadrática inteira mista e programação linear inteira mista, respectivamente.

Os métodos de solução aproximados (heurísticos e metaheurísticos) sobressaem na busca de soluções ótimas ou quase ótimas para problemas de otimização em grande escala, combinatoriais ou não convexos, onde os algoritmos exatos tradicionais enfrentam dificuldades devido à complexidade computacional. No entanto, de forma geral, não garantem que a solução encontrada seja a ótima global. Os autores Esmaeilian e Fadaeinedjad (2015) propuseram um método híbrido de algoritmos heurísticos e metaheurísticos para o problema da RSDEE e localização ótima de GD. Neste artigo, a reconfiguração é realizada considerando a localização de GD, bem como a variabilidade da demanda. Os autores Bagheri, Ali e Rizwan (2015) desenvolveram uma proposta de um algoritmo de *Otimização por Colônia de Formigas* (ACO) difuso para resolver simultaneamente o problema da RSDEE e a localização ótima de GD e DSTATCOM. O objetivo do modelo é diminuir perdas, melhorar o perfil de tensão e aumentar o balanceamento de carga no alimentador.

Outros métodos de solução mais recentes são baseados em inteligência artificial. Esses métodos, que incluem modelos de aprendizado de máquina e redes neurais, podem ser aplicados a todos os tipos de problemas, mostrando-se uma alternativa de grande flexibilidade. Para o caso da RSDEE, os autores Gao, Wang, Shi e Yu (2020) propõem um modelo de aprendizado por reforço restrito por lotes baseado em dados (data-driven batch-constrained reinforcement learning) para resolver o problema de reconfiguração dinâmica em SDE. O modelo não depende dos parâmetros do sistema e são usados dados históricos da operação do sistema para que o modelo "aprenda" as políticas de reconfiguração. Portanto, não é necessário que o modelo interaja diretamente com o SDE no mundo real. O objetivo do modelo é diminuir os custos de operação do sistema.

Como é evidente, o problema da RSDEE e os desafios da GD solar PV são de grande relevância. A RSDEE contribui para os ODS das Nações Unidas, facilitando uma maior

integração da GD solar PV. No entanto, um operador de rede não possui controle total sobre a localização das novas unidades de GD, sendo necessário realizar estudos que considerem diferentes níveis de inserção e localizações variadas da GD. Este artigo aborda a identificação da melhor topologia para a rede através da RSDEE, à medida que a inserção de GD aumenta.

2. FUNDAMENTAÇÃO TEÓRICA

Modelo Matemático Linear do Problema de Reconfiguração para RDEE

Seguindo a Figura 1, o modelo matemático linear do problema da RSDEE é definido pelas Eq. (1)-(29) (Gallego; López; Gómez, 2023[a]).

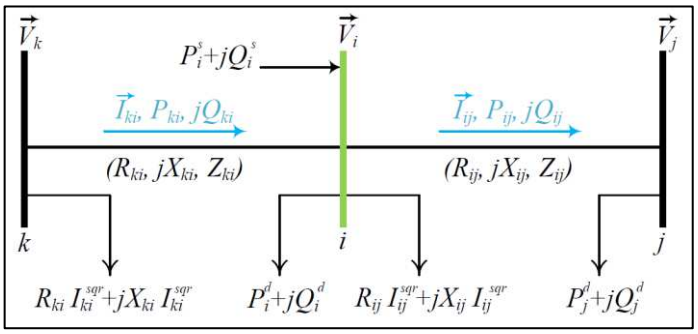

Figura 1. Representação básica dos SDE.

Fonte: Elaboração do autor (2024).

O modelo proposto considera que o sistema é balanceado e representado por um equivalente monofásico. Além disso, as potências são modelas como potências constantes, não se considera reatância capacitiva das linhas, e somente se considera uma fonte de fornecimento de energia; que neste caso é uma subestação de distribuição de energia.

$$\text{Minimizar } v = k_e \sum_{\forall ij \in \Omega_l} R_{ij} I_{ij}^{sqr} \tag{1}$$

$$\sum_{\forall ki \in \Omega_l} P_{ki} - \sum_{\forall ij \in \Omega_l} \left(P_{ij} + R_{ij} I_{ij}^{sqr}\right) + P_i^s = P_i^d;\ \forall i \in \Omega_b \tag{2}$$

$$\sum_{\forall ki \in \Omega_l} Q_{ki} - \sum_{\forall ij \in \Omega_l} \left(Q_{ij} + X_{ij} I_{ij}^{sqr}\right) + Q_i^s = Q_i^d;\ \forall i \in \Omega_b \tag{3}$$

$$V_i^{sqr} - 2\left(R_{ij}P_{ij} + X_{ij}Q_{ij}\right) - Z_{ij}^2 I_{ij}^{sqr} - V_j^{sqr} - b_{ij} = 0;\ \forall ij \in \Omega_l \tag{4}$$

$$\left(\underline{V}^2 + \frac{1}{2}\Delta V\right) I_{ij}^{sqr} + \sum_{s=1}^{S} P_{j,s}^c = \sum_{y=1}^{Y} m_{ij,y}^s \cdot \Delta P_{ij,y} + \sum_{y=1}^{Y} m_{ij,y}^s \cdot \Delta Q_{ij,y};\ \forall ij \in \Omega_l \tag{5}$$

$$0 \le I_{ij}^{sqr} \le \overline{I}_{ij}^2;\ \forall ij \in \Omega_l \tag{6}$$

$$\underline{V}_i^2 \le V_i^{sqr} \le \overline{V}_i^2;\ \forall i \in \Omega_b \tag{7}$$

$$\underline{V}^2 + \sum_{s=1}^{S}(\Delta V \cdot x_{j,s}) \leq V_j^{sqr} \leq \underline{V}^2 + \sum_{s=1}^{S}(\Delta V \cdot x_{j,s}) + \Delta V;\ \forall j \in \Omega_b \quad (8)$$

$$x_{j,s} \leq x_{j,s-1};\ \forall j \in \Omega_b; s = 2..S \quad (9)$$

$$x_{j,s} \in \{0,1\};\ \forall j \in \Omega_b; s = 1..S \quad (10)$$

$$0 \leq \Delta V \cdot I_{ij}^{sqr} - P_{j,s}^{c} \leq \Delta V \cdot \overline{I}_{ij}^{2}(1 - x_{j,s});\ \forall ij \in \Omega_l, s = 1..S \quad (11)$$

$$0 \leq P_{j,s}^{c} \leq \Delta V \cdot \overline{I}_{ij}^{2} x_{j,s};\ \forall ij \in \Omega_l \quad (12)$$

$$P_{ij}^{+} - P_{ij}^{-} = P_{ij};\ \forall ij \in \Omega_l \quad (13)$$

$$P_{ij}^{+} + P_{ij}^{-} = \sum_{y=1}^{Y} \Delta P_{ij,y};\ \forall ij \in \Omega_l \quad (14)$$

$$0 \leq \Delta P_{ij,y} \leq \overline{\Delta} S_{ij}; \forall ij \in \Omega_l;\ \forall y \in 1..Y \quad (15)$$

$$Q_{ij}^{+} - Q_{ij}^{-} = Q_{ij};\ \forall ij \in \Omega_l \quad (16)$$

$$Q_{ij}^{+} + Q_{ij}^{-} = \sum_{y=1}^{Y} \Delta Q_{ij,y};\ \forall ij \in \Omega_l \quad (17)$$

$$0 \leq \Delta Q_{ij,y} \leq \overline{\Delta} S_{ij}; \forall ij \in \Omega_l;\ \forall y \in 1..Y \quad (18)$$

$$0 \leq P_{ij}^{+}, P_{ij}^{-}, Q_{ij}^{+}, Q_{ij}^{-};\ \forall ij \in \Omega_l \quad (19)$$

$$m_{ij,y}^{s} = (2y - 1)\overline{\Delta} S_{ij} \quad (20)$$

$$\overline{\Delta} S_{ij} = \overline{V} \cdot \overline{I}_{ij} / Y \quad (21)$$

$$0 \leq I_{ij}^{sqr} \leq \overline{I}_{ij}^{2}(y_{ij}^{+} + y_{ij}^{-});\ \forall ij \in \Omega_l \quad (22)$$

$$0 \leq P_{ij}^{+} \leq \overline{VI} y_{ij}^{+}; \forall ij \in \Omega_l;\ \forall ij \in \Omega_l \quad (23)$$

$$0 \leq P_{ij}^{-} \leq \overline{VI} y_{ij}^{-}; \forall ij \in \Omega_l;\ \forall ij \in \Omega_l \quad (24)$$

$$|Q_{ij}| \leq \overline{VI}(y_{ij}^{+} + y_{ij}^{-}); \forall ij \in \Omega_l \quad (25)$$

$$|b_{ij}| \leq \left(\overline{V}^2 - \underline{V}^2\right)\left(1 - (y_{ij}^{+} + y_{ij}^{-})\right);\ \forall ij \in \Omega_l \quad (26)$$

$$\sum_{ij \in \Omega_l} (y_{ij}^{+} + y_{ij}^{-}) = N - 1;\ \forall ij \in \Omega_l \quad (27)$$

$$(y_{ij}^{+} + y_{ij}^{-}) \leq 1;\ \forall ij \in \Omega_l \quad (28)$$

$$y_{ij}^{+}; y_{ij}^{-}; \text{binary};\ \forall ij \in \Omega_l \quad (29)$$

onde Ω_l é o conjunto de linhas e Ω_b é o conjunto de barras. P_{ki}, P_{ij}, Q_{ki} e Q_{ij} representam o fluxo de potência nas linhas ki e ij. P_i^s, Q_i^s, P_i^d e Q_i^s representam as potências da subestação e da demanda na barra i. Z_{ij}, R_{ij} e X_{ij} são a impedância, resistência e reatância da linha ij. V_i^{sqr} é a tensão ao quadrado na barra i. I_{ij}^{sqr} é a corrente ao quadrado da linha ij. $\overline{V}_i$ e $\underline{V}_i$ representam os limites superiores e inferiores de tensão na barra i. $\overline{I}_{ij}$ é o limite superior de corrente da linha ij. ΔV é o passo de discretização, S é o número de discretizações, $P_{j,s}^{c}$ é a correção de potência usada em $V_j^{sqr} I_{ij}^{sqr}$, e $x_{j,s}$ é uma variável binária usada na discretização de V_j^{sqr}. Y é a quantidade de blocos da linearização segmentada. $m_{ij,y}^{s}$

indica a inclinação do bloco y_{th} do fluxo de carga na linha ij. $\Delta P_{ij,y}$ e $\Delta Q_{ij,y}$ representam os valores do bloco y_{th} de $|P_{ij}|$ e $|Q_{ij}|$, respectivamente. $\overline{\Delta} S_{ij}$ é o limite máximo de cada bloco do fluxo de carga na linha ij. P_{ij}^{+} e P_{ij}^{-} são implementados para obter $|P_{ij}|$; e Q_{ij}^{+} e Q_{ij}^{-} são usados para obter $|Q_{ij}|$. b_{ij} é zero se a linha ij estiver fechada, caso contrário, b_{ij} funciona como uma variável slack. y_{ij}^{+} e y_{ij}^{-} representam variáveis binárias relacionadas à direção do fluxo de potência da linha ij. Se qualquer uma das variáveis for igual a um, a linha respectiva está fechada; se ambas as variáveis forem zero, a linha está aberta. Finalmente, N é o número de barras.

A Equação (1) representa a função objetivo que consiste em minimizar as perdas de potência ativa. O balanço de potência ativa e reativa para cada barramento do sistema é descrito pelas Eq. (2) e (3), respectivamente. A restrição dada pela Eq. (4) modela a queda de tensão em cada linha ij. A Equação (5) é a potência aparente, representada como a soma de uma aproximação linear das potências ativa e reativa ao quadrado (P_{ij}^{2}, Q_{ij}^{2}) que é igual a uma aproximação linear de $V_{j}^{sqr} I_{ij}^{sqr}$. As Equações (6) e (7) representam os limites da corrente através da linha ij e da tensão na barra i, respectivamente. A Equação (8) especifica o intervalo de valores possíveis para a tensão (V_{j}^{sqr}) na linearização proposta. A Equação (9) afirma que a variável binária $x_{j,s-1}$ deve ser maior que a variável $x_{j,s}$. A Equação (10) indica a natureza da variável implementada no esquema de linearização (variável binária). Os valores de $P_{j,s}^{c}$ são definidos pelas Eq. (11) e (12). Se $x_{j,s} = 0$, $P_{j,s}^{c} = 0$, e $I_{ij}^{sqr} \leq \overline{I}_{ij}^{2}$; caso contrário, $P_{j,s}^{c} = \Delta V \overline{I}_{ij}^{2}$. As Equações (13) e (16) representam os possíveis valores das variáveis P_{ij} e Q_{ij} como função das variáveis auxiliares P_{ij}^{+}, P_{ij}^{-}, Q_{ij}^{+} e Q_{ij}^{-}. As Equações (14) e (17) indicam que $|P_{ij}|$ e $|Q_{ij}|$ são a soma dos valores em cada bloco de discretização. As Equações (15) e (18) definem os limites superior e inferior da contribuição de cada bloco para $|P_{ij}|$ e $|Q_{ij}|$, respectivamente. A Equação (19) representa a não negatividade das variáveis auxiliares P_{ij}^{+}, P_{ij}^{-}, Q_{ij}^{+} e Q_{ij}^{-}. As Equações (20) e (21) são usadas para calcular os valores de $m_{ij,y}^{s}$ e $\overline{\Delta} S_{ij}$. O limite de corrente é representado pela Eq. (22), que é uma função das variáveis y_{ij}^{+} e y_{ij}^{-}. O limite das variáveis P_{ij}^{+} e P_{ij}^{-} é representado pelas Eq. (23) e (24).

O limite do fluxo de potência reativa na linha ij é representado pela Eq. (25). A Equação (26) representa o limite de b_{ij}. A garantia de que o SDE seja radial é dada pelas Eq. (27) e (28). Por fim, as variáveis y_{ij}^{+} e y_{ij}^{-} são binárias de acordo com a Eq. (29).

Geração Distribuída Solar PV

A GD solar PV é modelada como uma injeção de potência na barra onde cada um dos geradores está conectado. Barras atrativas para conexão de GD são identificadas devido à sua alta demanda e diferentes casos de estudo são considerados. Desta forma, varia o número de barras onde os geradores são instalados. Neste caso, os geradores do tipo solar PV se consideram com fator de potência de 1 e a capacidade de geração é determinada para cada caso de estudo.

Por outro lado, é necessário modificar o modelo do problema da RSDEE para incluir o efeito da GD solar PV. Assim, a Eq. (2) é transformada na Eq. (30).

$$\sum_{\forall ki \in \Omega_l} P_{ki} - \sum_{\forall ij \in \Omega_l} \left(P_{ij} + R_{ij} I_{ij}^2\right) + P_i^s + P_i^{GD} = P_i^d;\ \forall i \in \Omega_b \qquad (30)$$

onde P_i^{GD} representa a potência ativa injetada pelo gerador distribuído solar PV conectado na barra i.

3. RESULTADOS

O modelo matemático descrito na seção anterior é implementado no AMPL e solucionado utilizando o CPLEX. O AMPL é uma linguagem de programação algébrica projetada para modelar diversos tipos de problemas matemáticos. O modelo é testado utilizando os sistemas de 69 e 136 barras para os diferentes níveis de inserção de GD solar PV da Tabela 1. Como o sistema de 136 barras é maior, sua demanda de potência é maior. Por esta razão, para manter a potência da GD a ser instalada em uma magnitude comparável em ambos os sistemas, é utilizado um percentual menor da carga total para este sistema.

Sistema 69 barras

O sistema de 69 barras é um sistema de distribuição de 12,66 kV que possui 69 barras, 73 linhas, 3802,19 kW e 2694,6 kVAr de potência demandada. As perdas de potência ativa na rede na configuração inicial são de 225 kW com as linhas 69, 70, 71, 72 e 73 abertas inicialmente. Os autores Gallego, López e Gómez (2023[b]) apresentam os dados do sistema.

Tabela 1. Casos de estudo (nb: número de barras, Pd: potência demanda total).

	Sistema 69 barras	Sistema 136 barras
Caso 1	10% nb, 30% Pd	15% nb, 10% Pd
Caso 2	15% nb, 30% Pd	20% nb, 10% Pd
Caso 3	17% nb, 30% Pd	30% nb, 10% Pd
Caso 4	10% nb, 50% Pd	15% nb, 20% Pd
Caso 5	15% nb, 50% Pd	20% nb, 20% Pd
Caso 6	17% nb, 50% Pd	30% nb, 20% Pd
Caso 7	10% nb, 70% Pd	15% nb, 30% Pd
Caso 8	15% nb, 70% Pd	20% nb, 30% Pd
Caso 9	17% nb, 70% Pd	30% nb, 30% Pd

Fonte: Elaboração do autor (2024).

Na Figura 2 são apresentados os perfis de tensão nas barras do sistema de 69 barras. Em geral, os perfis de tensão sofrem uma melhoria em relação ao caso base. Em alguns casos, por exemplo caso 4 e caso 7 apresentam comportamento diferente devido à seleção de linhas abertas da reconfiguração. Este comportamento é causado pela busca por uma topologia com perdas mínimas, mantendo os níveis de tensão nos níveis permitidos.

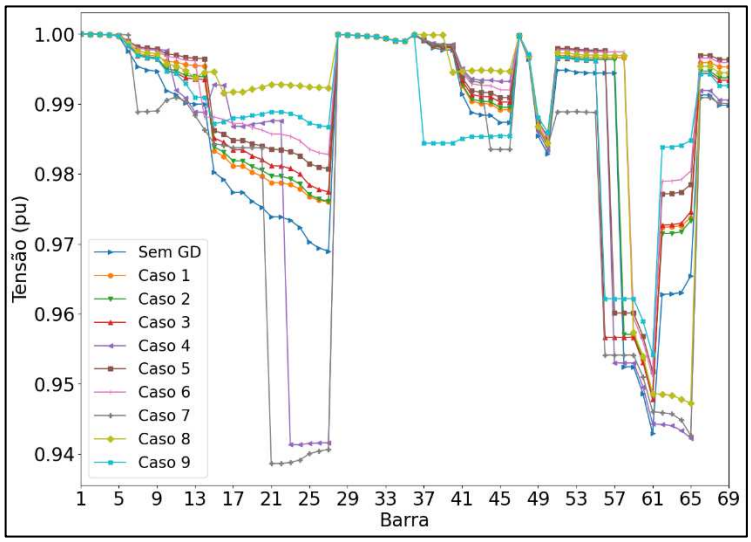

Figura 2. Perfis de tensão sistema 69 barras.
Fonte: Elaboração do autor (2024).

Na Tabela 2 são apresentados os resultados das simulações dos casos de estudo do sistema de 69 barras. É possível observar que as perdas do sistema e a potência fornecida pela subestação diminuem com a inserção de GD. Neste tipo de sistema, é possível observar

que a topologia ótima é afetada pela inserção de GD, mostrando uma variedade de resultados nas linhas abertas.

Tabela 2. Resultados sistema 69 barras.

Caso	Perdas (kW)	Potência subestação (MVA)	Redução perdas (%)	Barras com GD	Linhas abertas
Sem GD	99.62	4.80	58.41	-	14, 57, 61, 69, 70
1	68.55	3.89	69.53	11, 12, 49, 50, 61, 64	14, 58, 61, 69, 70
2	69.20	3.89	69.25	8, 11, 12, 21, 48, 49, 50, 59, 61, 64	14, 57, 61, 69, 70
3	69.44	3.89	69.14	8, 11, 12, 17, 21, 48, 49, 50, 59, 61, 64	14, 55, 61, 69, 70
4	67.94	3.40	69.80	11, 12, 49, 50, 61, 64	10, 14, 16, 22, 56
5	57.77	3.39	74.32	8, 11, 12, 21, 48, 49, 50, 59, 61, 64	14, 56, 61, 69, 70
6	58.42	3.39	74.03	8, 11, 12, 17, 21, 48, 49, 50, 59, 61, 64	13, 58, 61, 69, 70
7	69.31	3.02	69.20	11, 12, 49, 50, 61, 64	6, 20, 43, 55, 70
8	61.51	3.01	72.66	8, 11, 12, 21, 48, 49, 50, 59, 61, 64	13, 15, 39, 58, 73
9	61.60	3.01	72.62	8, 11, 12, 17, 21, 48, 49, 50, 59, 61, 64	14, 36, 55, 61, 69

Fonte: Elaboração do autor (2024).

Sistema 136 barras

O sistema de 136 barras é um sistema de distribuição de 13,8 kV que possui 136 barras, 156 linhas, 18313,809 kW e 7932,533 kVAr de potência demandada. As perdas de potência ativa na rede na configuração inicial são de 320,37 kW com as linhas 135 a 156 abertas inicialmente. O autor Possagnolo (2015) apresenta os dados do sistema.

Na Figura 3 são apresentados os perfis de tensão nas barras do sistema de 136 barras. Neste sistema, é possível observar uma relação entre o perfil de tensão e a inserção de GD, melhorando à medida que a inserção aumenta. Por ser um sistema maior e a GD ter magnitudes comparáveis aos casos do sistema de 69 barras, o efeito pode ser reduzido.

Na Tabela 3 são apresentados os resultados das simulações dos casos de estudo do sistema de 136 barras. Pode-se verificar que as perdas do sistema e a potência fornecida pela subestação diminuem com a inserção de GD. Para um sistema de maior tamanho, é possível observar que a topologia ótima sofre menor variação, resultados que podem ser confirmados nos perfis de tensão da Figura 3.

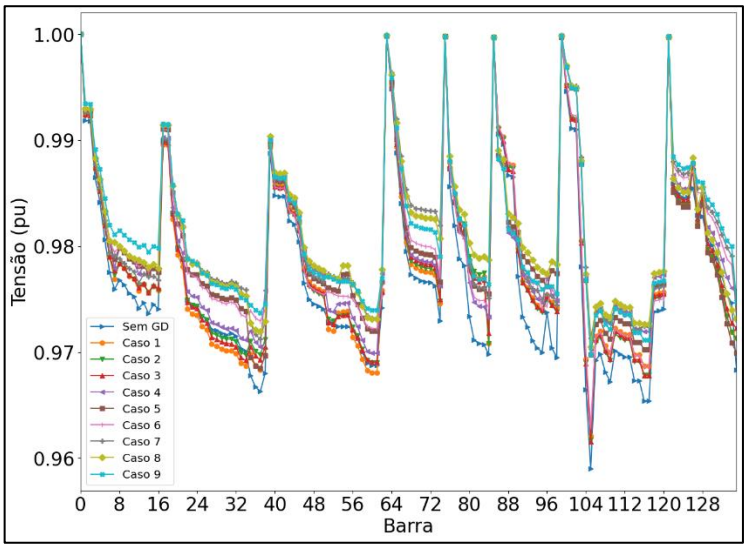

Figura 3. Perfis de tensão sistema 136 barras.
Fonte: Elaboração do autor (2024).

Tabela 3. Resultados sistema 136 barras.

Caso	Perdas (kW)	Potência subestação (MVA)	Redução perdas (%)	Barras com GD	Linhas abertas
Sem GD	280.19	20.45	15.46	-	7, 35, 51, 90, 96, 106, 118, 126, 135, 137, 138, 141, 142, 144, 145, 146, 147, 148, 150, 151, 155
1	228.26	18.72	28.75	5, 13, 14, 27, 34, 46, 47, 53, 64, 74, 79, 81, 87, 88, 89, 105, 106, 116, 132, 133	7, 51, 53, 84, 90, 96, 106, 118, 126, 128, 137, 138, 139, 141, 144, 145, 147, 148, 150, 151, 156
2	226.81	18.71	29.20	5, 7, 12, 13, 14, 27, 34, 37, 46, 47, 53, 64, 74, 79, 81, 83, 84, 87, 88, 89, 105, 106, 116, 131, 132, 133, 134	7, 38, 51, 53, 84, 90, 96, 106, 118, 126, 128, 137, 138, 141, 144, 145, 147, 148, 150, 151, 156
3	226.12	18.71	29.42	5, 7, 12, 13, 14, 15, 16, 21, 23, 27, 34, 36, 37, 46, 47, 48, 53, 59, 62, 64, 68, 70, 74, 79, 81, 83, 84, 87, 88, 89, 95, 105, 106, 110, 116, 129, 131, 132, 133, 134	7, 51, 53, 84, 90, 96, 106, 118, 126, 128, 137, 138, 139, 141, 144, 145, 147, 148, 150, 151, 156
4	190.11	17.03	40.66	5, 13, 14, 27, 34, 46, 47, 53, 64, 74, 79, 81, 87, 88, 89, 105, 106, 116, 132, 133	7, 38, 51, 53, 96, 106, 118, 126, 137, 138, 141, 144, 145, 146, 147, 148, 149, 150, 151, 155, 156
5	188.46	17.02	41.17	5, 7, 12, 13, 14, 27, 34, 37, 46, 47, 53, 64, 74, 79, 81, 83, 84, 87, 88, 89, 105, 106, 116, 131, 132, 133, 134	7, 35, 51, 54, 96, 106, 118, 126, 128, 137, 138, 141, 144, 145, 146, 147, 148, 149, 150, 151, 156
6	187.07	17.02	41.61	5, 7, 12, 13, 14, 15, 16, 21, 23, 27, 34, 36, 37, 46, 47, 48, 53, 59, 62, 64, 68, 70, 74, 79, 81, 83, 84, 87, 88, 89, 95, 105, 106, 110, 116, 129, 131, 132, 133, 134	7, 35, 51, 90, 95, 106, 118, 126, 135, 137, 138, 141, 142, 144, 145, 146, 147, 148, 150, 151, 155
7	182.05	15.42	43.17	5, 13, 14, 27, 34, 46, 47, 53, 64, 74, 79, 81, 87, 88, 89, 105, 106, 116, 132, 133	35, 51, 95, 106, 118, 126, 135, 136, 137, 138, 141, 142, 144, 145, 146, 147, 148, 149, 150, 151, 155
8	154.54	15.39	51.76	5, 7, 12, 13, 14, 27, 34, 37, 46, 47, 53, 64, 74, 79, 81, 83, 84, 87, 88, 89, 105, 106, 116, 131, 132, 133, 134	35, 51, 54, 96, 106, 118, 126, 128, 136, 137, 138, 141, 144, 145, 146, 147, 148, 149, 150, 151, 156
9	153.30	15.38	52.15	5, 7, 12, 13, 14, 15, 16, 21, 23, 27, 34, 36, 37, 46, 47, 48, 53, 59, 62, 64, 68, 70, 74, 79, 81, 83, 84, 87, 88, 89, 95, 105, 106, 110, 116, 129, 131, 132, 133, 134	7, 35, 51, 95, 106, 118, 126, 135, 137, 138, 141, 142, 144, 145, 146, 147, 148, 149, 150, 151, 155

Fonte: Elaboração do autor (2024).

4. CONCLUSÃO

O modelo de RSDEE proposto neste artigo demonstrou sua eficácia independentemente do tipo de sistemas usados nos casos de estudo. As principais características do modelo são a possibilidade de ser resolvido por qualquer solucionador comercial e sua alta precisão. Da mesma forma, ficou evidente nos testes realizados que o impacto da GD solar PV foi maior no sistema de menor porte, considerando geradores de tamanho similar para ambos os casos. Uma das grandes vantagens da inserção da GD é a redução da potência requerida nas subestações. Esta diminuição foi medida e está alinhada com os ODS ao reduzir a potência exigida nos SDE. Como resultado, há menor necessidade de geração de energia nas grandes centrais, sejam hidrelétricas ou termelétricas. Este benefício destaca a importância da RSDEE, pois promove a inserção da GD solar PV e contribui para a sustentabilidade do setor elétrico. Neste artigo, foram estudados os efeitos que ocorrem em um SDE devido à inserção de GD solar PV, realizando um estudo determinístico. Para futuros trabalhos, propõe-se realizar estudos semelhantes levando em consideração propostas de otimização robustas; ou seja, modelos que levem em conta a variabilidade na localização e na dimensão dos geradores. Esse tipo de proposta permitirá obter outros tipos de resultados, pois haverá uma maior quantidade de cenários prováveis.

5. AGRADECIMENTOS

O presente trabalho integra pesquisas do NAPI-SOLAR e conta com o financiamento da Fundação Araucária de Apoio ao Desenvolvimento Científico e Tecnológico do Estado do Paraná.

REFERÊNCIAS BIBLIOGRÁFICAS

BAGHERI TOLABI, H.; ALI, M. H.; RIZWAN, M. Simultaneous reconfiguration, optimal placement of dstatcom, and photovoltaic array in a distribution system based on fuzzy-aco approach. **IEEE Transactions on Sustainable Energy**, v. 6(1), p. 210–218, 2015.

ESMAEILIAN, H. R.; FADAEINEDJAD, R. Energy loss minimization in distribution systems utilizing an enhanced reconfiguration method integrating distributed generation. **IEEE Systems Journal**, v. 9(4), p. 1430–1439, 2015.

GALLEGO PAREJA, L. A.; LÓPEZ-LEZAMA, J. M.; GÓMEZ CARMONA, O. Optimal feeder reconfiguration and placement of voltage regulators in electrical distribution networks using a linear mathematical model. **Sustainability**, v. 15(1), 854, 2023ª.

GALLEGO PAREJA, L. A.; LÓPEZ-LEZAMA, J. M.; GÓMEZ CARMONA, O. Optimal integration of distribution network reconfiguration and conductor selection in power distribution systems via MILP. **Energies**, v. *16*(19), 6998, 2023[b].

GAO, Y.; WANG, W.; SHI, J.; YU, N. Batch-constrained reinforcement learning for dynamic distribution network reconfiguration. **IEEE Transactions on Smart Grid**, v. 11(6), p. 5357–5369, 2020.

HASHEMINAMIN, M.; AGELIDIS, V. G.; SALEHI, V.; TEODORESCU, R.; HREDZAK, B. Index-based assessment of voltage rise and reverse power flow phenomena in a distribution feeder under high pv penetration. **IEEE Journal of Photovoltaics**, v. 5(4), p. 1158–1168, 2015.

HILL, C. A.; SUCH, M. C.; CHEN, D.; GONZALEZ, J.; GRADY, W. M. Battery energy storage for enabling integration of distributed solar power generation. **IEEE Transactions on Smart Grid**, v. 3(2), p. 850–857, 2012.

HONG, H.; HU, Z.; GUO, R.; MA, J.; TIAN, J. Directed graph-based distribution network reconfiguration for operation mode adjustment and service restoration considering distributed generation. **Journal of Modern Power Systems and Clean Energy**, v. 5(1), p. 142–149, 2017.

MAHDAVI, M.; SCHMITT, K. E. K.; JURADO, F. Robust distribution network reconfiguration in the presence of distributed generation under uncertainty in demand and load variations. **IEEE Transactions on Power Delivery**, v. 38(5), p. 3480–3495, 2023.

MERLIN, A.; PACK, H. Search for a minimal-loss operating spanning tree configuration in an urban power distribution system. **Fifth Power Systems Computation Conference Proceedings**, Cambridge, UK, 1975, p. 1–18.

MINISTÉRIO DE MINAS E ENERGIA - MME; EMPRESA DE PESQUISA ENERGÉTICA - EPE (2019). **Plano Decenal de Expansão de Energia 2029**. Brasília. Disponível em: https://www.epe.gov.br/sites-pt/publicacoes-dados-abertos/publicacoes/Documents/PDE%202029.pdf. Acceso em: 24 abr. 2024.

MORTAZAVI, H.; MEHRJERDI, H.; SAAD, M.; LEFEBVRE, S.; ASBER, D.; LENOIR, L. A monitoring technique for reversed power flow detection with high PV penetration level. **IEEE Transactions on Smart Grid**, v. 6(5), p. 2221–2232, 2015.

NAÇÕES UNIDAS (2015). **Transformando Nosso Mundo: A Agenda 2030 para o Desenvolvimento Sustentável**. Nova York, setembro. Disponível em: https://brasil.un.org/sites/default/files/2020-09/agenda2030-pt-br.pdf. Acesso em: 24 abr. 2024.

POSSAGNOLO, L. H. F. M. **Reconfiguração de sistemas de distribuição operando em vários níveis de demanda através de uma meta-heurística de busca em vizinhança variável**. Dissertação de mestrado, Universidade Estadual Paulista, Ilha Solteira, SP, 178, Brasil. 2015.

Universidade Estadual de Londrina

Juan Esteban Suarez Patino <juanes.suarezp@uel.br>

Confirm co-authorship of submission to Results in Engineering

1 mensagem

Results in Engineering <em@editorialmanager.com> 23 de janeiro de 2025 às 15:04
Responder a: Results in Engineering <noreply_emsupport@elsevier.com>
Para: Juan Esteban Suarez Patiño <juanes.suarezp@uel.br>

This is an automated message.

Journal: Results in Engineering
Title: Optimal Placement, Sizing and Operation of D-STATCOMs in Power Distribution Systems Using a Mixed-Integer Linear Programming Model
Corresponding Author: Professor Luis Alfonso Gallego Pareja
Co-Authors: Oscar Gómez Carmona, Ph.D.; Juan Esteban Suarez Patiño, Ing.
Manuscript Number: **RINENG-D-25-01050**

Dear Juan Esteban Suarez Patiño,

The corresponding author Professor Luis Alfonso Gallego Pareja has listed you as a contributing author of the following submission via Elsevier's online submission system for Results in Engineering.

Submission Title: Optimal Placement, Sizing and Operation of D-STATCOMs in Power Distribution Systems Using a Mixed-Integer Linear Programming Model

Elsevier asks all authors to verify their co-authorship by confirming agreement to publish this article if it is accepted for publication.

Please read the following statement and confirm your agreement by clicking on this link: Yes, I am affiliated.

I irrevocably authorize and grant my full consent to the corresponding author of the manuscript to: (1) enter into an exclusive publishing agreement with Elsevier on my behalf (or, if the article is to be published under a CC BY license, a non-exclusive publishing agreement), in the relevant form set out at www.elsevier.com/copyright ; and (2) unless I am a US government employee, to transfer my copyright or grant an exclusive license of rights (or for CC BY articles a non-exclusive license of rights) to Elsevier as part of that publishing agreement , effective on acceptance of the article for publication. If the article is a work made for hire, I am authorized to confirm this on behalf of my employer. I agree that the copyright status selected by the corresponding author for the article if it is accepted for publication shall apply and that this agreement is subject to the governing law of the country in which the journal owner is located.

If you did not co-author this submission, please contact the corresponding author directly at luispareja@uel.br.

Thank you,
Results in Engineering

More information and support
FAQ: What is copyright co-author verification?
https://service.elsevier.com/app/answers/detail/a_id/28460/supporthub/publishing/
%CUSTOM_GENERALSUPPORT%

In compliance with data protection regulations, you may request that we remove your personal registration details at any time. (Remove my information/details). Please contact the publication office if you have any questions.